GEOLOGY OF HEBES CHASMA, VALLES MARINERIS, MARS

Gene Schmidt, BSc.

MSc, Earth Sciences

Submitted in partial fulfillment
of the requirements for the degree of

Master of Science

Faculty of Earth Sciences, Brock University
St. Catharines, Ontario

Abstract

Hebes Chasma is an 8 km deep, 126 by 314 km, isolated basin that is partially filled with interior layered deposits (ILD), massive deposits of water altered strata. By analyzing the ILD's structure, stratigraphy and mineralogy, as well as the perimeter faults exposed in the plateau adjacent to the chasma, the evolution and depositional history of Hebes Chasma is interpreted.

Three distinct ILD units were found and are informally referred to as the Lower, Upper and Late ILDs. These units have differing layer thicknesses, layer attitudes, mineralogies and erosional landforms. Based on observations of the plateau, wall morphology and slump blocks within the chasma's interior, chasma evolution appears to be controlled by cross-faults that progressively detached sections of the wall. A scenario involving the loss of subsurface volume and ash fall events is proposed as the dominant setting throughout Hebes' geologic history.

Table of Contents

List of Figures

Chapter 1

Chapter 2

Chapter 3

List of Abbreviations

CRISM	Compact Reconnaissance Imaging Spectrometer
CTX	Context Imager
HiRISE	High Resolution Imaging Science Experiment
HRSC	High Resolution Stereo Camera
ILD	Interior Layered Deposit
LLO	Light-tone layered deposits
MOLA	Mars Orbiter Laser Altimeter
SWEET	Slope wind enhanced erosion and transport
THEMIS	Thermal Emission Imaging system
VM	Valles Marineris

Chapter 1

1.1 Introduction

Mars' similarity and close proximity to Earth makes it a valuable research subject that spans several fields of science. The discovery of water ice and large fluvial channels has further increased our interest in Mars, particularly as a planet where life could have inhabited. Dating events on Mars is largely derived by crater counting the surface, a method calibrated from impact samples taken from the moon, as well as general observations using the law of superposition. Other data sources include meteorites, landers, and orbital spectrometers. The Martian geologic timescale is divided into three periods [Hartmann, 2001]. The Noachian period spans from the accretion of Mars at 4.5 to 3.7 Ga, ending just after the Late Heavy Bombardment. It is characterized by high rates of cratering and valley formation. The Hesperian (3.7-3.0 Ga) is characterized by high rates of volcanism. The Amazonian extends from 3 Ga to the present which is about two thirds of Martian history. The Amazonian shows less volcanism and cratering than the earlier periods, but shows evidence of widespread glaciations [Carr and Head, 2010] (Fig. 1.1).

Climate has changed dramatically throughout Martian history due to loss of the atmosphere and large shifts in obliquity. Although the atmosphere during the Noachian was dense enough for liquid water to exist on the surface [Bibring et al., 2006], Mars has experienced substantial atmospheric loss [Leshin et al., 2013] due to the relatively small size of the planet. This resulted in a global climate change early in Martian history when liquid water was no longer stable on the surface. Swings in obliquity of up to 60˚ also resulted in significant changes in the local environment which may be responsible for many of the geologic features observed at the equator and mid-latitudes such as outwash channels, layered strata, and glacial deposits.

Obliquity change is the foundation of various proposed climate models [Jakosky et al., 1995; Haberle, 1998; Head et al., 2006; Madeleine et al., 2009] and provides vital insight on the geologic history of Mars, particularly for the Late Amazonian.

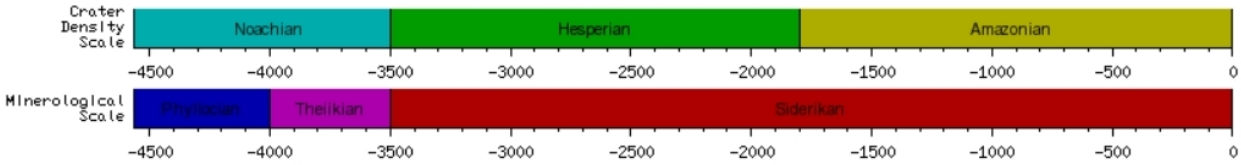

Fig. 1.1: Martian geologic time scale [Gangale, 2007].

Due to the loss of a magnetic dynamo and absence of mantle convection, no plate tectonics ever developed on Mars [Williams, 2004]. However, large-scale volcano-tectonics persisted throughout the planet's history producing the Tharsis Bulge [Mege and Masson, 1996]. The Tharsis Bulge is a massive volcanic plateau known for its shield volcanoes. It is home to several tectonic provinces including the large canyon system called Valles Marineris (VM). VM is subdivided into twelve chasmata, eleven of which contain large deposits of layered strata called interior layered deposits (ILD). The subject of this thesis, Hebes Chasma, is unique to the other chasmata in that it has no outwash channel.

1.2 Valles Marineris

VM is located on the east side of the Tharsis Bulge, at the Lunae Planum boundary (Fig. 1.2). It is 4,000 km long and the chasmata are collinear, trending 102-105˚. VM reaches 11 km in depth and is the origin of two large outflow channels, Kasei Valles in the north and the outflow from Capri and Ganges chasmata in the east.

The formation of VM began in Late Noachian or Early Hesperian [Tanaka, 1997; Schultz, 1998; Okubo et al., 2008]. It has been described as a multi-staged event beginning with the formation of isolated ancestral basins which were later linked by further extension [Schultz, 1998; Lucchitta et al., 1994]. Although commonly compared to rift valleys on Earth, vertical

collapse has been shown to be the primary driver in basin formation because the tensile stresses required in an extensional setting conflict with the observed topography and our understanding of the Martian lithosphere [Andrews-Hanna, 2012; Mege and Masson, 1996].

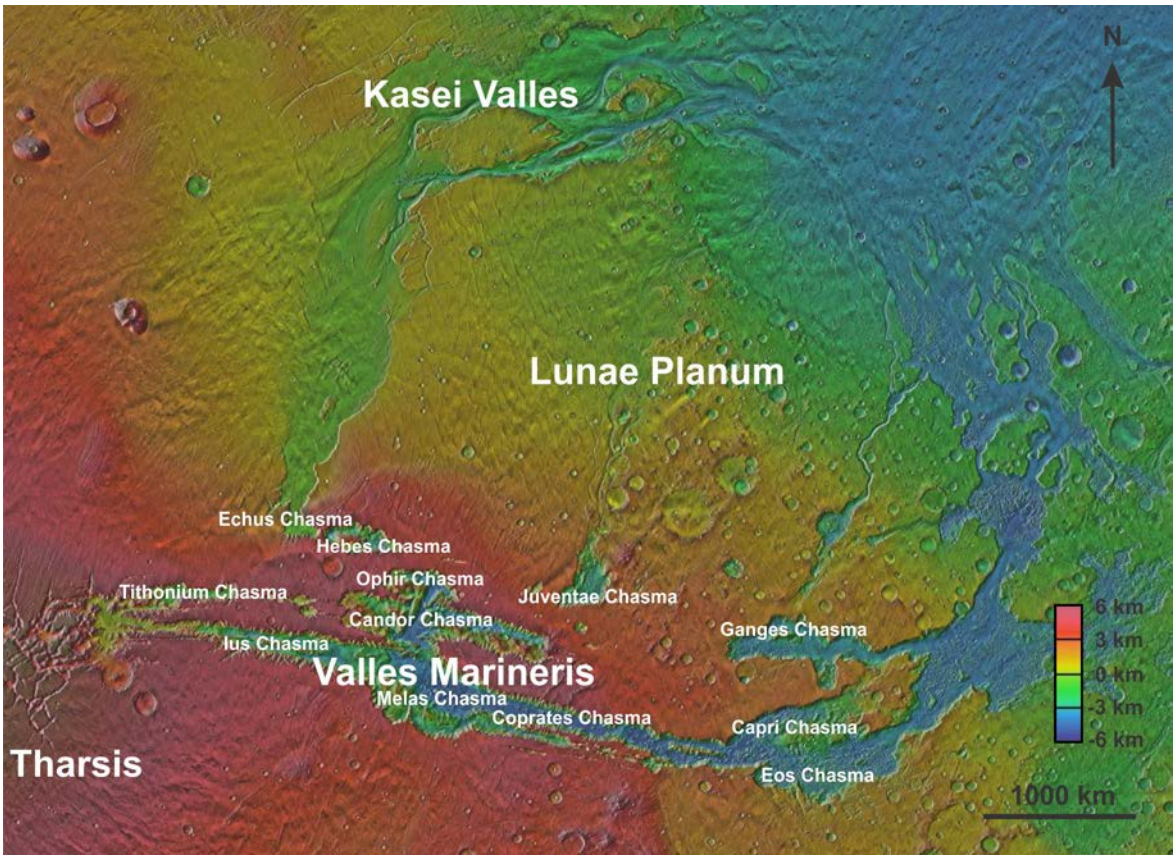

Figure 1.2: THEMIS imagery and MOLA colorized elevation of Valles Marineris and surrounding region.

Several methods of collapse have been proposed. Loss of volume by melting of ground ice [Sharp, 1973], dissolution of carbonates in the subsurface [Spencer and Fanale, 1990; Jackson et al., 2011], tension fractures [Tanaka and Golombek, 1989], dyke intrusion [Mckenzie and Nimmo, 1999], and isostatic subsidence from the Tharsis load and sediment infill [Andrews-Hanna, 2012]. Valles Marineris is likely a tensional feature because it is oriented perpendicular to the wrinkle ridges, which are compressional features [Zuber, 1994].

Valles Marineris is surrounded by Late Noachian and Hesperian-aged plateau. The plateau's lithology is comprised of tectonically contracted lava flows and undifferentiated impact breccias [Tanaka, K.L. 2014]. Numerous graben and wrinkle ridges have been observed in the plateau [Watters, 1993; Zuber, M.T. 1994; Mangold et al., 1998; Schultz, 2000] as well as cross faults [Wilkins and Schultz, 2003].

All chasmata, with the exception of Ius, contain layered strata referred to as interior layered deposits (ILD). Hebes Chasma contains an exceptionally large ILD deposit, making it important for the examination ofValles Marineris' formation. The relationship between ILD deposition and chasma collapse particularly concerns the loss of volume and subsidence hypotheses.

1.3 Interior Layered Deposits

The Martian surface shows a complex history of sedimentary deposition by water and eolian processes. Sedimentary strata are commonly observed outcropping as crater rims, the tops of chasma walls, mounds within basins, and outflow deposits. Strata outcropping within basins such as craters, valleys, or chasmata are of particular interest because they may represent changes in Martian paleoclimate [Lewis et al., 2008]. Formation of these ILD can be explained by processes akin to those seen on Earth [Grotzinger and Milliken, 2012]. A variety of processes and depositional regimes, including sedimentary and volcanic settings, have been proposed over the last four decades to explain ILD formation: lacustrine [Needell et al., 1987], groundwater springs [Rossi et al., 2008; Mangold et al., 2008], ash fall [Lucchitta, 1990; Chapman, 2002; Komatsu et al. 2004; Fueten et al., 2014], diapiric uplift [Milliken et al., 2007; Jackson et al., 2011], dust-rich glaciers [Michalski and Niles 2011], and katabatic winds [Kite et al., 2013]. These mechanisms are discussed in more detail below.

An ILD mound's size correlates to the size of the basin containing it. The timing of deposition during the stages of chasma formation may influence mound size. In general, ILD are several hundred thousand cubic kilometers in volume [Lucchitta et al., 1994]. ILD mounds within chasma are generally more massive than ILDs observed within craters. ILD within Hebes, Ophir and Candor Chasmata reach nearly 8 km in elevation [Jackson et al., 2011; Lucchitta et al., 1994]. ILD in Ganges chasmata reaches 4.25 km in elevation [Hore, A. et al., 2013]. However the ILD mound within Gale Crater reaches 5 km in elevation [Edgett and Malin, 2000]. ILDs generally comprise 60-80% of the total volume the basin [Kite et al., 2013, Lucchitta et al., 1994].

1.3.1 ILD Formation Mechanisms

1.3.1.1 Lacustrine Setting

The lacustrine hypothesis of ILD formation proposes that Valles Marineris was a series of isolated troughs before being connected by further extension [Lucchitta et al., 1994]. This is the generally accepted model for VM and therefore should apply to all ILDs. Many of the ILDs exhibit hundreds to thousands of meters-thick layered sequences with a paucity of bedforms, and they are best interpreted to have been deposited in low-energy environments such as slow settling in lacustrine or fall-out in subaerial conditions [Komatsu et al., 2004]. Constraints of a lacustrine origin include: (1) The requirement of a dense enough atmosphere to increase the surface air pressure to sustain liquid water for a period of time long enough to deposit 6-8 km of sediment [Peterson, 1981]. (2) During the last stages of ILD deposition, the lake level would have had to have been as high as the chasma (or crater) wall to create mounds that reach their current heights. However, if the infilling was syntectonic and at the same rate or faster than the subsidence, then the lake level does not to be this high (3) In the case of Valles Marineris ILDs,

lakes could not be sustained in chasmata if they were interconnected at the time of deposition. Hebes Chasma would be an exception to this, as it has remained enclosed.

Observations of ILD in Viking imagery (150-300m resolution) led to the first inferences about lacustrine settings. In 2005 the orbiting spectrometer, CRISM, revealed an abundance of hydrous sulfates within Valles Marineris [Murchie et al., 2007]. This provides evidence of a lacustrine environment during ILD formation, but other wet environments cannot be ruled out [Fueten, 2014].

1.3.1.2 Groundwater Spring Deposits

ILD formation by groundwater spring deposits explains some aspects of ILD mounds [Rossi et al., 2008], notably the high concentrations of hydrous sulfates associated with them [Chojnacki and Hynek, 2008; Catling, 2006; Hauber et al., 2008]. A groundwater spring could have existed within Hebes' ILD mound due to pressure gradients brought on by the mound [Grindrod, 2010]. The spring could deposit new layers [Hauber et al., 2008]. The extent of groundwater's influence on ILD formation, however, continues to be debated. There is an absence of fluvial erosion on the ILD mounds and groundwater springs do not explain their laterally continuous layering.

ILD with high albedo are referred to as light-tone layered deposits (LLO) [Catling et al., 2006]. These types of ILD tend to have high detections of hydrous sulfates and are interpreted to be consolidated salt deposits mixed with dust and sand [Catling et al., 2006]. Although there is some discrepancy of when to use the term "light-tone layered deposit" in place of "interior layered deposit", a LLO generally describes an ILD that is sulfate-rich and therefore lighter in tone, which is interpreted to be deposited specifically by groundwater springs. This is due to

their high albedo coupled with high levels of sulfates as observed by the CRISM and OMEGA orbiting spectrometers [Ehlmann et al., 2009].

1.3.1.3 Ash Fall Deposits

According to this hypothesis ILD mounds consist of a thick sequence of ash, with interbedded layers of relatively resistant welded tuffs [Peterson, 1981; Lucchitta, 2010]. For mounds to form, the ancestral troughs of Valles Marineris must have been interconnected early in their development, preventing the formation of a lacustrine setting [Lucchitta et al., 1994]. The pyroclastic material could have been issued from the Tharsis volcanoes or from beneath the chasmata themselves [Peterson, 1981; Fueten et al., 2014].

Layered sequences are best interpreted as the product of a low-energy depositional regime [Komatsu et al., 2004]. Ash fall is one way to get low-energy layered sequences, particularly when combined in a lacustrine setting. Pyroclastic deposits on Earth are often used as an ILD analog [Luchitta et al., 1994; Peterson, 1981; Wietz, 1999]. ILD mounds have also been compared to tuyas which are a type of volcano that erupts through a thick ice sheet [Luchitta et al., 1994; Chapman, and Tanaka, 2001]. One comparison was made between ILD and the Bishop Tuff in California [Wietz, 1999]. Erosional fluting visible along the edges of ILD mounds is also indicative of tuffs and other terrestrial ignimbrites.

1.3.1.4 Diapiric Uplift

In this hypothesis karstic collapse via subterranean piping drives chasma formation. ILD mounds are interpreted as uplifted floor produced from salt diapirism. Salt diapirism and subterranean piping between chasmata has been inferred in Valles Marineris several times [e.g., Milliken et al., 2007; Popa et al., 2007; Baioni and Wezel, 2008; Jackson et al., 2011]. Subterranean piping explains the apparent lack of material on chasmata floors [Luchitta et al.,

1994] as eroding an entirely filled basin into a mound by aeolian processes is problematic. This scenario, coupled with a basin that lacks an outflow channel, makes use of subterranean piping to explain the loss of material. For example, some infer that Hebes and Echus chasmata are connected via groundwater canals [Grindrod, P.M. 2010; Jackson et al., 2011].

Opponents argue there is no terrestrial analogue that combines diapirism and collapse [Andrews-Hannah, 2012]. Distinct layers in mounds are not explained by this model and are only hinted to be material that was brought up from depth. The internal layering of diapirs tends to be deformed and faulted, and these features are rarely seen in ILDs. Also, subterranean flow would produce carbonates instead of detritus [Luchitta et al., 1994]. ILD mounds are not associated with high levels of carbonates [Quantin et al., 2010] and the amount of carbonates needed to create the chasmata conflicts with global spectral analysis that shows carbonates are spatially and volumetrically limited on Mars [Ehlmann et al, 2008].

1.3.1.5 Dusty Glaciers

The dusty glacier hypothesis is perhaps the most imaginative. It suggests that ILD are deposited in cold, dry climates by receding dust-rich glaciers that fill much of the chasmata [Michalski, 2012]. Sulfur from volcanic eruptions also gets trapped in these glaciers, explaining the abundance of sulfates within ILD. Layers are thus viewed as an expression of Mars' obliquity. Proponents argue that the topographic highs of ILD contradict groundwater upwelling. It is also argued that sulfate deposition from groundwater upwelling implies the chasmata was entirely filled with sulfur-rich sediments, a scenario that requires more sulfur than would have ever been available on Mars [Michalski, 2012].

Many landforms within VM suggest glaciations. The massive outflow channel that connects chasmata in Valles Marineris has been interpreted to have been a large ice dam that

gave way [Lucchitta et al., 1994]. ILD often display features suggestive of periglacial environments: freeze-thaw polygons, solifluction lobes, rock glaciers, and pingos [Hauber et al., 2008; Blame et al., 2011].

Although there is a consensus that glacial activity has played an active role in the ILD's past, glaciation as a method of deposition is debated. It does not easily explain ILD mounds that contain uniform layers over 12 m thick [Fueten et al., 2013]. Also, many find it implausible that 6-8 km high mounds of strata could be created by repeated glaciations because it implies a longstanding Martian seasonal cycle. The detection of abundant sulfates within ILDs [Gendrin et al., 2005; Chojnacki and Hynek, 2008] suggests wetter conditions because on Earth sulfates are difficult to form in glacial environments and more commonly are associated with liquid water.

ILDs were deposited in the Hesperian, in the period 3-3.5 Ga [Head et al., 2001]. Mars' unique obliquity is known to slowly increase and decrease between about 15 degrees and 35 degrees over a 124,000-year cycle. Recent studies suggest that at intervals of a few tens of millions of years Mars' obliquity may swing from 0 degrees up to 60 degrees [Wordsworth et al., 2013]. Certainly there has been a cycle of freezing and thawing of subsurface ice, but ILD formation as a result of glaciers will continue to be debated although there is considerable evidence for their existence throughout VM’s history.

1.3.1.6 Katabatic Winds

Katabatic winds (wind that moves down the chasma/crater wall) have been shown to create an aeolian flow that may lead to deposition of ILD mounds [Kite et al., 2013]. This process is referred to as “wind-topography feedback”. However, for Aeolis Mons in Gale Crater, it is argued that if the crater was filled with ILD and then eroded to form a mound, the erosion required to remove the $\approx 10^6$ km^3 of material is not feasible [Kite et al., 2013]. The model

demonstrates that mounds reach a terminal height dependent on the basin size. Once a mound reaches this height, the wind begins to erode it in a process called slope wind enhanced erosion and transport.

This model is constrained by requiring the existence of a "moat" during mound growth [Kite et al., 2013]. Wind plays a role in the erosion of ILD mounds, but it is hard to conceive that it could create 6-8 km mounds. The model is ideal for circular mounds, but not irregular or oval shaped mounds particularly those with layer thicknesses that are uniform. Katabatic winds also do not explain craters with mounds that exceed the crater rim's height (Fig. 1.2). The model does, however, leave room for intermittent fluvial/lacustrine deposits that were perhaps reworked by aeolian processes.

1.3.2 Crater ILD vs. Chasma ILD

It is important to understand the difference between ILD contained within craters and ILD contained within chasmata. ILDs tend to take the shape of the depression they are deposited in [Kite et al., 2013; Lucchitta et al., 1994; Jackson et al., 2011; Peterson, 1981] which is useful when determining the extent of an eroded deposit. An ILD mound within a crater, which is a circular shape, will thus have the shape of a circle. ILD mounds within chasmata are more irregularly shaped and often trend the axis of the chasma. If we assume that crater and chasmata ILD were deposited by the same mechanism and that deposition occurred during the early stages of chasma extension [Lucchitta et al., 1994; Peterson, 1981], then the gap between the mound and crater wall is not explained. However, craters often continue to collapse around the original crater rim as a result of isostatic rebound in the interior [Head, 1975].

The lacustrine hypothesis could explain ILD mounds in both craters and chasmata because they are both enclosed basins that could hold water. Deposition by ash fall explains

ILDs in Valles Marineris because of the close proximity to the major Martian volcanoes: Olympus Mons, Ascraeus Mons, Pavonis Mons, and Arsia Mons. However, many of the craters that contain mounds are not within proximity to volcanoes [Anderson, R. B., 2010].

Many of the crater mounds are covered with dust, consequently making layers hard to distinguish from orbit. Many also show no expression of layering, or shelf-bench features. This could suggest that the material is not layered (i.e., massive), the layers are much finer than can be resolved, or that the layers are so uniform in composition that differences in their erosional expression are not visible. For the case of Gale Crater, some argue that the lower layers represent the lucastrine hypothesis and the upper layers represent the katabatic wind hypothesis [Anderson, 2010]. The Mars Science Laboratory (MSL) has the opportunity to examine these deposits in situ and observations thus far suggest that Aeolis Mons in Gale Crater contains at least one ash deposit [Milliken, et al. 2008].

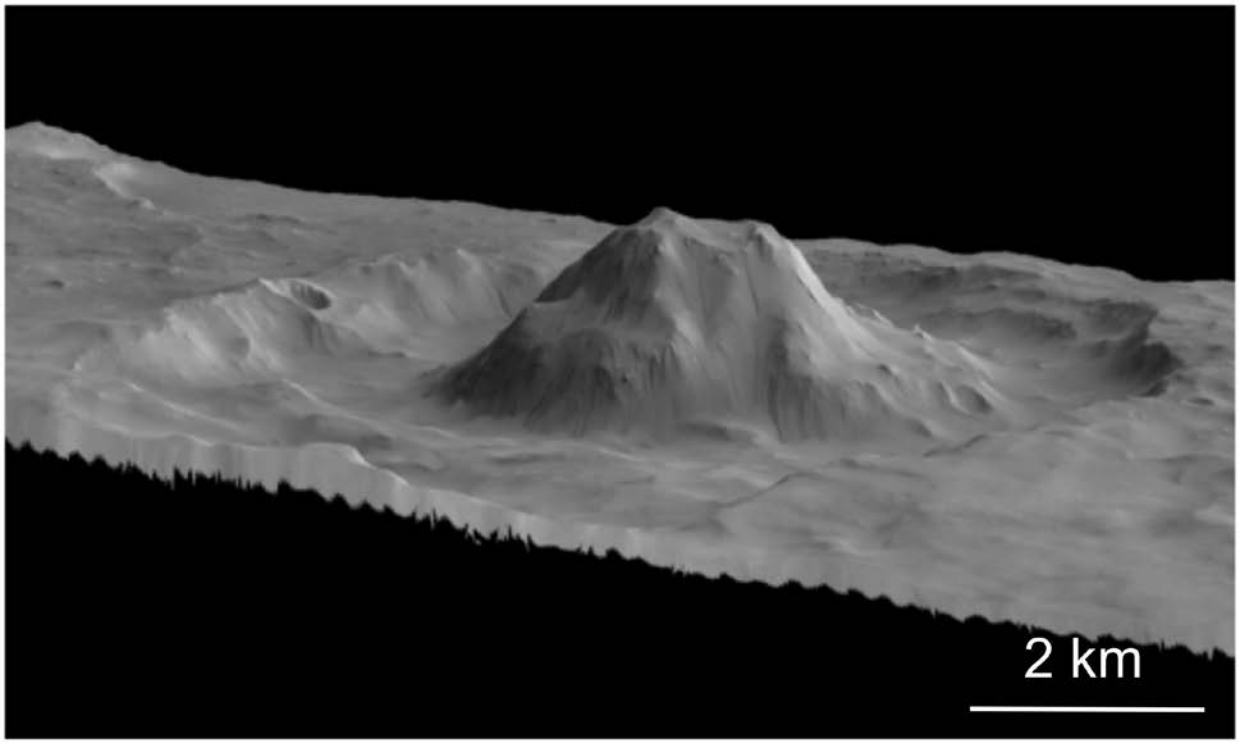

Figure 1.3: Unnamed crater in Arabia Terra with mound rising 1 km above the crater rim, 5x vertical

exaggeration [NASA/JPL-Caltech/Malin Space Science Systems].

The height of ILD mounds suggests that both craters and chasmata were once completely filled and buried [Malin and Edgett, 2000]. ILDs are also considered to be less resistant than the wall material that encloses them. However, there are examples of crater mounds where the associated crater rim has been completely eroded away (e.g. Fig. 1.3), leaving the central mound higher than the surrounding rim. Another example, similar to Aeolis Mons yet with differing erosional expressions and layer thickness, is a mound contained in Henry Crater (Fig. 1.4). The mound has numerous layers and appears to be cross-cut by a series of parallel faults. Not far to the southwest from Henry Crater, there is a crater with a mound displaying yet another unique erosional appearance [Malin, 2000]. This is only one example of many locations exhibiting craters with mounds that differ in their erosional expression and layering.

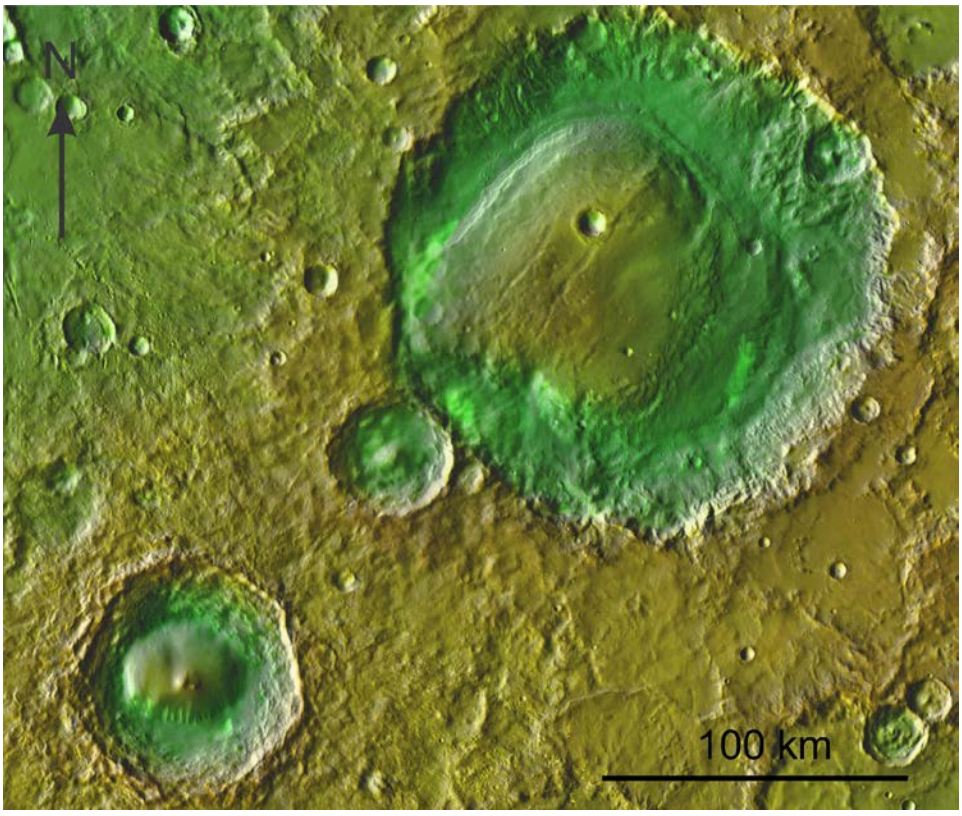

Figure 1.4: THEMIS imagery and MOLA colorized elevation of Henry Crater (northeast) and an unnamed crater (southwest) containing unique mounds.

These observations suggest to the interpretation that groups of craters in close proximity to each other existed in different depositional environments with varying supplies of clastic material (assuming it is not chemically precipitated). Despite differing dimensions, locations, and erosional features, the basic conditions during sedimentation and erosion of ILD could not have varied greatly because comparable mineralogies and morphologies are found among all ILD [Sowe et al., 2011].

1.3.4 Timing Constraints

The tops of ILD mounds are impacted by large craters, implying ILD mounds formed in the Lower Hesperian (3-3.5 Ga), which is equivalent to Earth's Archean [Quantin et al., 2010; Head at al. 2001]. However, the duration of deposition, number of depositional episodes, and the stage of basin formation at deposition are questions currently debated. Different modes of deposition will require various durations of ILD formation. For example, Aeolis Mons may have taken at least 10-100 My to accumulate [Kite et al., 2013], which falls in the same time range as the ILD formation model proposed by Andrews-Hanna, [2012]. However, this disagrees with other models of ILD formation that are on the order of hundreds of millions of years [Head, 2001].

In an attempt to explain the large 5- 20 km distances between ILD mounds and chasma walls, it has been argued the mounds formed during chasmata extension [Peterson, 1981] (Fig. 1.5), or ILD mounds have experienced extensive erosion[Grindrod and Warner, 2014]. This model explains how mound geometry represents the shape of the ancestral basin and that the ILDs took less time to form than the chasma.

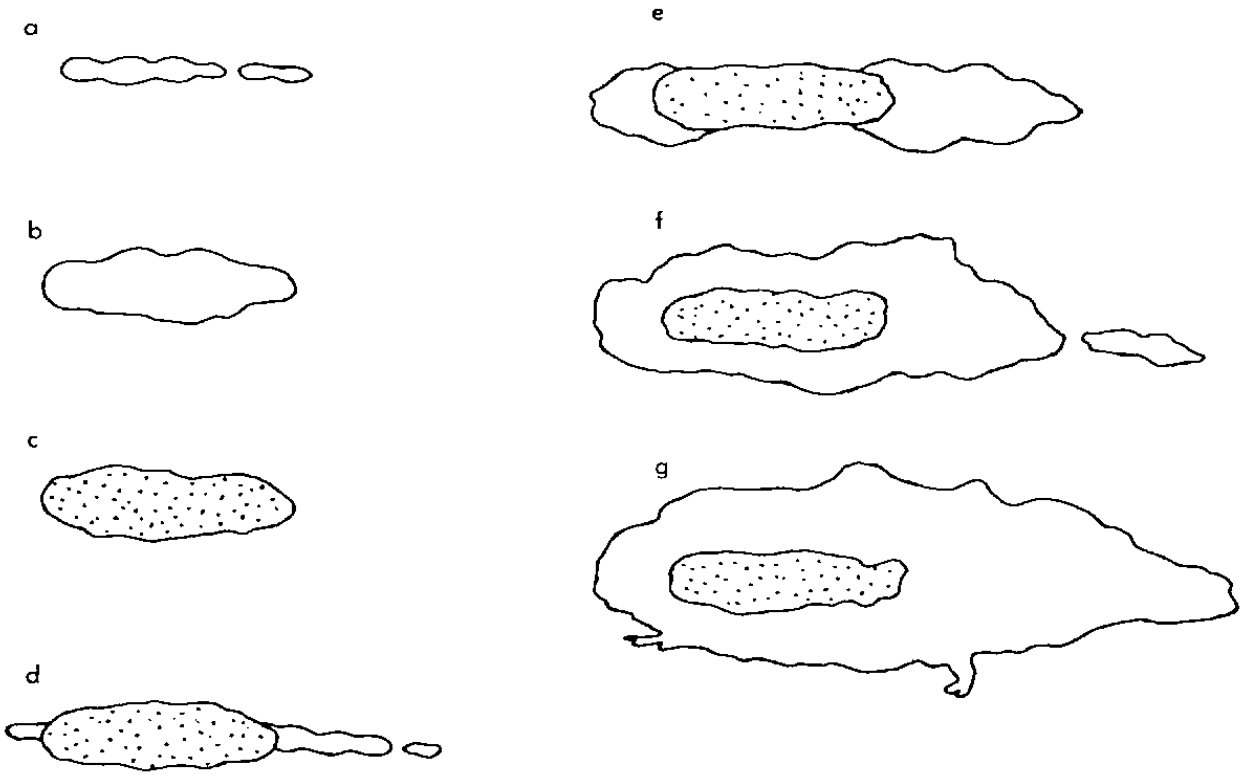

Fig. 1.5: Sketch of proposed geologic history of Hebes Chasma. (a) Linear collapse of crater chain by evaporation of ground ice along a graben. (b) Widing of trough by landslides. (c) Infilling of trough by volcanic ash or eolian material. (d) Continued collapse along graben and lengthening of trough. (e) Widening by landslides. (f) Isolation of central plateau from main chasma walls by landslides. (g) Present configuration. [From Peterson, 1981]

One of the focuses of this study was the determination of the timing of Hebes' collapse relative to the ILDs' deposition. Two central questions arise: did ILD deposition occur before chasma formation or is deposition post-formation and were there multiple periods of deposition?

1.3.5 Erosional Features of ILDs

There is no clear consensus for the erosional processes of ILDs. There is however the consensus that Martian climate has changed dramatically since the Hesperian, which implies changing erosional processes throughout ILD history [Head et al., 2001]. ILDs display a diverse array of erosional features making the labeling of one dominant erosional process difficult. Despite this, wind is widely accepted as the major erosional process influencing ILD as it is the

most predominate on Mars today [Armstrong and Leovy, 2005]. Yardangs and dunes are observed on all ILD [Grotzinger and Milliken, 2012]. Flutes are also observed [Wietz, 1999]. Outflow events that formed the channels merging Juventae, Ganges, and Capri/Eos chasmata, are thought to have eroded some of the ILD in Valles Marineris as well [Luchitta et al., 1994]. There are also numerous features suggestive of glacial erosion [Hauber et al., 2008].

1.3.6 Water-Altered Minerals

Spectral analysis of ILD within Valles Marineris [e.g. Bibring et al., 2005, 2006; Poulet et al., 2005; Gendrin et al., 2005; Murchie et al., 2007; Mustard et al., 2008] used to infer their mineralogy [e.g. Murchie et al., 2009; Flahaut et al., 2010] indicates that both poly and monohydrated sulfates comprise a significant amount of the ILDs. Hematite was also found in ILDs within Ophir, Candor and Capri Chasmata [Chojnacki and Hynek, 2008]. A slope stability analysis suggests that ILDs consist of relatively weak and hydrated sediments [Komatsu et al., 2003].

Conditions favoring the formation of hydrous minerals on Mars may have persisted during the entire history of Mars from the Early Noachian to the Amazonian [Quantin et al., 2010]. Most fluvial landforms were formed in Middle Noachian and later, although many early fluvial landforms may not have been preserved [Head et al., 2001]. Monohydrated sulfates comprise about 10,263 km^2, polyhydrated sulfates about 3,419 km^2, and hematite about 1,915 km^2 of the total area within Valles Marineris [Chojnacki and Hynek, 2008]. There is also evidence that monohydrated sulfates occur at lower elevations and polyhydrated sulfates occur at higher elevations [Flahaut et al., 2010; Fueten et al., 2014]. Hydrated sulfates usually form where water has been concentrated and exposed to prolonged evaporation in a sulfur rich environment. A polyhydrated sulfate contains an extra water molecule and its detection implies a more porous

material or possibly more fluid pressure.

These discoveries have encouraged ILD research as their apparent relevance to our understanding of Mars' paleoclimate becomes clearer.

1.4 Purpose of Study

This study focuses on the geology of Hebes Chasma. The Hebes Chasma ILD mound is particularly significant due to its isolation. This provides an opportunity to observe an intact ILD that has not undergone a major outwash event and thus has the potential for use as a foundation for correlating all the ILDs within Valles Marineris. Determining the mineralogy, layer thickness, and layer attitudes within ILDs will contribute to our scientific understanding of the Martian paleoclimate. Furthermore, examination of Hebes will contribute to our understanding of Valles Marineris' formation, and in a broader sense the technicalities of Tharsis' structure. Findings are organized into two chapters that separate the geology of the ILDs and of the chasma itself.

Chapter 2 analyzes the structure and mineralogy of ILDs within Hebes Chasma. Layer thicknesses and attitudes show three depositions of ILD with unique mineralogies. A geologic map was then constructed in an attempt to improve upon previous interpretations of the chasma.

Chapter 3 focuses on wall morphology and wall collapse in Hebes Chasma and their relationship to perimeter faults. An effort is made to determine chasma extent during ILD deposition by looking at ILD-wall contacts and collapse structures. The regional structure between Echus Chasma and Hebes Chasma is also discussed to address the possibility of groundwater flow between them.

Chapter 2: Structure and Mineralogy of ILD in Hebes Chasma, Mars: Evidence for multiple episodes of deposition

2.1 Introduction

The formation of Valles Marineris (VM) is thought to involve a process of collapse in combination with slight amounts of extension followed by erosion [Mege and Masson, 1996]. Although the exact mechanism is debated, most studies describe a multi-stage event that began in the Late Noachian or Early Hesperian [Tanaka, 1997; Schultz, 1998; Okubo, et al., 2008] to form isolated ancestral basins that were later linked by further extension and collapse [Schultz, 1998; Lucchitta et al., 1994].

Large mounds of sedimentary strata that are several kilometers high are well known throughout VM. Formation of such strata, called Interior Layered Deposits (ILDs), can be explained by processes observed on Earth [Lucchitta et al., 1994; Grotzinger and Milliken, 2012]. Fluvial, aeolian, and volcanic process have been proposed to explain ILD formation [Needell et al. 1987; Rossi et al., 2008; Mangold et al., 2008; Lucchitta, 1990; Chapman, 2002; Komatsu et al. 2004; Fueten et al 2014; Milliken et al 2007; Jackson et al. 2011; Michalski and Niles, 2011; Kite et al 2013]. The abundance of water-altered minerals within ILD implies the presence of liquid water during deposition [Flahaut et al., 2010].

Hebes Chasma is the only large isolated basin within VM (Fig. 2.1). It measures 126 km (North-South) by 314 km (East-West) and reaches over 8 km at its deepest point. It is unique to VM in that unlike other chasmata, it lacks an outwash channel. The absence of any massive outwash event provides an opportunity to observe its intact, undisturbed ILD mound, which is often referred to as Hebes Mensa [Jackson et al., 2011; Grindrod and Balme, 2010; Rossi et al., 2008; Ori et al., 2005]. In this study three distinctly different ILDs resting at differing elevations were identified within Hebes. Differing mineralogy, layer thickness, layer attitude, and overall

geometry within the ILDs indicates a complicated depositional regime during various stages of chasma formation. Erosional differences amongst the ILDs point toward changing environments, including glacial, periglacial, fluvial, and aeolian within the chasma since their deposition. These discoveries may aid the stratigraphic correlation of ILDs throughout VM.

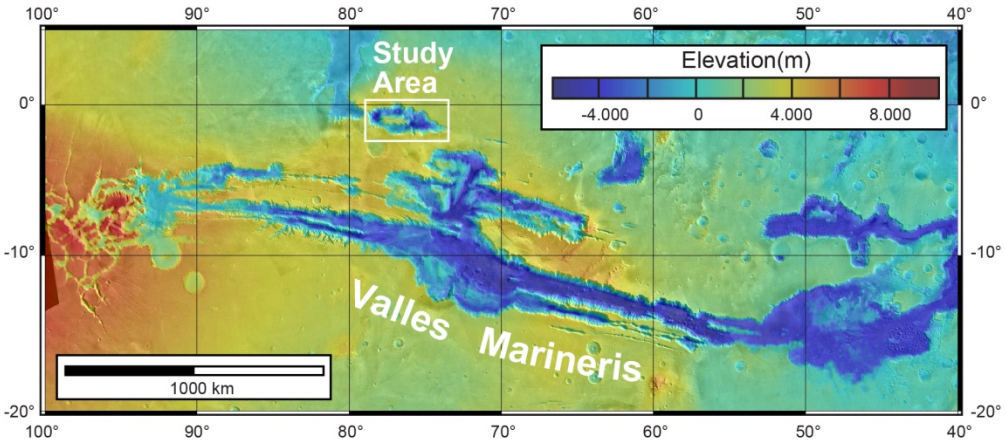

Figure 2.1: MOLA colorized DTM showing the location of Hebes Chasma

2.2 Background

Hebes Chasma (-1.1° S, -76.2° W) is the northern-most chasma of VM located at the Tharsis and Lunae Planum boundary (Fig. 2.1). The surrounding plateau is mostly Hesperian in age with the exception of Noachian plateau in the northwest [Tanaka, 2014]. The plateau contains an extensive network of graben and several wrinkle ridges. The southern plateau's surface is largely covered with impact ejecta, but some faulting and wrinkle ridges have been observed there as well [Tanaka, 2014]. Directly west of Hebes is Echus Chasma, an open-ended flat-floored depression that marks the beginning of the Kasei Valles outflow system [Chapman et al., 2010]. To the southwest of Hebes is Perrotin Crater, a large 80 km wide Hesperian-aged crater [Tanaka, 2014]. A 95 km long pit chain is located 147 km east of Hebes (Fig. 2.2). Echus, Hebes, and the pit chain are collinear with an orientation of 102˚.

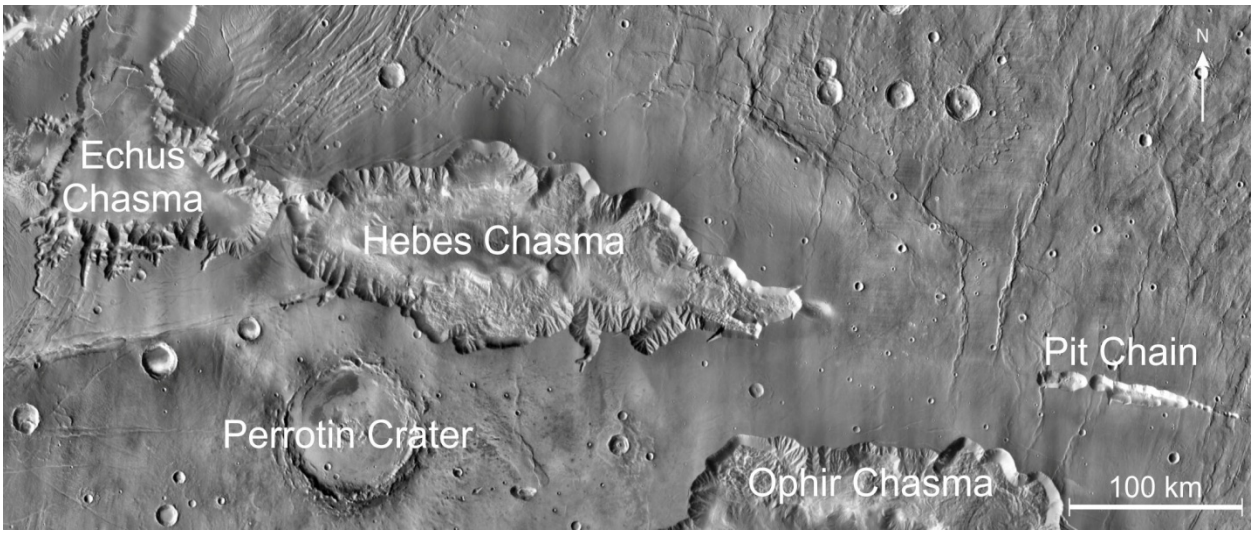

Figure 2.2: THEMIS daytime infrared imagery of Hebes Chasma (center), Echus Chasma (west), Perrotin Crater (southwest), Ophir Chasma (southeast), and pit chain (east). Note the wrinkle ridges on the northeast plateau and the graben field between Hebes and Echus.

The ancestral basin that became Hebes Chasma was formed during post-Early Hesperian time [Schultz, 1998]. Hebes Chasma is thought to have been formed prior to the opening of VM [Lucchitta et al., 1994]. The formation of Valles Marineris is thought to have been complete by the Middle Hesperian [Head et al., 2001], although late faulting in the Amazonian may have contributed to a small fraction of chasma collapse [Schultz, 1998].

The age of Hebes Mensa, like other ILD in VM, is thought to be Hesperian [Schultz, 1998; Head et al., 2001]. The ILD within Hebes Chasma has previously been described as having an upper layered unit and a more massive lower light-toned unit [Komatsu et al., 1993; Lucchitta, 1999]. Lucchitta [1990] described tuff-like weathering on VM's isolated ILD mounds and Weitz, [1999] compared Hebes Mensa to the Bishop Tuff in California.

Several origins have been proposed for Hebes Mensa. Peterson [1982] argued an aeolian or pyroclastic origin on the grounds that the removal of water and sediments in a lacustrine origin was problematic in an isolated chasma. Similarly, Hauber et al., [2006] favored a pyroclastic origin to explain the down-slope dipping of ILD layers and argued against any deep

bodies of standing water in Hebes. However Lucchitta [2010] argued that eolian and pyroclastic origins still required a lake to trap the sediments. Proposed ash sources for the pyroclastic theory of origin have included supply from beneath the chasma, either as fissures, caldera or tuya [Peterson, 1981; Croft, 1990; Chapman, M.G. and Tanaka, K.L., 2001], or from distal volcanoes [Fueten et al., 2014]. Mangold et al., [2008] proposed a groundwater deposition origin for ILD in Candor Chasma, but Fueten et al., [2014] argued that the high elevation of the ILD mound would leave its upper portions isolated from groundwater flow. Hebes Mensa reaches 3,830 m in elevation, which is approximately 500 m below the western plateau and level with the eastern plateau. Grindrod and Balme, [2010] produced a model of groundwater upwelling in Hebes Chasma driven by pressure gradients caused by the ILD mound. Although the study did not consider the origin of the ILD, it demonstrated the possibility of groundwater processes within Hebes Mensa. Similarly, Hauber et al., [2006] proposed that groundwater might have played a major role in the occurrence of alteration minerals within the ILD in Hebes. Conversely, Jackson, et al. [2011] proposed that Hebes Mensa was not deposited material, but rather deep basement rock produced by diapiric uplift.

2.3 Methodology

2.3.1 Data Source

A CTX mosaic registered to a HRSC composite DTM (orbits 0360, 2116, 2138, 2149, 5142, 5160, 5178) forms the base data for the study (Fig. 2.2a). With the exception of several areas, CTX DTMs with a resolution of 5 m/pixel cover the majority of the chasma (Fig. 2.2b). Layer thickness measurements were taken using a 50 m/pixel HRSC DTM in one area that lacked a CTX DTM. Thirteen HiRISE images with five accompanying DTMs with resolutions ranging 100-40 cm/pixel were used as well. All CTX and HiRISE DTMs were computed using

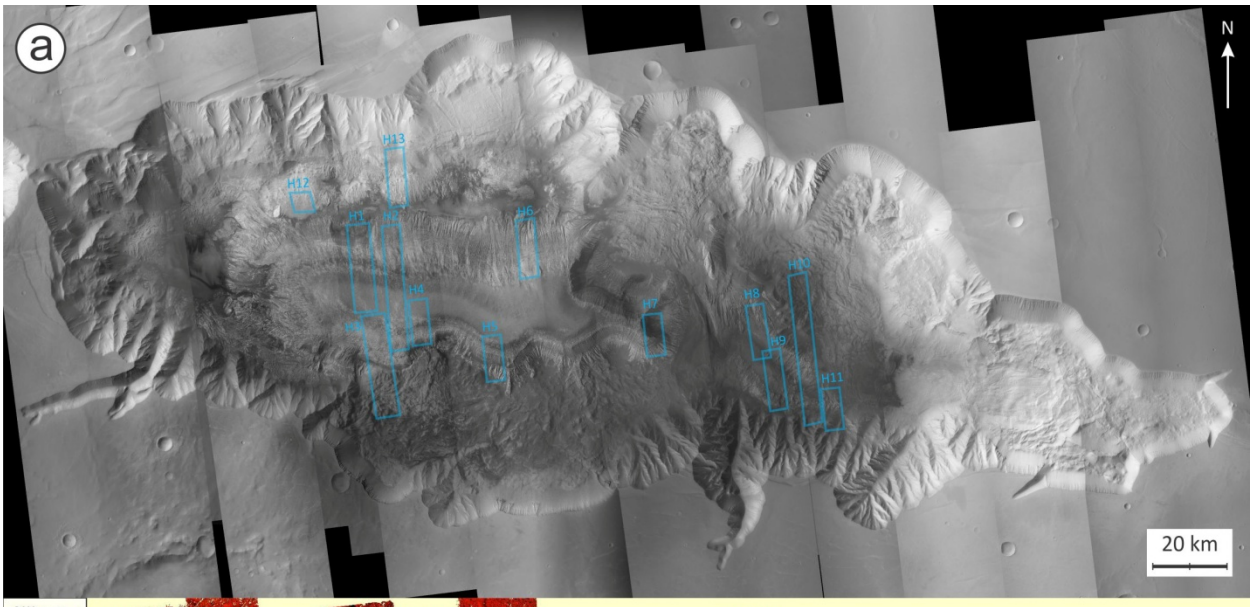

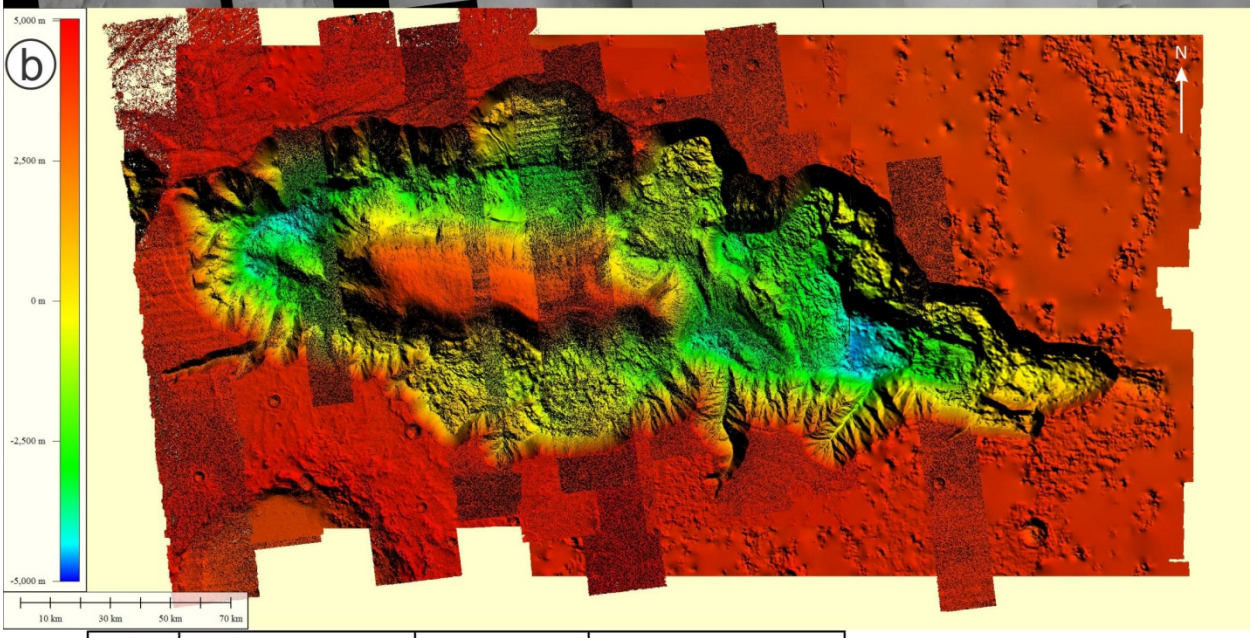

c

Label	HiRISE Image Number	ILD Formation	Elevation Range (m)
H1	PSP_005808_1790	Upper ILD	-1,140 to 3,680
H2	PSP_006520_1790	Upper ILD	
H3	ESP_016462_1785	Upper ILD	
H4	ESP_033380_1790	Upper ILD	
H5	ESP_030479_1785	Upper ILD	
H6	ESP_021565_1785	Upper ILD	
H7	PSP_003975_1790	Upper ILD	
H8	ESP_014418_1790	Lower ILD	-3,302 to -1,552
H9	ESP_024400_1790	Lower ILD	
H10	ESP_017319_1785	Lower ILD	
H11	ESP_018664_1785	Lower ILD	
H12	ESP_019297_1795	Late ILD	-1,666 to -738
H13	ESP_013772_1795	Late ILD	

Figure 2.3: CTX mosaic of Hebes Chasma with HiRISE image locations. (a) Location of HiRISE images outlined in blue. (b) CTX DTM coverage over HRSC DTM. (c) List of HiRISE images with corresponding labels and ILD unit with elevation ranges.

the NASA Ames Stereo Pipeline [Moratto et al., 2010; Broxton and Edwards, 2008].

2.3.2 Geometric Measurements

Layer attitudes and thicknesses were measured using five HiRISE stereo pairs and eight HiRISE images registered to CTX DTMs (Fig. 2.2). Dip measurements typically had an error between ±1˚ and ±5˚. Uncertainty was kept to less than the value of the dip to ensure that the correct dip direction was identified. Layer thicknesses were obtained by measuring elevation and distance between each layer along a line parallel to slope. Multiple transects were measured for each HiRISE image as well as two CTX images to confirm measurements. A HRSC DTM was used in a small section of the western side of the central ILD mound where both HiRISE and CTX topography were not available. In this instance layer thicknesses were obtained by counting the number of layers along transects over known elevations and calculating the mean thickness for each transect. Layer attitudes were obtained using Orion software [Pangaea Scientific, 2006-2011]. Attitudes that showed folding were plotted on Schmidt nets to determine fold axes. Schmidt nets were produced using SpheriStat3 [Pangea Scientific, 2014].

2.3.3 Geologic Mapping

A geologic map was created in CorelDraw [© 2010 Corel Corporation] using the CTX mosiac (Fig. 2.3). Geologic units and features were interpreted on the basis of their location, elevation, size, attitude, erosional features, tone, and mineralogy. All available CRISM data sets for Hebes were analyzed by J. Flahaut. Layer strike and dip was measured using both CTX and HiRISE DTMs. Each strike and dip measurement depicted on the map represents an average of several measurements taken in the area surrounding the symbol. Geologic nomenclature is that of Tanaka, 2014 and Lucchitta, 1999. Hebes Chasma has also been mapped before with Viking, HRSC and MOLA data [Croft, *1990;* Jackson, et al., 2011]. The map presented in this study

expands interpretations made by previous maps by taking advantage of mineralogical data and higher resolution imagery.

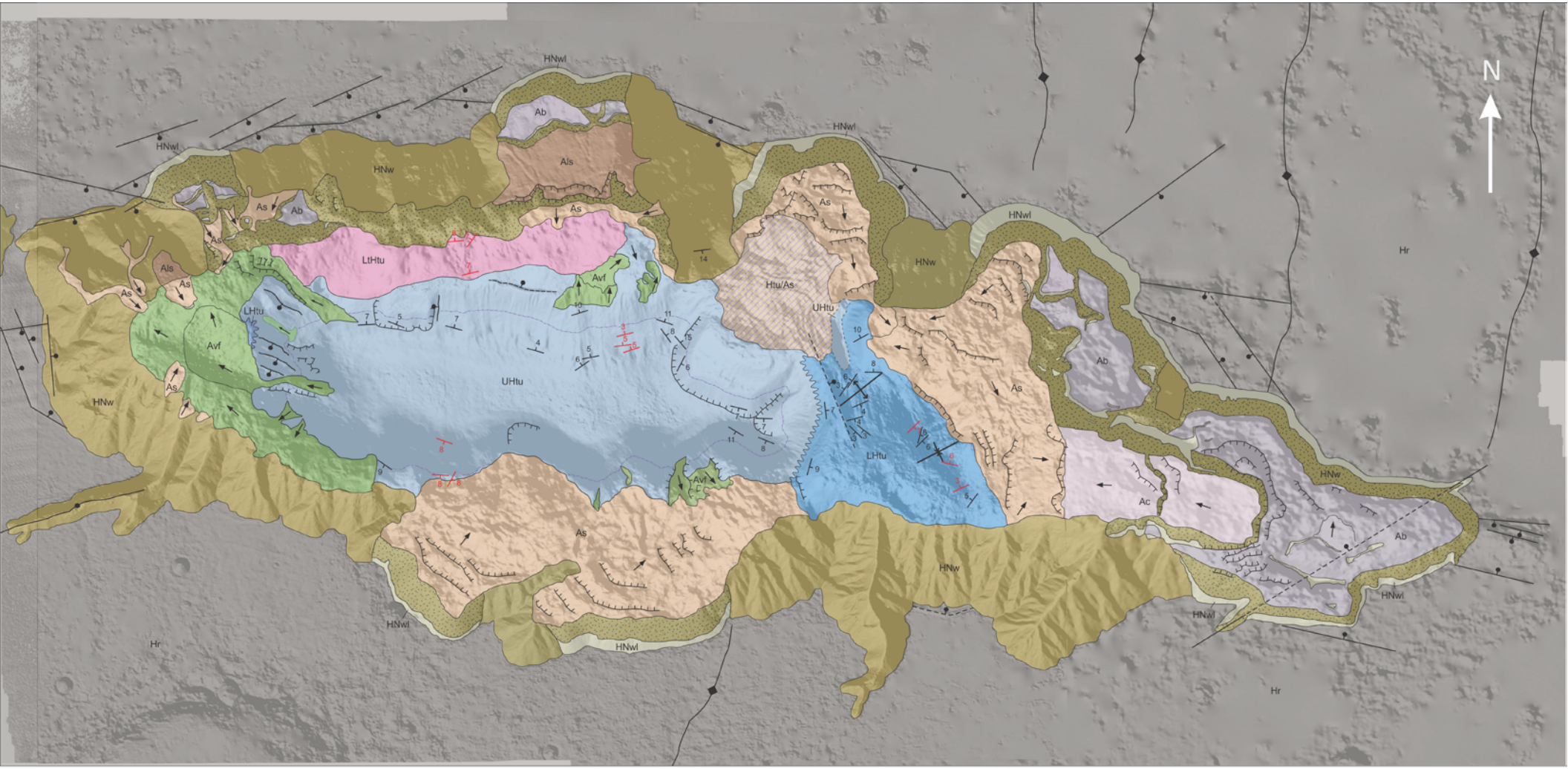

SCALE 1 : 1 000 000 (1 mm = 1 km) 1°S 75°W
EQUIRECTANGULAR PROJECTION
0 10 20 30 40 50 60 70 80 90 100 KILOMETERS

Description of Map Units:

UHtu — **Upper ILD Formation:** Forms central mound. Monohydrated sulfates overlain by polyhydrated sulfates intermixed with mafic material. Average layer thickness of 2.38 m.

LHtu — **Lower ILD Formation:** Mono- and polyhydrated sulfates and gypsum. Some clays. Large scale folding. Average layer thickness of 28.09 m.

LtHtu — **Late ILD:** Mono- and polyhydrated sulfates. Average layer thickness of 0.89 m. Hummocky terrain.

HNwl — **Layered wall material:** VM cap unit. Forms 1 km high cliffs lining the upper extent of the chasma's perimeter. Rests above smooth talus slopes.

HNw — **Wall material, stippled where smooth:** Forms spur-and-gully topography or smooth talus slopes.

Avf — **ILD mound flows:** Forms moraines and low energy lobate flows of ILD material possibly driven by freeze-thaw creep.

As — **Landslide material:** Forms chaotic material on chasma floor. Comprised of wall material deposited by multiple landslide events.

Ab — **Slumped Wall Blocks:** Forms large blocks up to 3 km thick of plateau and wall material that has detached into the chasma.

Ac — **Smooth material:** Forms smooth veneer of wasted colluvium over older plateau collapse. Material flows into deepest part of the chasma (8.4 km from chasma rim).

Als — **Landslide scar:** Forms smooth surfaces on the chasma wall.

Hr — **Plateau material:** Undifferentiated volcanic/impact/eolian materials [Tanaka, K.L. 2014] with numerous graben and wrinkle ridges.

Htu/As — **Mixed ILD and landslide debris:** Forms a homogeneous chaotic terrain of Upper ILD and landslide material.

Contact - dashed where inferred.

Scarp

Wrinkle Ridge

Unconformity

Graben

Fault - bar and ball on downthrown side. Dashed where inferred.

5 HiRISE

5 CTX

Strike and dip

Fold Axis

Direction of landslides and mound flows

Mineralogical transition between mono and polyhydrated sulfates. Monohydrated at elevations < 800 m. Polyhydrated > 900 m.

Figure 2.4: Surficial Geologic Map of Hebes Chasma over HRSC DTM.

2.4 Results

2.4.1 Geologic Map

Geologic units include four main groups common among VM maps: ILD, chasma wall, plateau, and mass wasting deposits (Fig. 2.4). The map contains strike and dip measurements as well as mineralogy. Many boundaries are obscured by the late deposition of dust or fine veneer, particularly in the west and northwest areas of the chasma.

2.4.1.1 ILD Units

Differences in layer thickness, layer attitude, erodibility and mineralogy indicate that Hebes contains three distinct ILD units. They are referred to as the Lower, Upper and Late ILD units. Together these units form a deposit over 7.5 km in height.

2.4.1.1.1 Lower ILD (LHtu)

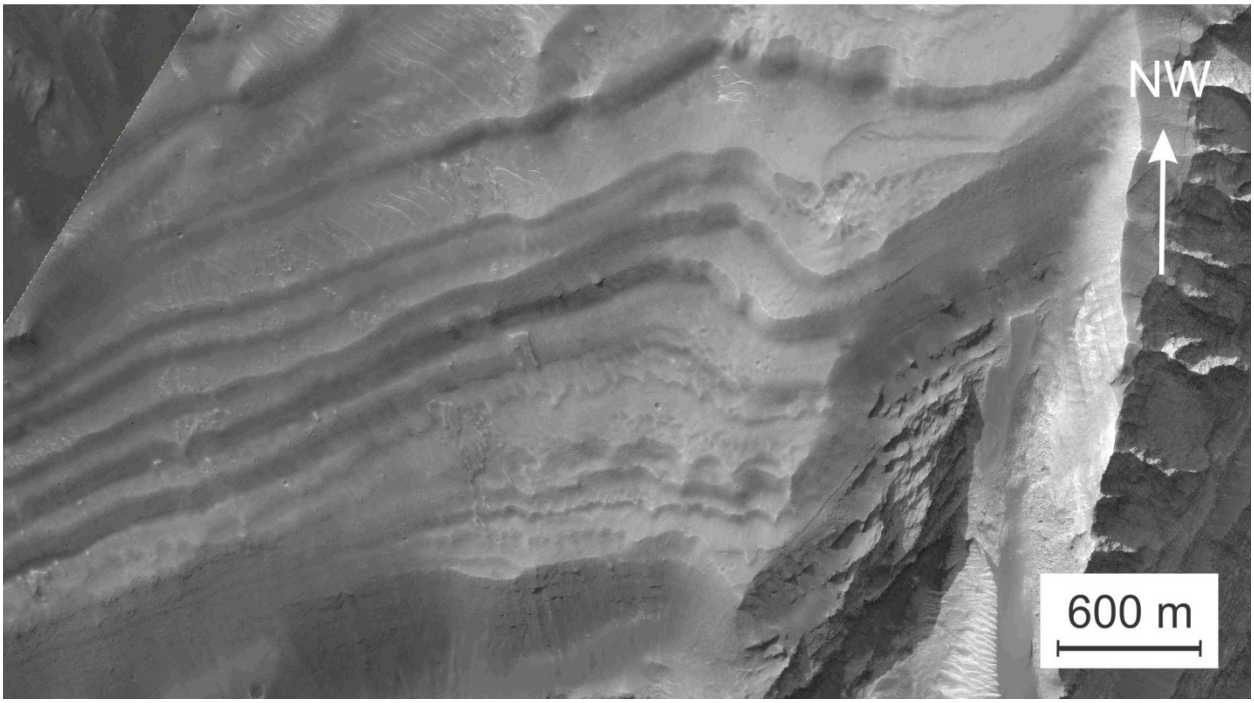

Figure 2.5: HiRISE imagery of layers within the Lower ILD.

The Lower ILD (Fig. 2.5) is observed between elevations from about -3,682 to -1,400 m. It is well exposed in the eastern side of the chasma with approximately 700 km^2 of outcrop

containing mono- and polyhydrated sulfates, gypsum, and phyllosilcates. It also contains a wide range (0.7 to 100.1 m) of layer thicknesses averaging 28 m and includes Hebes' thickest ILD layers. Layers are of uniform thickness laterally and unit boundaries display little deformation, with the exception of several vertical faults and a large eroded valley. Layers are observed in contact with the chasma wall at three locations, dipping toward and away from the wall. Layer dips range from 3˚ to 10˚ and vary in direction throughout the unit. The Lower ILD has an overall darker tone than the other ILD units, but upper elevations provide surfaces that show light tones as well.

2.4.1.1.2 Upper ILD (UHtu)

The Upper ILD (Fig. 2.6) comprises the majority of visible ILD within Hebes and forms the main ILD mound with a total area of roughly 4,500 km^2. It is observed between elevations from about -1,400 to 3,830 m and rests unconformably on top of the Lower ILD. A mineralogical transition from mono to polyhydrated sulfates exists throughout the Upper ILD between 800 -

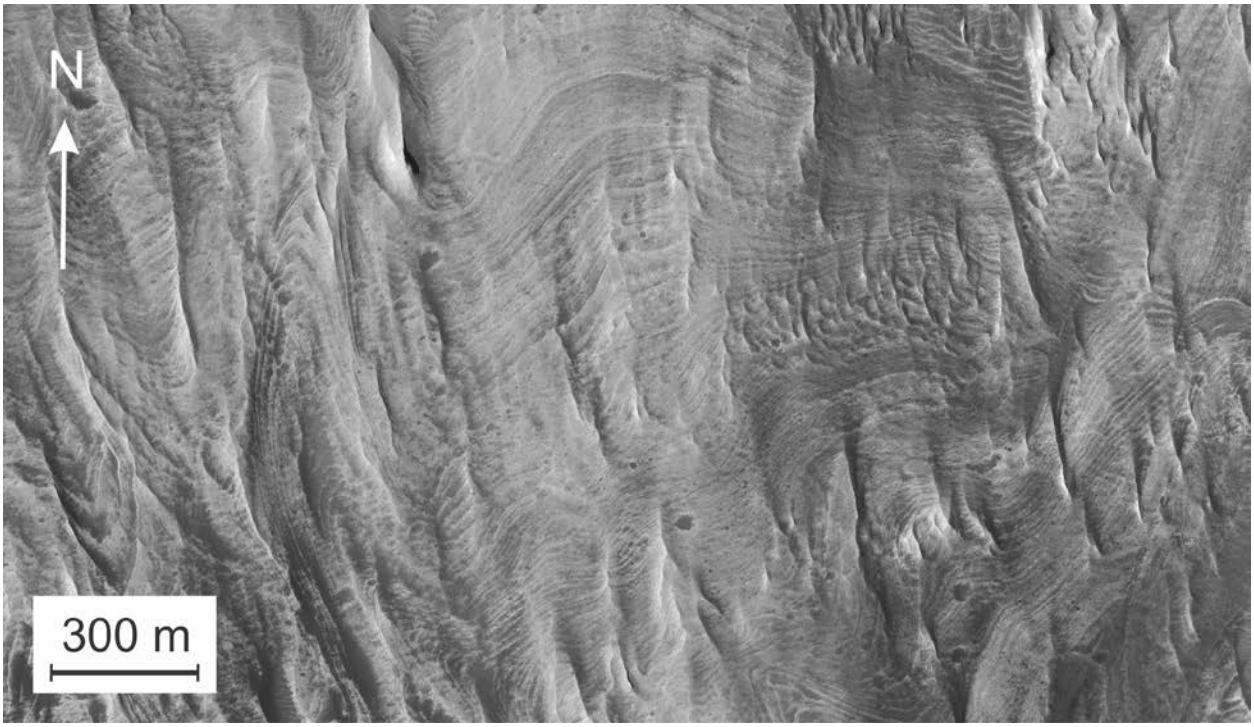

Figure 2.6: HiRISE imagery of layers within the Upper ILD.

900 m of elevation. Monohydrated sulfates are found at elevations < 800 m and polyhydrated sulfates are found at elevations > 900 m. Olivine and pyroxene are common as well. The Upper ILD has an average layer thickness of 2.38 m. Layers are uniform and have attitudes ranging from 3˚ to 11˚that are radial to the center of the mound. Layers are in contact with the chasma wall in two locations, dipping toward and away from the wall. The unit contains yardangs, slump scars and also lobate flows, but relatively little faulting and deformational features compared to Candor Chasma [Birnie, et al., 2009]. Layers alternate dark and light tones, but the unit is generally lighter toned than the other two ILD units.

2.4.1.1.3 Late ILD (LtHtu)

The Late ILD (Fig. 2.7) is confined to the valley between the north chasma wall and Hebes Mensa. It is observed between elevations from about -2,800 to -100 m with over 700 km^2 of exposure. The Late ILD contains both mono- and polyhydrated sulfates. It is a particularly light toned unit with the thinnest average layer thickness in Hebes of less than one meter. It appears to cover areas of Hebes Mensa, but contacts are not well defined. Its surface has numerous layered hummocks, which is a characteristic erosional pattern of the unit.

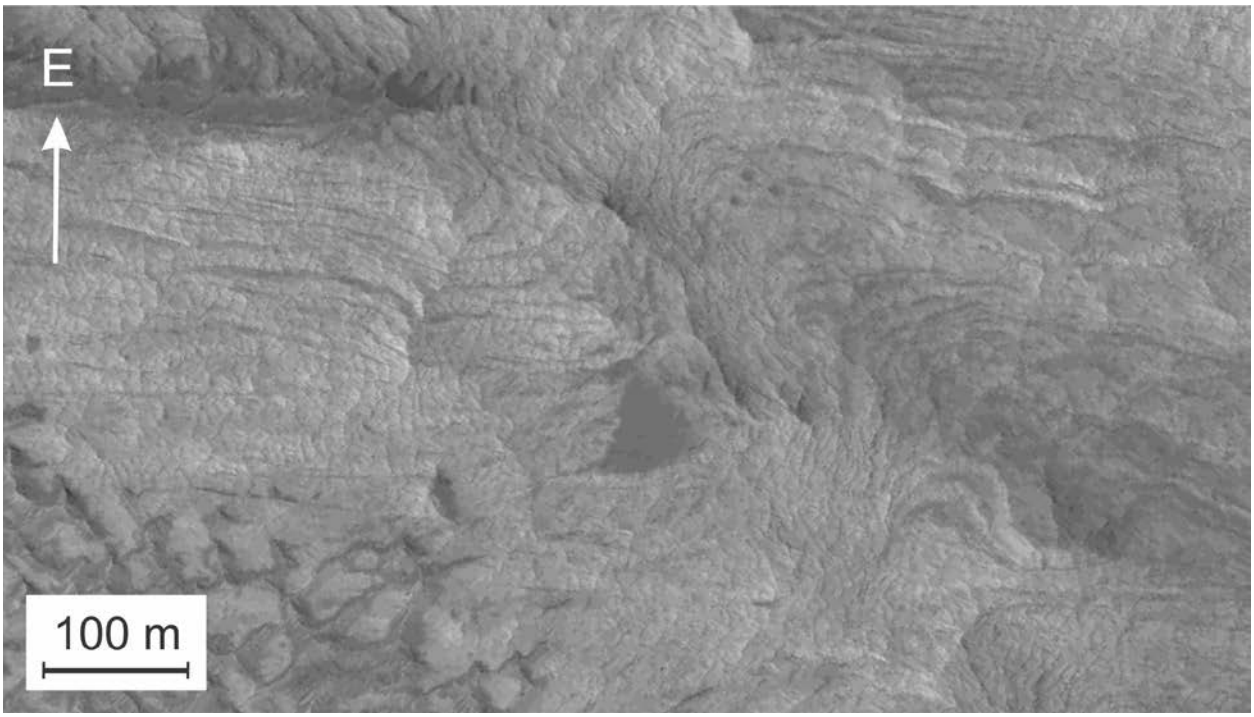

Figure 2.7: HiRISE imagery of layers within the Late ILD.

2.4.1.2 Wall Units (HNw, Ab)

Wall morphology varies from spur and gully to smooth talus. Faults are generally associated with observed grabens and could also be interpreted as half-graben. The upper sections of the chasma wall contain a “plateau-capping unit” (HNwl) observed throughout VM [Lucchitta, 1979; Lucchitta, 1999; McEwen et al., 1999; William et al., 2003]. The cap unit is generally about a kilometer thick although in several areas it can be up to two kilometers thick. Sections of smooth talus form concave indentations and are associated with landslide debris down slope. Spur and gully sections protrude into the chasma. Slumped wall blocks (Ab) observed in the north and east areas of the chasma have dropped over four kilometers from the plateau.

2.4.1.3 Faults, Graben, Wrinkle Ridges, and Scarps

Faults and fault scarps are observed both in and outside of the chasma. In some areas graben are identified by long u-shaped valleys extending from the chasma that are believed to have been produced from preferential weathering by means of groundwater sapping [Sharp and Malin, 1975; Pieri, 1980; Howard et al., 1988]. The western side of Hebes Mensa has undergone significant mass wasting and several parallel faults were observed there as well. Wrinkle ridges are observed in the northeastern area of the plateau. Their expressions are not observed within the chasma wall or floor. One wrinkle ridge visible in the northern plateau was correlated across the chasma to the southern plateau. Landslide scarps and steep cliffs along the edge of a slumped wall block were identified as well.

2.4.1.4 Erosional Features

Erosional features attributed to aeolian, fluvial, and glacial mechanisms were identified throughout the chasma. However the only erosional features represented on the map are mass wasting events such as landslides from the wall and flows from the mound. Landslide debris covers large sections of the chasma floor particularly in the southern valley between the Upper ILD and the chasma wall, as well as the northwestern area of the chasma adjacent to the Lower ILD.

2.4.2 Large scale Geometry of the Central Mound

Hebes Mensa is 120 by 43 km and ranges in elevation from -3,680 m to 3,830 m with the deepest exposure located on its eastern side. The mound's maximum height reaches 3,830 m, ≈ 500 m below the plateau's elevation of ≈ 4,380 m.

The top surface of the ILD mound has a shallow dip of 3° to the north. The northern and southern slopes of the mound have an average inclination of 17° and 27° respectively, making the mounds topography asymmetrical. Yardangs are widespread along the northern slope, but are

scarce along the southern slope. Overall, the northern side of the ILD mound is significantly more weathered (Fig. 2.8a).

Four large erosional features, interpreted as landslide scars (Fig. 2.8b), occur on three sides of the mound. Each landslide scar follows the distinct geometry of a steep slope grading to an almost horizontal shelf which extends several kilometers before the slope steepens again (Fig. 2.8c). Landslide material appears to have been deposited off the mound as units can be traced across the scar boundary immediately below the shelf. The elevation of the shelf varies around the mound, but tends to be higher on the southern side (Fig. 2.8c). To determine the possibility of these shelves being an exhumed bedding surface, points were placed along the upper boundary of each nearly horizontal section of the landslide scars. This placement of points covers an elevation range of 1,960 m for all the shelf surfaces. The best-fit plane through these points has a maximum deviation of only 264.62 m, and an attitude with strike 278.9°±8.5°, dip 4°±2°.

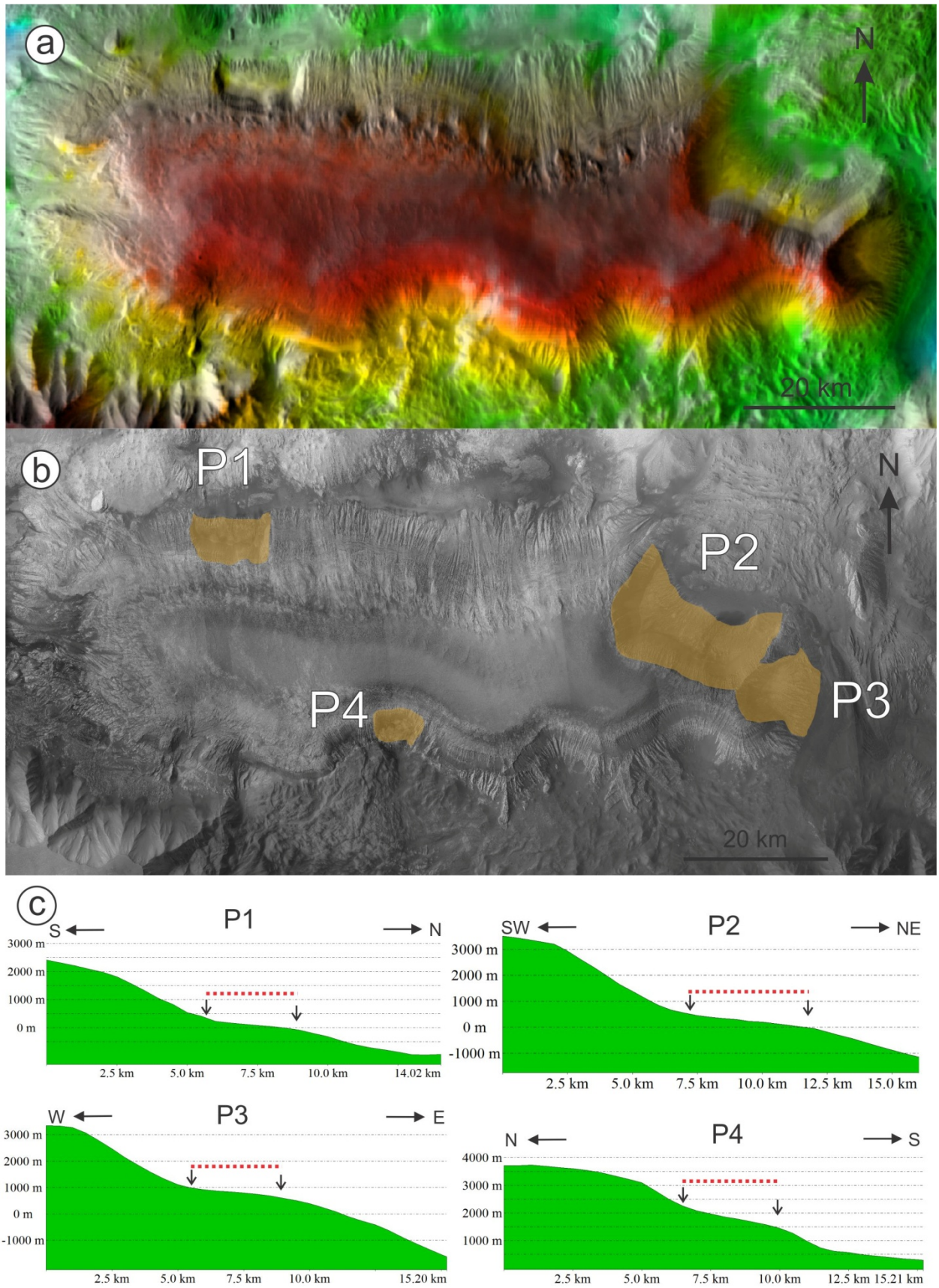

Figure 2.8: Physiography of Hebes Mensa (a) MOLA color over THEMIS imagery showing the weathered northern slope and the relatively smooth southern slope of the ILD mound. (b) Locations of landslide scars P1, P2, P3, and P4. (c) Cross sections of landslide scars P1, P2, P3, and P4 with shelf indicated by dotted red line.

The margins of the chasma and the ILD mound are concentric, leading Peterson (1982) to suggest that the ILD formed during an early stage of chasma formation and that the shape of the mound loosely represents the chasma's extent at the time of deposition. Several indentations within the south side of the mound correlate uniformly with convex shapes within the collapsed material of the chasma's southern wall (Fig. 2.9). These boundaries display a distinct similarity between the mound and chasma.

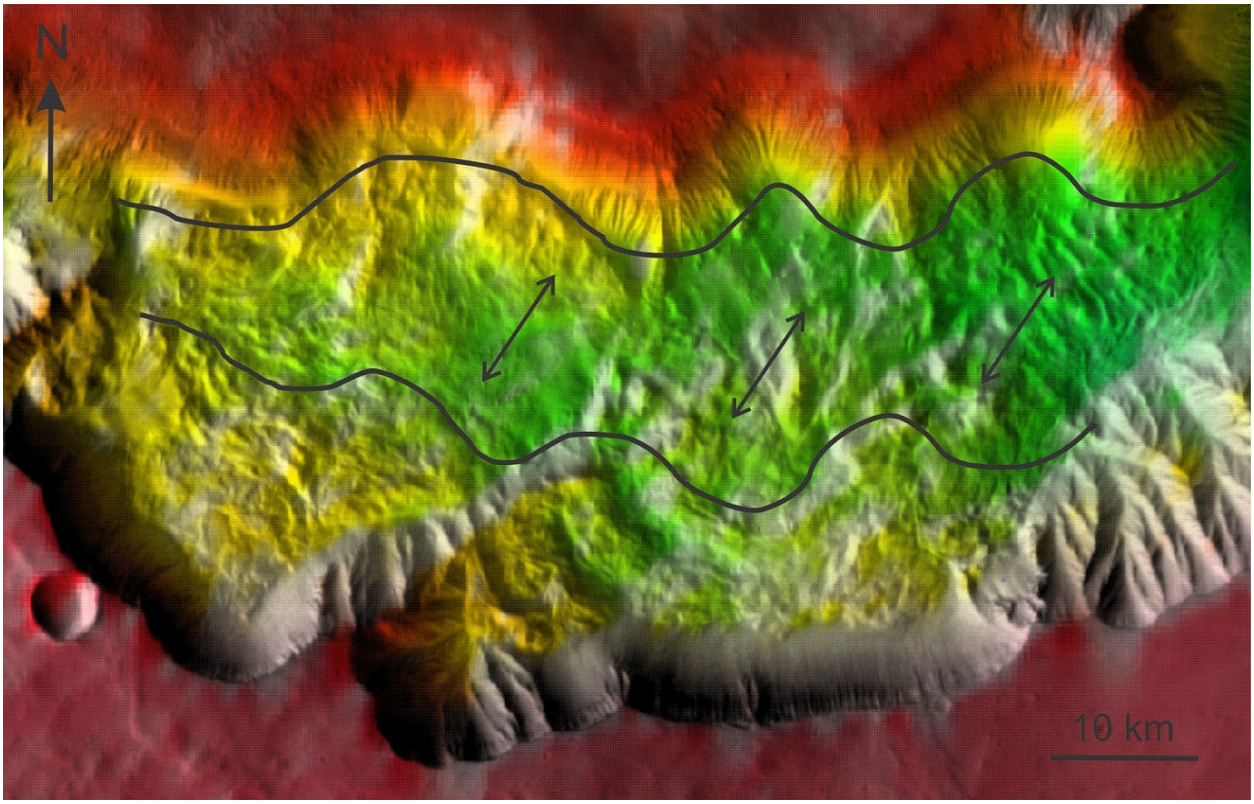

Figure 2.9: MOLA color over THEMIS imagery of the southern area of Hebes Chasma. Arrows indicate scarps within collapsed wall material and areas of the ILD mound that have similar boundary outlines. Their resemblance suggests that the outlines may correlate to each other.

2.4.3 Layering and Layer Attitudes

Layering is laterally persistent throughout the three ILD units. Many layers can be traced for tens of kilometers. Layering is generally thicker at lower elevations and dips were typically less than 10°. Layers often alternate from dark to light tones.

2.4.3.1 Lower ILD Layer Attitudes and Folds

Dip direction varies throughout the Lower ILD. A 1.4 km wide valley cuts through it, but layers can be matched on either side. Layers west of this valley are directly beneath the Upper ILD contact and dip 7-9° E. Layers east of the valley have dips of about 6° NW. Starting from this location along a 38 km long southward transect, layer dip direction changes to 4° SE. Further south, layers steepen slightly to 7° SE before changing dip direction to 6° N. Layers continue to dip north along this transect until their contact with the chasma wall.

These layer attitudes form a 38 km long monoclinal structure within the Lower ILD directly east of the main mound (Fig. 2.11). Exposed layering can be traced through both limbs of the structure. The upper limb spans an elevation of -2.8 to -1.5 km and the lower limb spans an elevation of -3.3 to -2.7 km producing about 1.2 km of structural relief. The fold axes are nearly parallel, with attitudes of the upper and lower hinges at 052°/~2-5° and 063°/~2-5° respectively (Fig. 2.10).

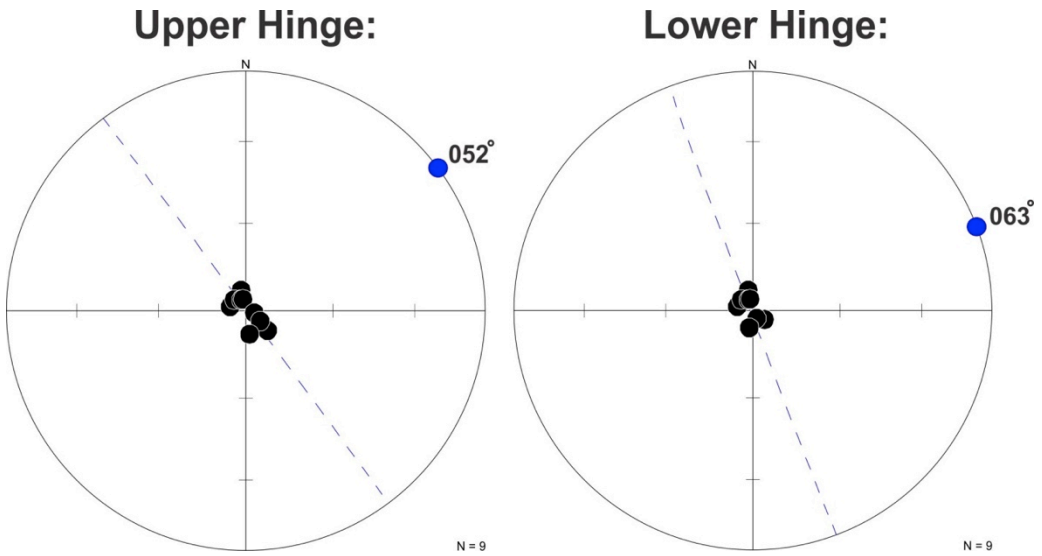

Figure 2.10: Layer attitudes were plotted in lower hemisphere Schmidt projections to determine hinge attitudes. Dashed line marks best fit great circle.

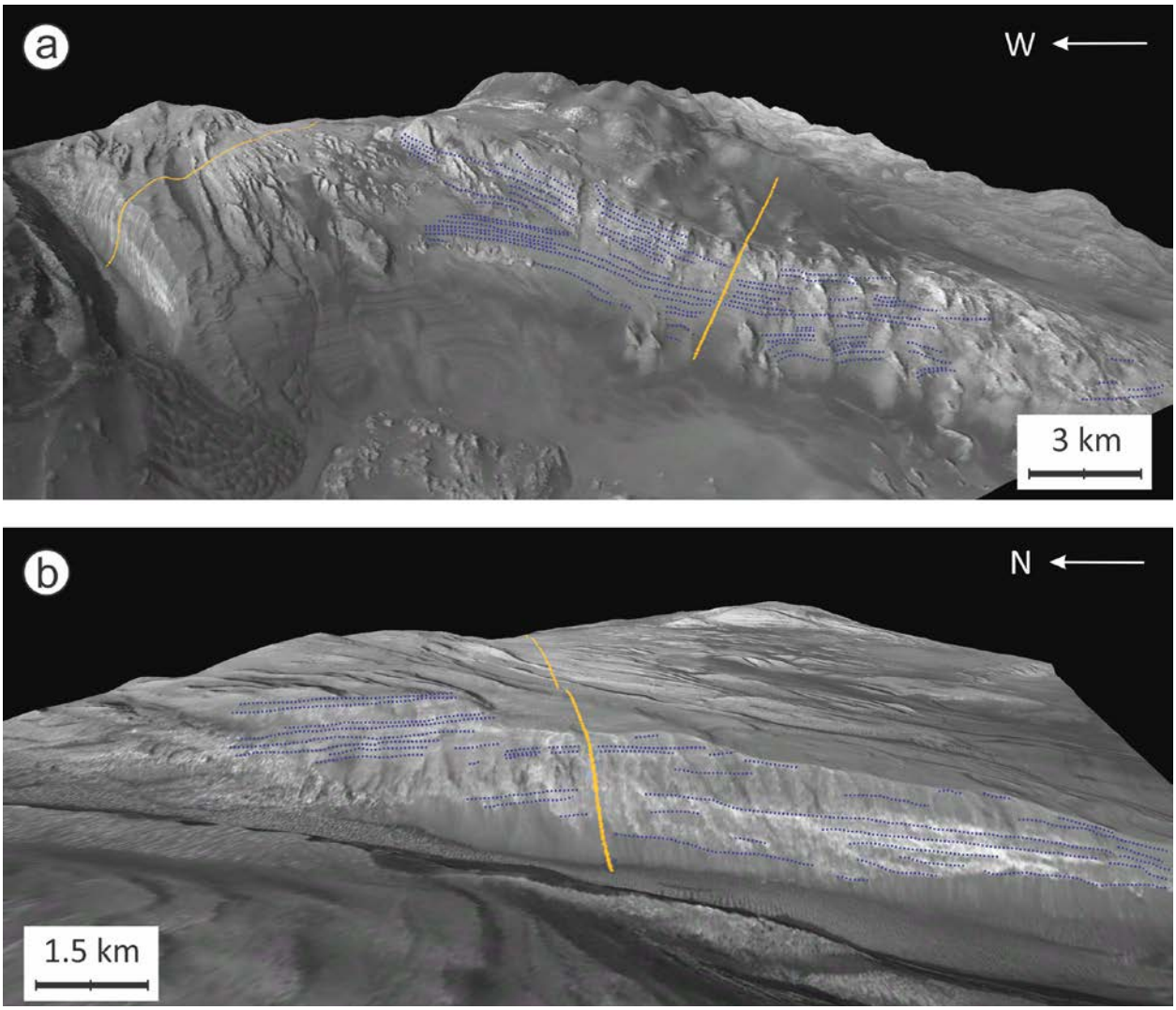

Figure 2.11: 3D views of two broad folds in the Lower ILD, axial traces are in orange and the layering is in blue. (a) 3D view of the upper and lower hinges. (b) 3D view of the upper hinge.

2.4.3.2 Lower and Upper ILD Contact

The contact between the Upper and Lower ILD on the East side of the chasma is readily identifiable in both CTX and HiRISE imagery. It is a horizontal erosional surface at an elevation of approximately -1,400 m. Thick layers in the Lower ILD are truncated by a surface overlain with mottled material from the Upper ILD which grades into finely layered beds (Fig. 2.12a). Layers above the contact dip to the north (Fig. 2.12b) and layers below the contact dip to the east (Fig. 2.12c).

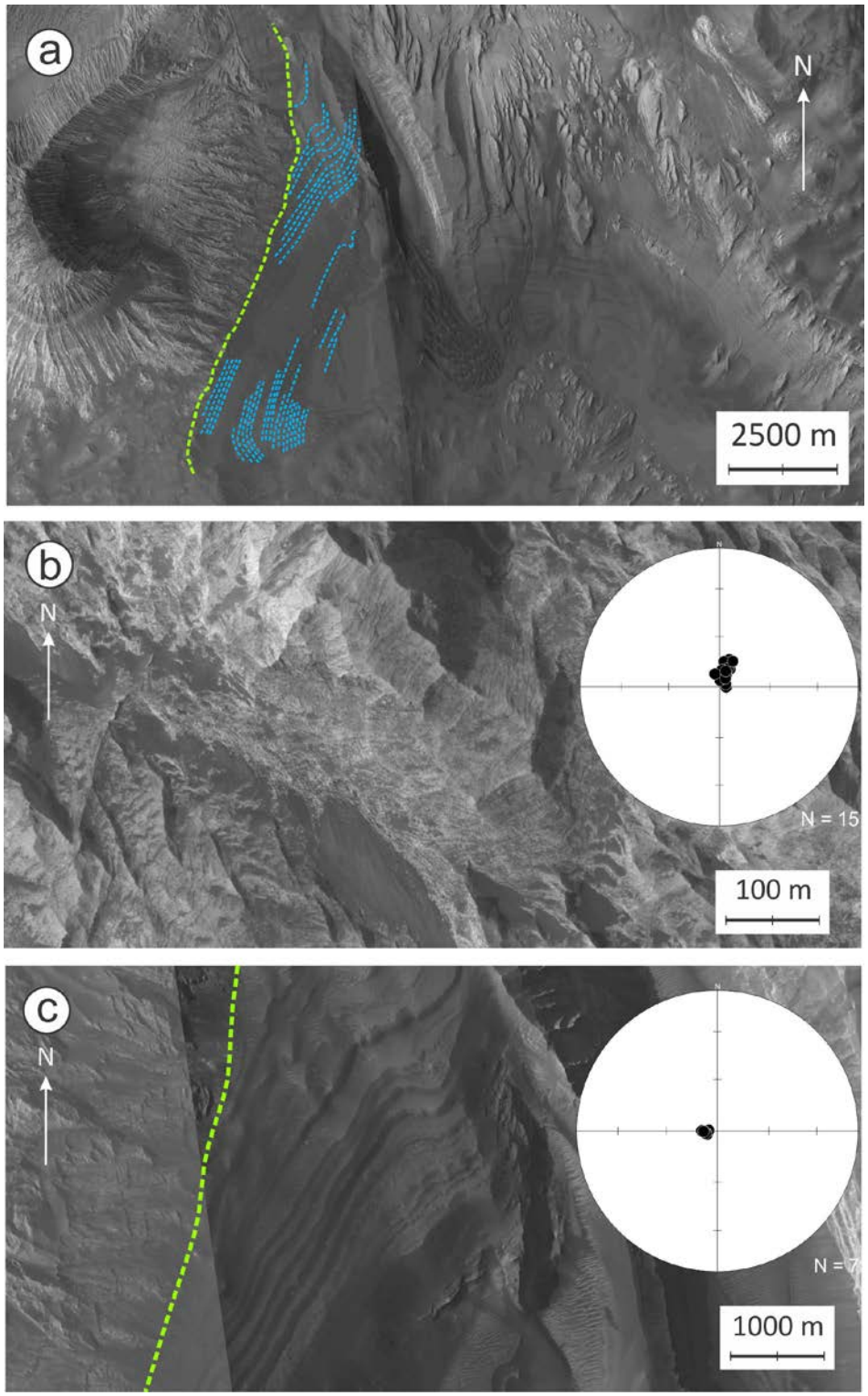

Figure 2.12: The contact between the Upper and Lower ILD. (a) The contact is traced in green with the Upper ILD to the west and Lower ILD to the east. Layers below the contact (blue lines) are seen truncated by material above. (b) HiRISE image PSP_003975_1790 with layer attitudes plotted in lower hemisphere Schmidt projection. (c) CTX image P08_003975_1790 with layer attitudes plotted in lower hemisphere Schmidt projection.

The western extent of the Lower ILD is uncertain. The southern area of the chasma is completely covered by wall debris. The mound's top is relatively smooth and does not indicate that the Lower ILD's boundary is beneath it. Layers observed at the western edge of the mound possibly correlate with the Lower ILD but are in an area lacking HiRISE imagery and CTX topography.

2.4.3.3 Upper and Late ILD Attitudes

Layer attitudes within the mound are generally shallow (<10˚) and dip in the direction of the surface slope (Fig. 2.4). This is consistent with previous measurements in Hebes [Jackson, M.P.A. et al, 2011] and is consistent with observations of ILDs elsewhere in VM [Fueten, F. et al. 2011]. Mt. Sharp, a large layered mound within Gale Crater, also displays these types of radial dips and are often attributed to draping [Kite et al., 2013].

Attitudes in the Late Stage ILD all show consistent dips of approx. 7° N. Eight kilometers south of these measurements, layers observed in the Upper ILD have the same dip (Fig. 2.4). Internally layered hummocks are scattered across the Late ILD's terrain.

2.4.4 Layer Thicknesses

Layer thickness measurements within the 13 HiRISE images cover a significant range of elevations (Fig. 2.3c). HiRISE images H1-H7 of the Upper ILD cover a nearly continuous range of elevations from -1,140 m to 3,680 m (Fig. 2.13). HiRISE images H8-H11 of the Lower ILD cover elevations from -3,302 m to -1,552 m (Fig. 2.13). HiRISE images H12 and H13 of the Late ILD cover elevations from -1,666 m to -738 m (Fig. 2.17).

A total of 901 layer thicknesses measurements were taken along 101 lines parallel to slope. Elevations of measured layers overlap frequently (Fig. 2.13). Lower ILD layers range in

thickness from 100.12 m to 0.76 m with an average of 28.09 m. Upper ILD layers range in thicknesses from 0.13 m to 13.39 m with an average of 2.38 m.

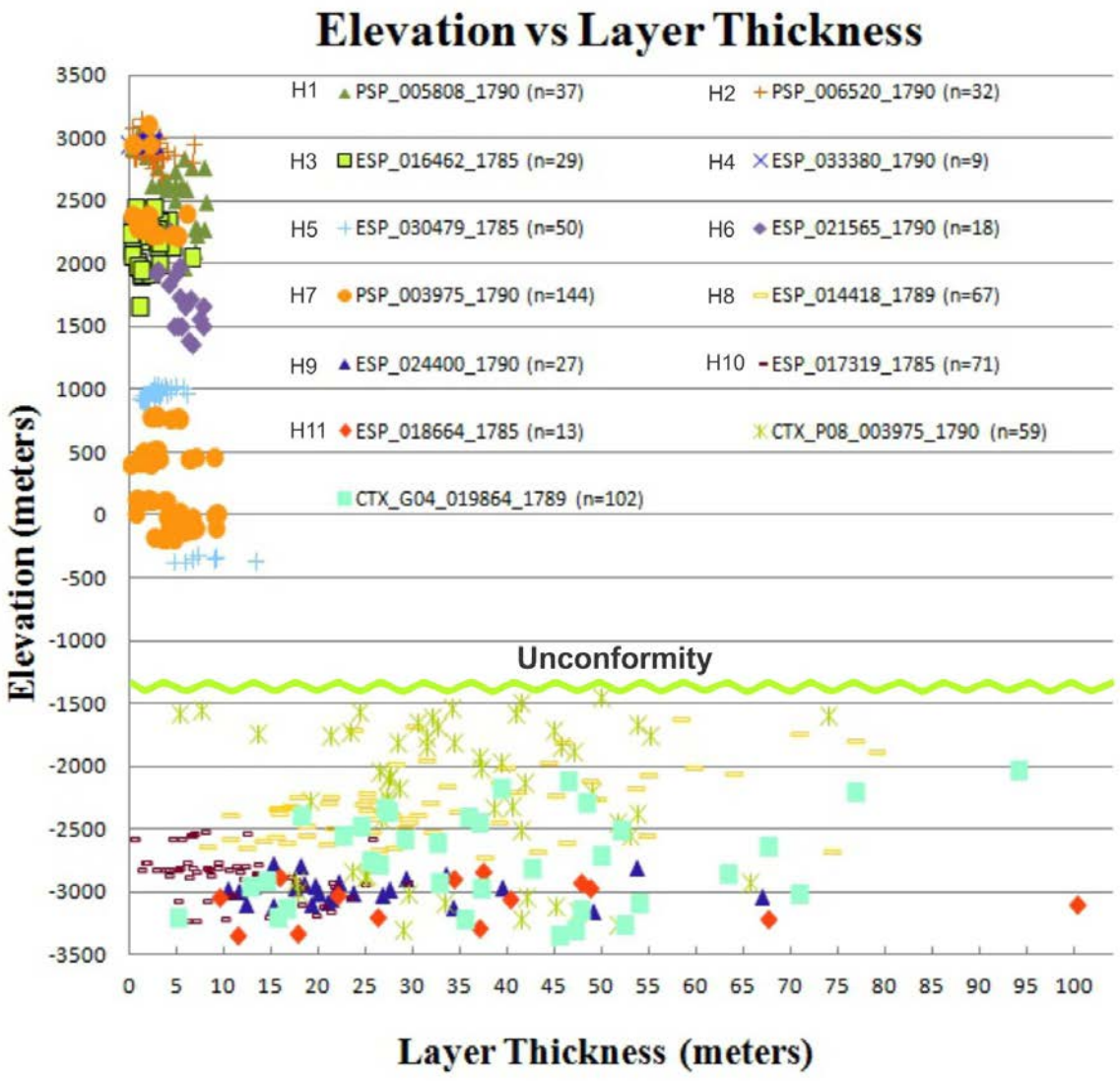

Figure 2.13: Elevation vs. layer thickness of the Upper and Lower ILDs in HiRISE images H1-H11 and CTX images G04_019864_1789 and P08_003975_1790.

Immediately above the unconformity is a 900 m section of the Upper ILD where layering was not observed. However it may contain thin layering that cannot be resolved. Layers are observed again at about -400 m elevation. Several thinning upwards sequences were found in the

Upper ILD (Fig. 2.15). The mineralogical transition between mono and polyhydrated sulfates (discussed in section 2.4.7) occurs in the top half of a thinning upwards sequence and is overlain by a thickening upwards sequence. Within individual HiRISE images, five thinning upwards sequences were identified as well (Fig. 2.13). Measurements within H7 cover the largest elevation range from -186 to 3,120 m and showed an average thickness change from 3.3 to 1.6 m. Measurements within H5 showed an average thickness change from 7.9 to 2.6 m over elevations from -358 to 1,032 m. Measurements within H6 showed a thickness change from 6.5 to 4.2 m over elevations from 1,370 to 2,261 m. Measurements within H1 showed a thickness change from 5.9 to 1.0 m over elevations from 1,965 to 3,039 m. Lastly, Measurements within H2 showed a thickness change from 3.2 to 1.2 m over elevations from 2,715 to 3,152 m.

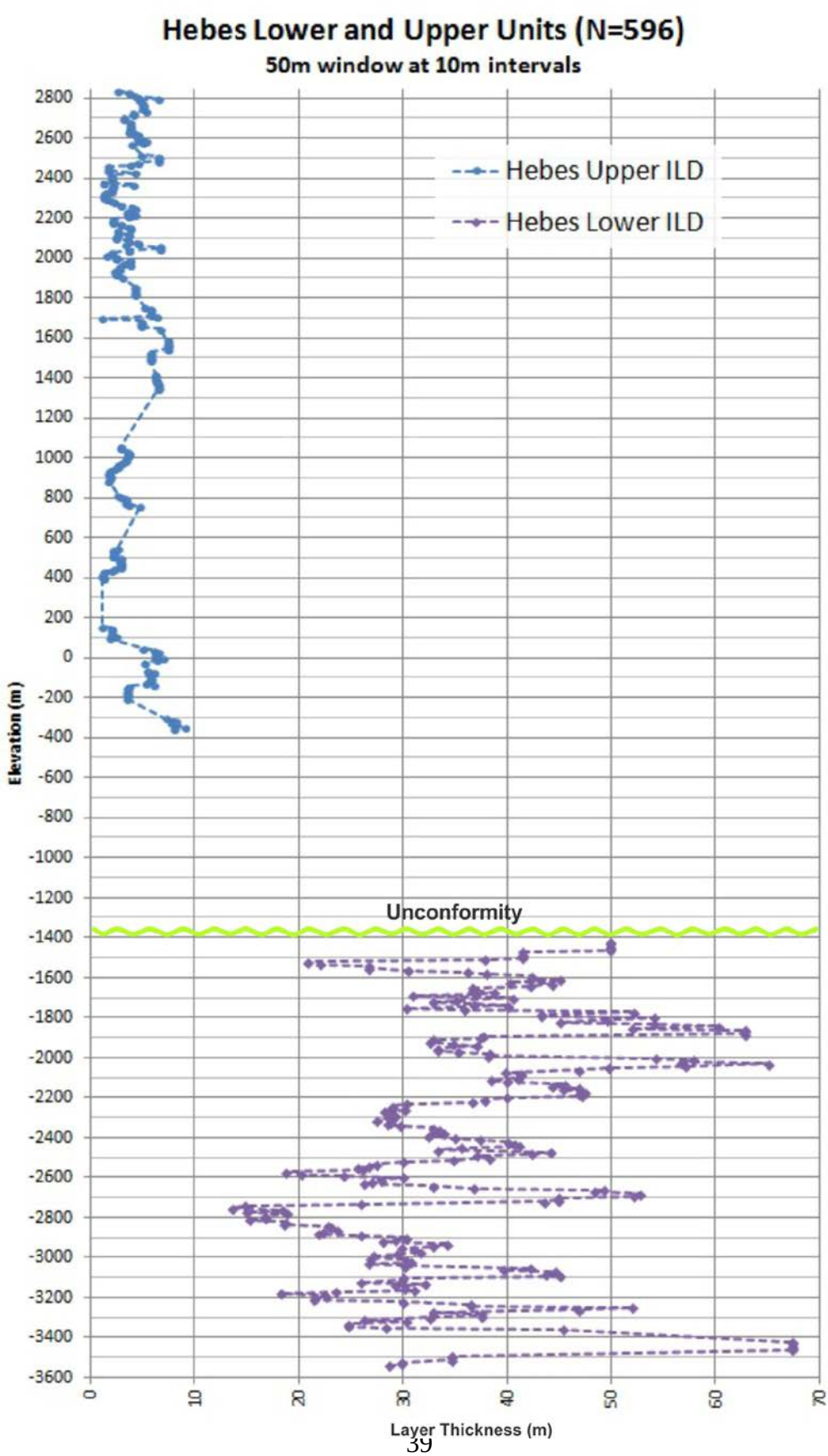

Figure 2.14: Smoothed elevation vs. layer thickness graph of the Upper and Lower ILDs.

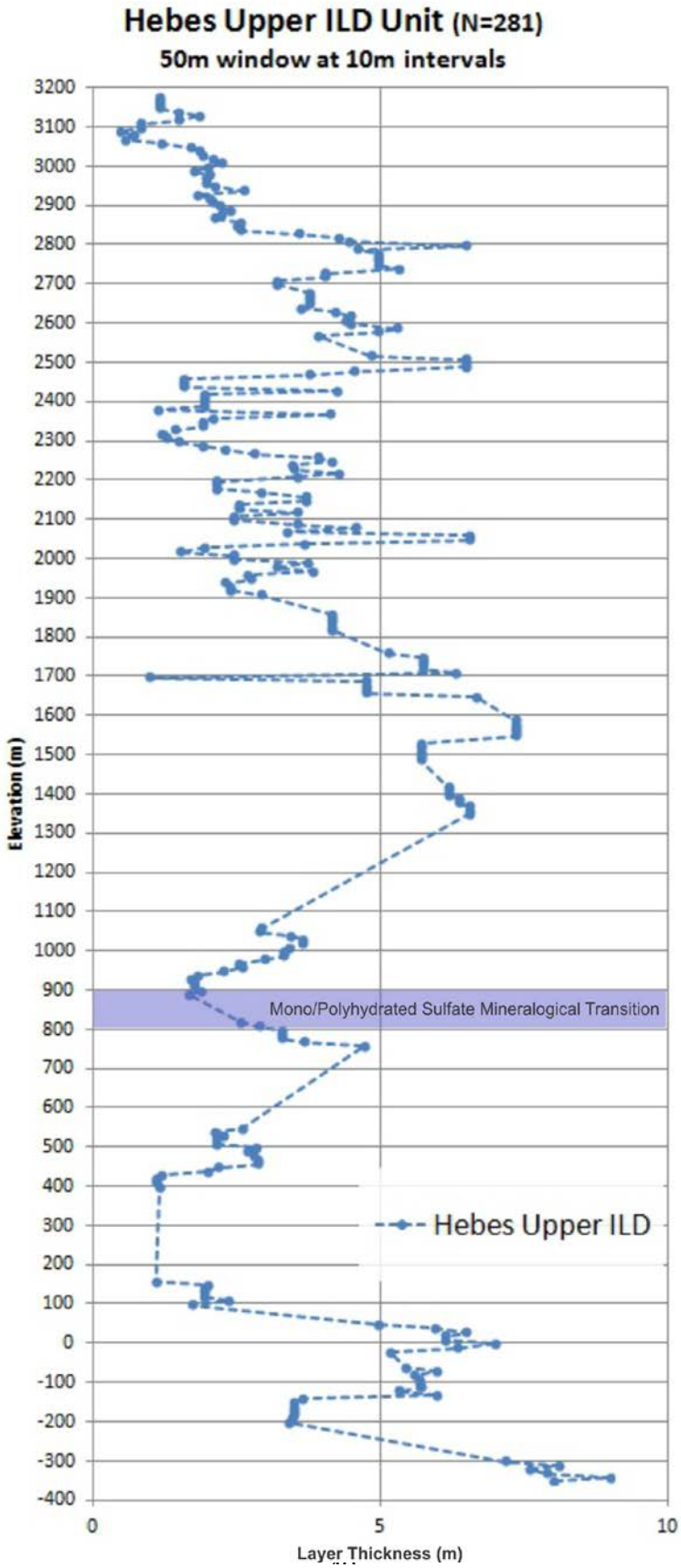

Figure 2.15: Zoomed in elevation vs. layer thickness graph showing only measurements above the unconformity in the Upper ILD. Mineralogical boundary of mono and polyhydrated sulfates has been highlighted in purple. Monohydrated sulfates are below 800m and polyhydrated sulfates are above 900m.

The Lower ILD observed in the western side of Hebes Chasma (Figs. 2.16, 2.17) is in an area lacking HiRISE imagery and CTX topography. Measurements in this area within the Lower ILD were taken using a 50m/pixel HRSC DTM, while measurements in the Upper ILD used 10m/pixel CTX DTMs. Because there is a lack of high-resolution imagery in this area, thin layers may be present that cannot be resolved. Measurements in this area indicate that the Lower ILD has an average layer thickness of 24.17 m (Fig. 2.17). This is similar to the average layer thickness of 28.09 m observed in the eastern side (Fig. 2.13). The Upper ILD basal contact is not as definable on the west side as it is on the east side of the mound. However an upward change in average layer thickness to 6.73 m is observed between -2,000 m and 0 m on the west side. This puts the contact in the same range of elevation as the east side. Measurements above the west contact in the Upper ILD were taken between elevations of -2,640 m and 1,036 m and average 7.7 m in thickness.

Figure 2.16: Approximate outlines of the Upper ILD (orange), Lower ILD (blue), and the Late Stage ILD (green) in the western side of Hebes Chasma.

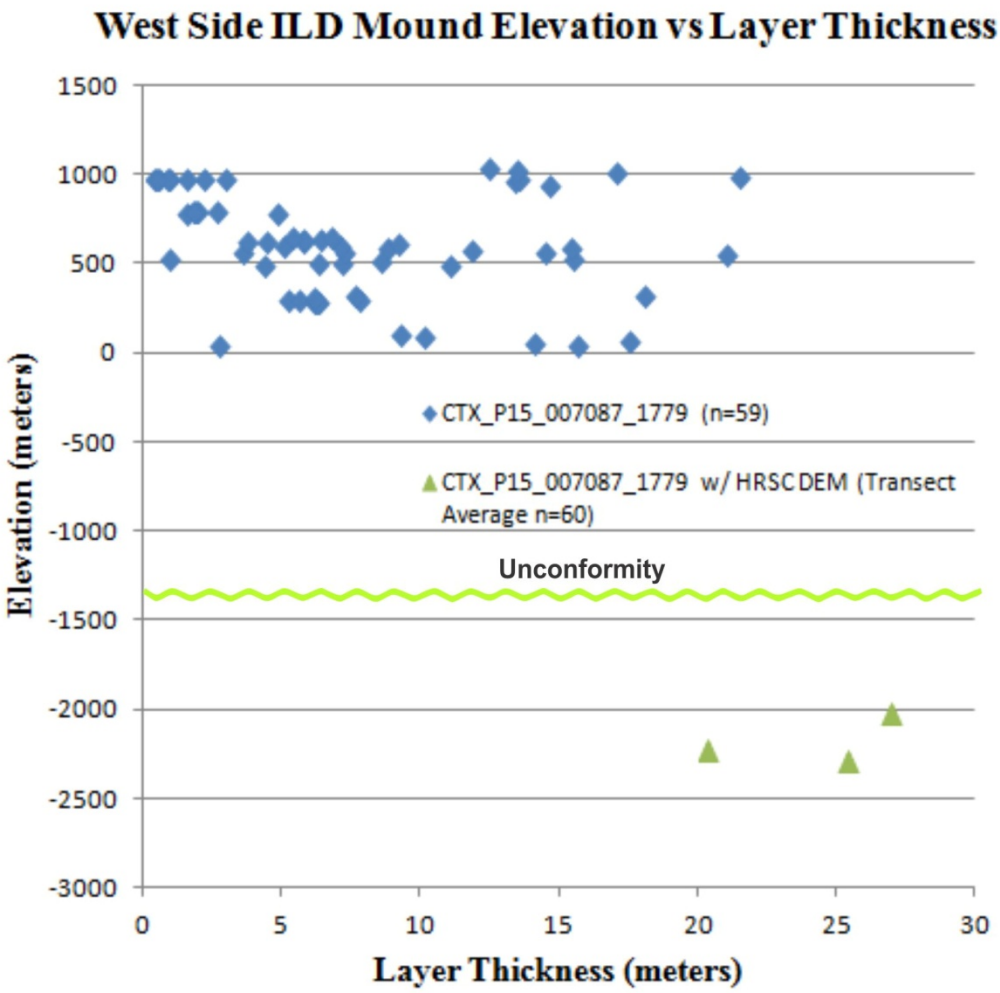

Figure 2.17: Elevation vs. layer thickness of the Upper and Lower ILD along the western side of the mound observed in CTX image P15_007087_1779. The Lower ILD (green) was measured with HRSC DTM and thicknesses were averaged to compensate for the 50m/pixel resolution.

The Late ILD is located between the chasma's north wall and the ILD mound and was measured between elevations of -738 m to -1,666 m (Figs. 2.16, 2.18), which is within the elevation range of the Lower ILD. Layers are significantly thinner than layers within the Upper and Lower ILDs, ranging in thickness from .05 m to 3.62 m with an average of 0.89 m.

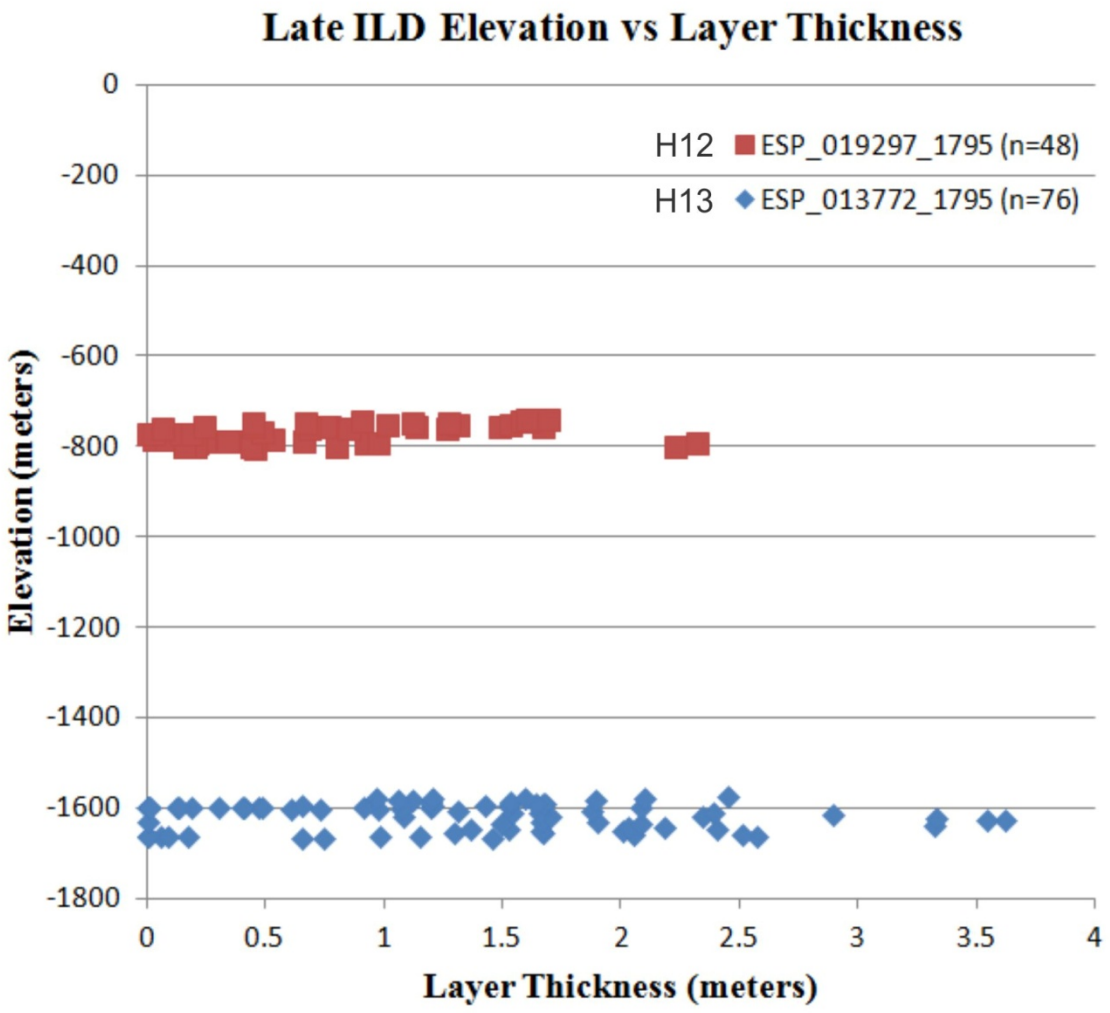

Figure 2.18: Elevation vs. layer thickness of HiRISE images H12 and H13 within the Late Stage ILD (green outline in figure 2.16).

2.4.5 ILD Faulting

Fractures within the ILD are rarely observed, but usually strike parallel to the slope of the mound. Most are isolated such as those depicted on the north slope of the ILD mound (Fig. 2.19a). No orthogonal fracture sets were found, as those documented in the ILDs of western Candor Chasma [Birnie et al., 2012]. Vertical faults were observed in the lower hinge of the Lower ILD monocline (Fig. 2.19b). Vertical offset on these is about 45 m.

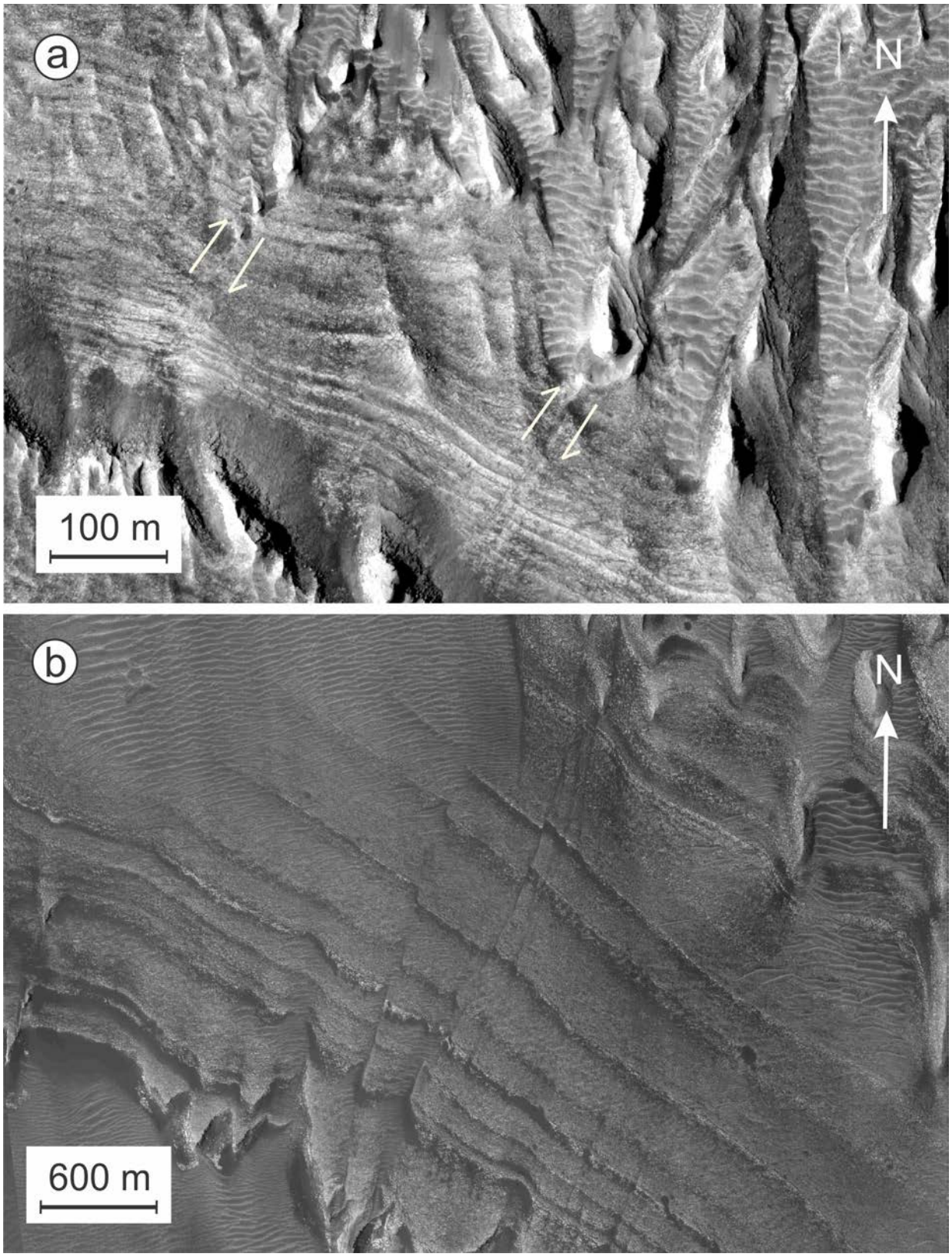
a
N
100 m
b
N
600 m

Figure 2.19: HiRISE imagery of ILD faulting (a) Parallel faults observed in the Upper ILD with several meters of offset. (b) Vertical faults observed in the lower fold hinge of the Lower ILD.

On the western side of the mound, there appears to be a large fault within the Upper ILD (Fig. 2.20) with 700 m of vertical displacement. This area of the mound has undergone significant mass wasting and probably represents an immature slump scar that did completely erode. There is a large area of ILD debris extending over 17 km from the mound. It is 12.2 km wide and over a kilometer high.

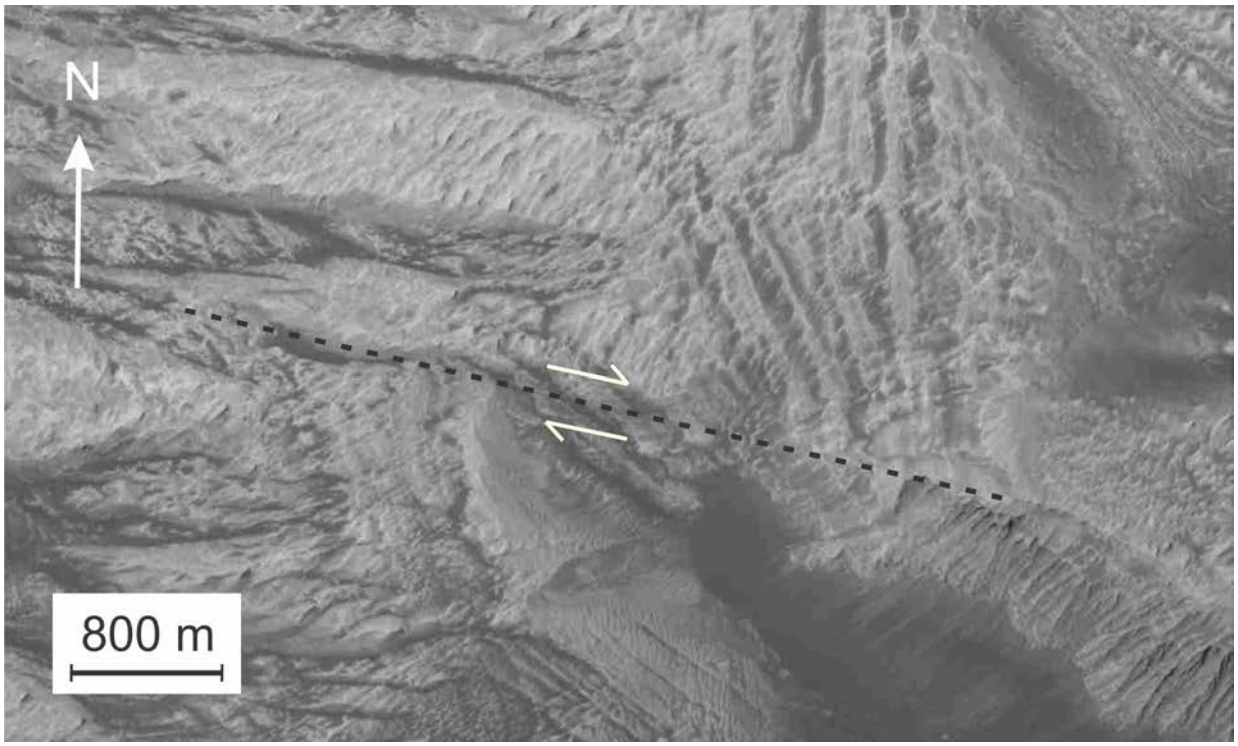

Figure 2.20: CTX imagery of a fault observed in the Upper ILD with 700 m of vertical displacement.

2.4.6 Large Scale Post-Depositional Landforms

A large mass wasting structure measuring over 16 km long and 5 km wide is observed on the northeast side of the ILD mound (Fig. 2.21a). It extends from an elevation of approximately 700 m to -3,500 m terminating against the chasma wall and contains a succession of lobes.

The Late ILD's surface contains abundant hummocks and polygons which are not observed in the Upper and Lower ILD. The hummocks are layered and average 380 m wide and 120 m tall (Fig. 2.21a). The polygons average 8 m in diameter (Fig. 2.21b).

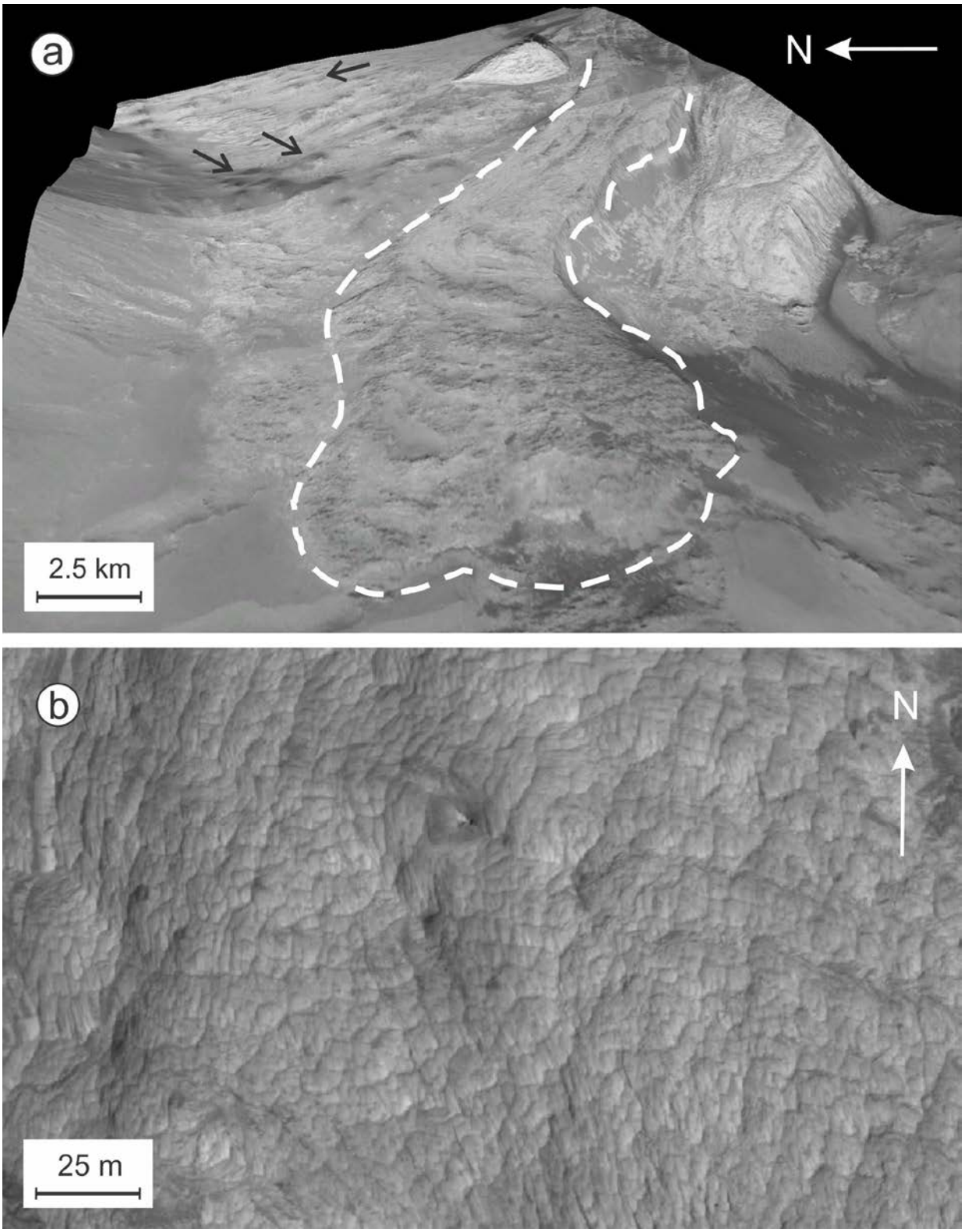

Figure 2.21: (a) CTX imagery of a debris flow protruding from the northwest area of the ILD mound, outlined in white. Hummocky terrain within the Late Stage ILD is seen to the east of the moraine. Arrows indicate several hummocks. (b) Late Stage ILD polygons observed in HiRISE image ESP_019297_1795.

A 1.4 km wide and 15 km long valley, over 800 m deep cuts through the Lower ILD (Fig. 2.22). What is interpreted as an alluvial fan is observed at the southern extent of the valley. Layer attitudes differ on each side of the valley with layers on the westside dipping east and layers on the eastside dipping north and south.

Figure 2.22: A large valley cutting through the Lower ILD directly East of the unconformity.

2.4.7 CRISM Analysis

Analysis of CRISM data shows differing mineral compositions between the Upper and Lower ILD (Fig. 2.23). There appear to be two chemically distinct units within the Upper ILD. Monohydrated sulfates comprise elevations below 800m while polyhydrated sulfates dominate elevations above 900m. There is also a significant amount of olivine, low-calcium pyroxene and high-calcium pyroxene throughout the ILD mound. The composition of the Lower ILD is more complicated. It is rich in monohydrated sulfates, but also contains signatures of Fe:Mg-rich phyllosilicates and gypsum (Fig. 2.24).

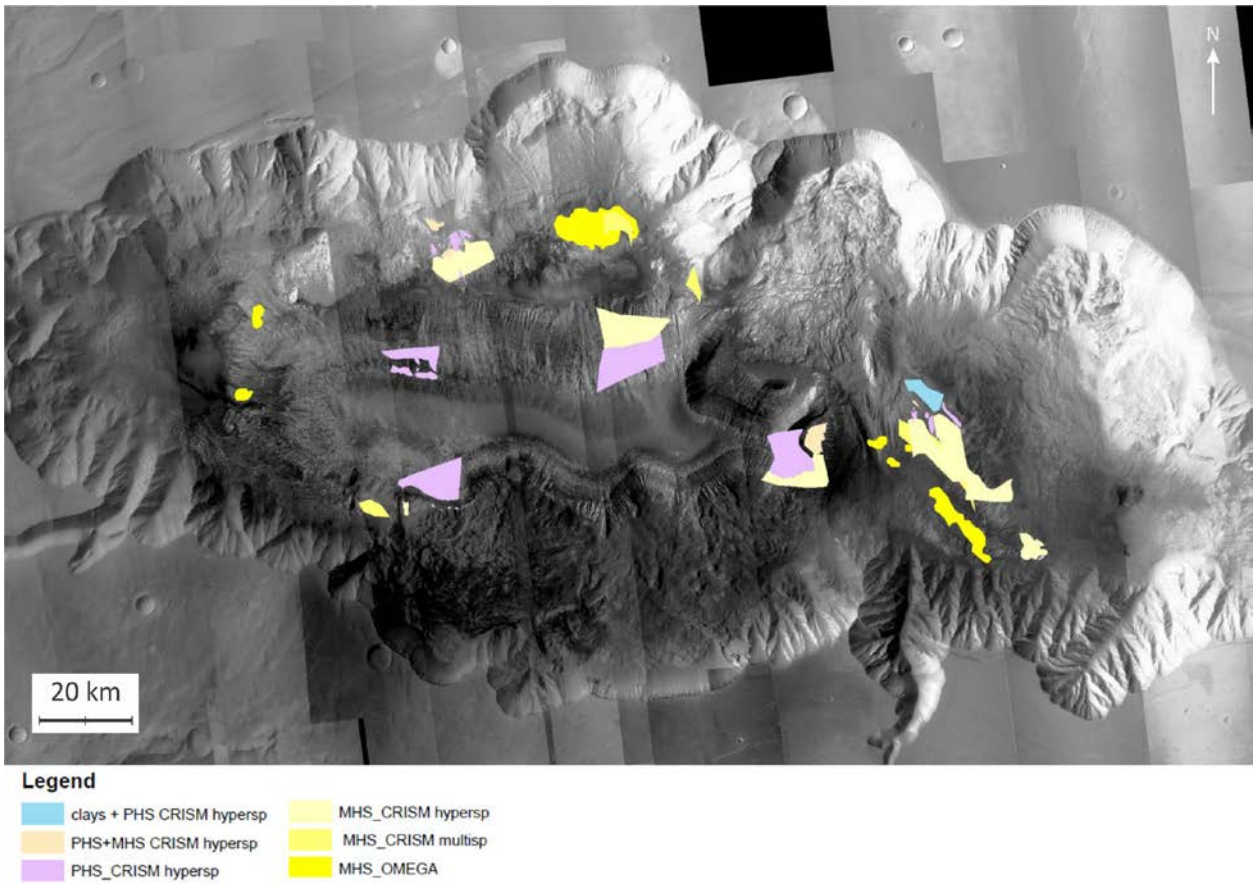

Figure 2.23: Generalized CRISM hyper and multi-spectral analysis of Hebes Chasma indicates clays (light blue), monohydrated sulfates (yellow), and polyhydrated sulfates (dark pink). OMEGA analysis of monohydrated sulfates (bright yellow) included as well [pers. com. Flahaut, 2015].

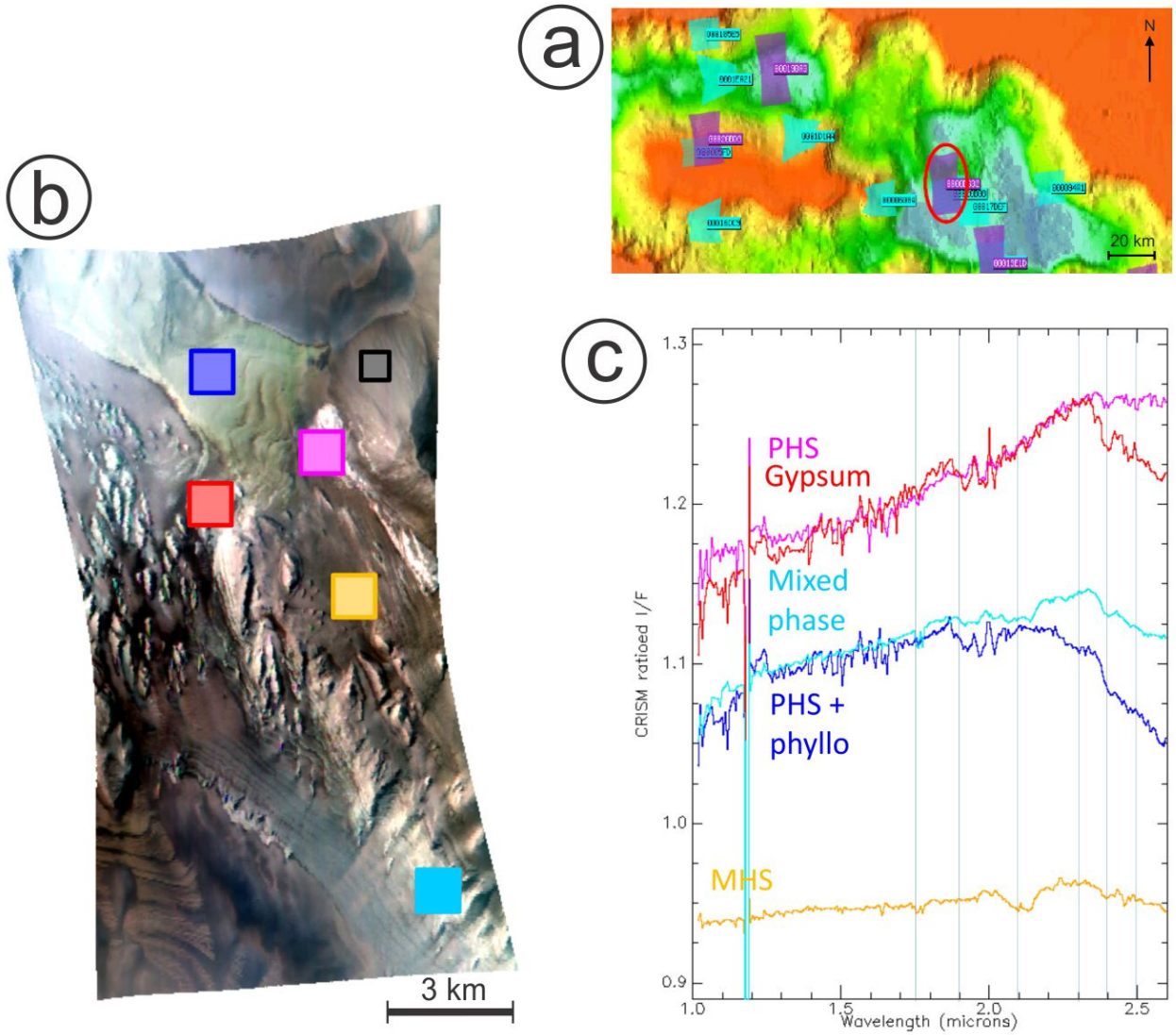

Figure 2.24: CRISM analysis of the Lower ILD. (a) MOLA DTM showing the locations of several CRISM images taken in Hebes, red ellipse locates image b. (b) CRISM image 0000D632 with color coded locations of minerals to correspond to graph c. (c) The ratioed spectra of 0000D632 indicating gypsum, phyllosilicates, and hydrated sulfates [pers. com. Flahaut, 2015].

The Late ILD is similar in composition to the Upper ILD, containing both mono and polyhydrated sulfates. However, it bears no resemblance to the Upper ILD's separation of the two, where monohydrated sulfates are detected at elevations below 800 m and polyhydrated sulfates are seen at elevations above 900 m. Mixed mono and polyhydrated sulfates are observed in the Late Stage at elevations below -1,100 m (Fig. 2.25).

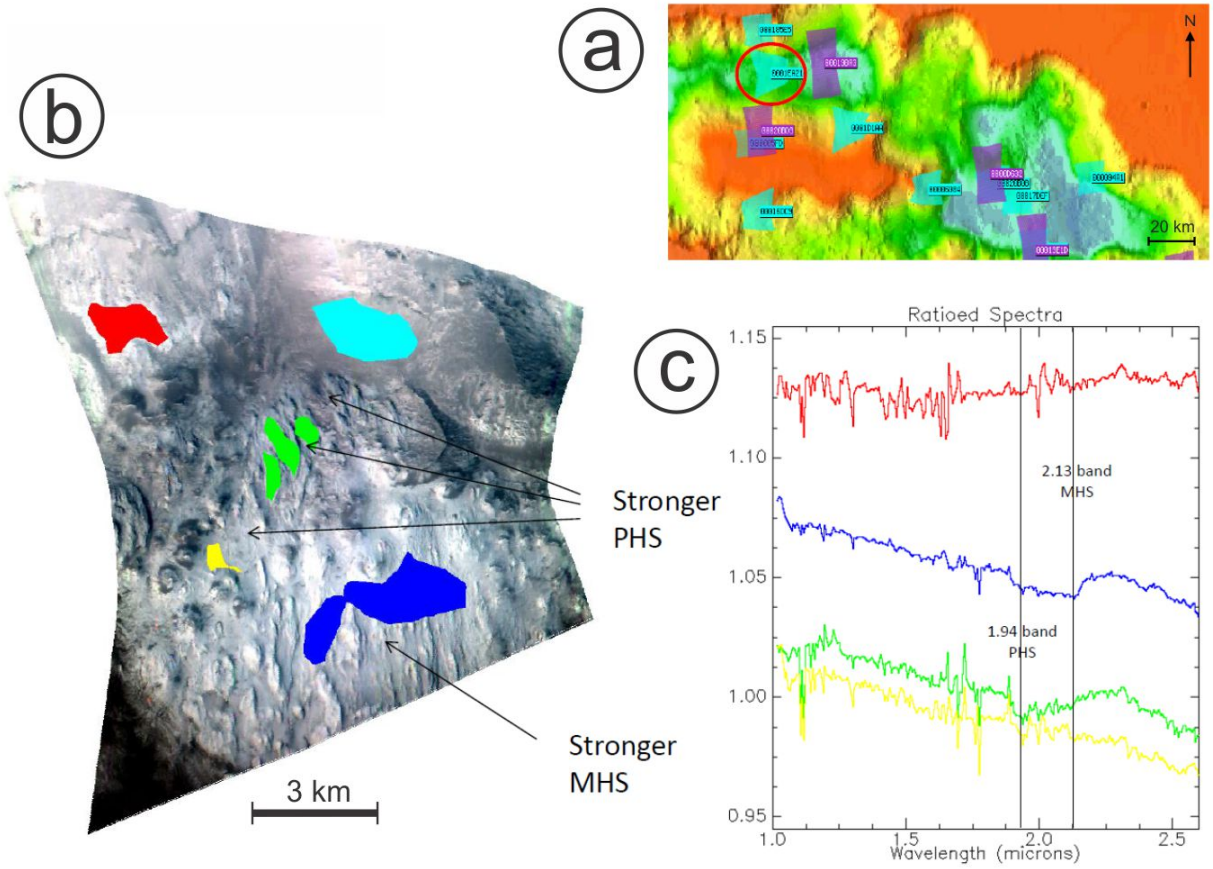

Figure 2.25: CRISM analysis of the Late Stage ILD. (a) MOLA DTM showing the locations of several CRISM images taken in Hebes, red circle locates image b. (b) CRISM image 0001EA21 with color coded locations of minerals to correspond to graph c. (c) The ratioed spectra of 0001EA21 mono- and poly hydrated sulfates [pers. com. Flahaut, 2015]

2.5 Discussion

Mapping, structural analysis and layer measurements have led to the identification of three distinct ILD units that are distinguished on the basis of elevation, extent, layer thickness and attitude, differential weathering, and mineralogy. The Lower and Upper ILD contact is interpreted as an unconformity. Folding, deposition and sulfate formation mechanisms are presented, as well as a brief sequence of the geologic events within Hebes.

2.5.1 Lower ILD Folding Mechanisms

The observed folding in the Lower ILD could have been formed from late faulting beneath the ILD or from draping during deposition over a pre-existing topography. Both mechanisms are ideal, however drape folding is more fitting to the presented observations.

Late faulting beneath the ILD could produce the folding if a fault that was located at one of the fold hinges had vertical offset of 1.2 km. This movement would have been gradual as the layers have not been disturbed by large scale faulting. The only faults observed in the Lower ILD produced 45 m of offset (Fig. 2.19b), however these may have formed from tension within the ILD created from the folding. The faulting could have taken place as late as the Early-Mid Amazonian (1-1.5 Ga) [Head et al., 2001]. This mechanism would presumably have folded the Upper ILD as well, which no evidence for was found.

Drape folding over a pre-existing topography has previously been proposed for the ILD in Hebes Chasma [Hauber et al., 2006] and agrees well with the observations described here. Drape folding is a mechanism that was first proposed to explain monoclines observed in the Colorado Plateau [Stearns, 1978]. Although these monoclines are now considered to be the result of post-depositional thrust faulting [Brown, 1988], the Lower ILD's folds could have formed from air fall material draping over the early chasma floor. Faults on the plateau that may also exist on the chasma floor were examined to determine if they could be related to the Lower ILD fold axes. Several wrinkle ridges were observed in the plateau and strike roughly 5° (Fig. 2.4). Wrinkle ridges are thought to be blind thrust faults caused by stresses associated with the Tharsis bulge [Zuber, 1994; Golombek et al., 1991]. Strikes of 5˚ do not match the fold hinges' trends of 58˚ and 63˚. However, sets of graben striking 60° are observed in the northwest area of the

plateau and make good candidates for the origins of the folds, provided they had enough vertical relief to influence layer attitude during deposition (Fig. 2.26).

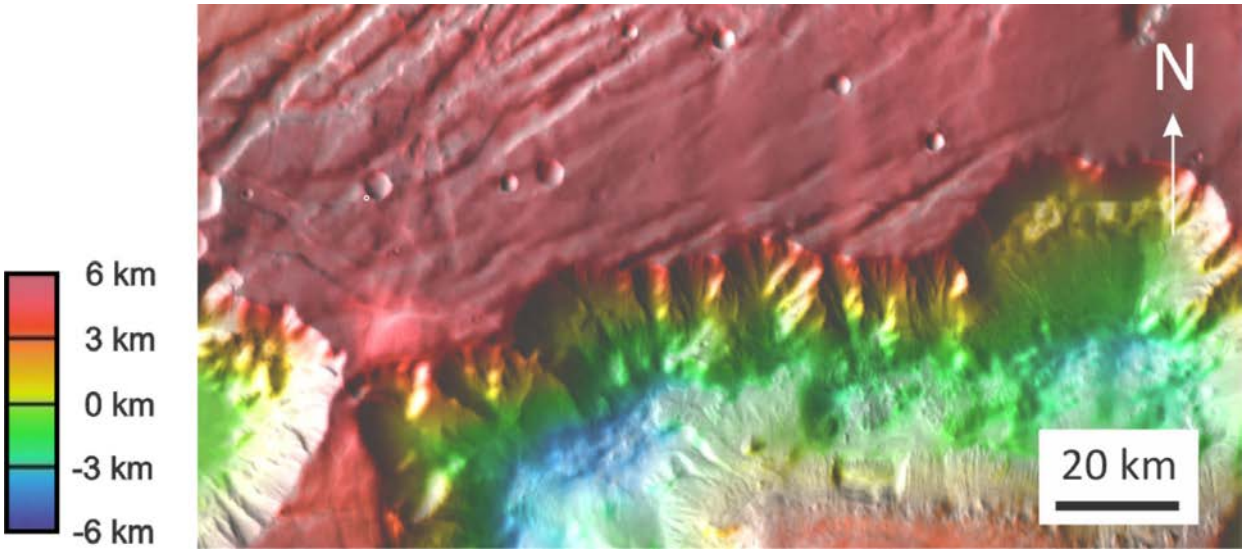

Figure 2.26: MOLA color over THEMIS imagery of the graben plateau northwest of Hebes Chasma. Echus Chasma in the west.

2.5.2 Unconformity

The horizontal contact between the Upper and Lower ILD rests at about -1,400 m. Layers below the contact dip due east and above the contact layers dip to the south. Regionally, layers within the Upper ILD dip outward around the mound with dips < 10˚ while layer attitudes measured in the Lower ILD display more complex attitudes with multiple changes in dip direction. The Lower ILD also displays deformation features including faults and open folds. Layer thickness measurements provide evidence of the existence of the Lower ILD on the mound's west side at approximately the same elevation. Layers of the Upper ILD are relatively uniform and continuous. It is reasonable to assume that the Lower ILD extends west beneath the mound. The mound composed of Upper ILD lacks any features such as ramping or large faults that would indicate significant changes in the topographic expression of the Lower ILD. For

these reasons the contact is interpreted as an unconformity, which indicates an interval of little or no deposition.

2.5.3 Deposition of the ILDs

Given their sizable mafic and sulfur content, draping structure and sheer height, the ILDs are best interpreted as ash fall deposits within shallow standing water, a lacustrine setting or possibly upon intervals of melting or sublimating ice. A groundwater origin for the ILDs does not explain several observations including laterally continuous layering and thinning upwards trends. A groundwater origin for the ILDs also implies the deposition of sulfur-rich sediments on the chasma walls. Although there is evidence of water alteration in the walls of VM, no abundant sulfate material is found [Roach, 2010; Viviano-Beck, 2014]. Thinning upwards sequences within the layers of the Upper ILD may indicate eruptions of differing intensity and duration. Layers alternating between dark and light tones may also represent periodic volcanic eruptions within varying levels of water and/or melting ice.

There is evidence that during the Noachian abundant water was present on the surface of Mars [Baker, 2006; Williams, 2001; Harrison, 2005] as well as liquid precipitation in mid-latitudes [Pollack, 1987; Hynek, 2003]. Water within the chasma prior to the ILDs' deposition could have entered Hebes Chasma in a variety of ways including surface runoff [Lucchitta, 2010], ground ice [Sharp, 1973], or the burial of aquifers during the formation of the Tharsis Bulge [Andrews-Hanna, 2007].

Hydrated minerals are either syndepositional or post-depositional, forming from either ash fall into water and immediately becoming hydrated or from a fluctuating groundwater table that altered sulfur-rich ILDs and repeated evaporitic sequences. If groundwater was the source of

sulfur then sulfur material would be observed more often on the chasma walls. Acid rain does not explain the ILD mound's thickness and hydrothermalism would form a heterogeneous distribution of the sulfates which is not observed in Hebes. A mineralogical transition exists within the Upper ILD at an elevation between 800-900 m; below 800 m are monohydrated sulfates and above 900 m are polyhydrated sulfates. Similar boundaries between mono- and polyhydrated sections of ILD have been detected elsewhere in VM [Quantin et al., 2005; Bishop et al., 2009; Murchie et al., 2009; Fueten et al., 2014]. This boundary indicates the lower section of the Upper ILD is more competent and/or resistant and the upper section is porous and became more saturated. Four large landslide scars formed close to this boundary because the lower monohydrated section is more competent and forms a slip surface for the upper polyhydrated section to slide upon. Sulfates are likely a large part of the composition of the ILDs and not merely a vaneer because they are only detected in association with the ILDs and not on other surfaces like the chasma wall [Gendrin et al., 2005]. They are also detected on the landslide scars that expose internal portions of the mound. This suggests Hebes Mensa may have been completely water saturated after ILD formation.

Layering was not observed in a 900 m section of the Upper ILD immediately above the unconformity. This implies deposition was continuous for the first 900 m above the unconformity or that the scale of layering is below the resolution of the orbital images. Deposition of this section may have been rapid and constant in a low energy lacustrine condition, or possibly as the result of the melting of a frozen lake that had accumulated a thick deposit of sediment [Lucchitta, 1994; Fueten et al., 2014].

The layer attitudes within the Late ILD most likely represent draping upon Upper ILD's slope. Layer attitudes within the Late ILD are approx. 7˚ N, the same layer attitudes seen in the

adjacent area of the Upper ILD. Although the contact between the Upper and Late ILD is not easily identifiable, layer thickness and overall appearance (tone and morphology) of the Late ILD differs significantly from the Upper and Lower ILD. The Late ILD also does not have the mineralogical boundary detected in the Upper ILD, although it is located within the elevation range.

Periodic glacial activity may have been present during ILD deposition [Le Deit, 2010; Mege, 2011; Gourronc, 2014]. Glaciers could have formed the thinly layered hummocks of the Late ILD, although it is unclear whether they are depositional or erosional features. The Late ILD is confined to the area between the chasma wall and the ILD mound, a regional low where ice would be prone to develop. The layered hummocks could have been deposited by receding ice or formed from the erosion of a flooding event that also produced the large valley cutting through the Lower ILD (Fig. 2.18). Differing layer attitudes on each side of the valley may mean that it is a fault that preferentially eroded in response to large influxes of melt water.

A possible sequence of depositional events within Hebes Chasma involves initial ash fall to deposit the 2.2 km thick Lower ILD within a proto-chasma that contained standing water or ice, followed by an interval of little or no deposition. Ash fall then deposited the 5.2 km thick Upper ILD on top of the Lower ILD followed by collapse of the northern wall to its current extent. Collapse of the northern wall led to longer exposure of the mound's north side which in turn created the shallower slope and weathered surface. Areas of the southern and eastern walls may have collapsed slightly as well. The Late ILD was then deposited within the valleys between areas of pre-existing ILD and chasma wall, either by glaciers or ash fall. After deposition of the Late ILD, the southern and eastern sides of the chasma collapsed to their present extent. Some of this collapsed wall material may be covering Late ILD. Hydrated sulfates and gypsum formed by

alteration of the ILD from a combination of changing chemical conditions within the chasma and differing ILD composition. Given that hydrated sulfates require liquid water to form, the environment within Hebes during this time was relatively warm and wet. Hydrated mineral formation eventually ceased as the changes in climate no longer supported liquid water at the surface. During this time, large amounts of ice were present in the chasma, producing the observed glacial morphology. Gypsum localized to the eastern outcrop of the Lower ILD could have formed hydrothermally from beneath the chasma or during a period of evaporation and may have been formed before or after deposition of the Upper ILD.

At present there is no good explanation for the lack of Upper ILD in the eastern side of the chasma, where the folded Lower ILD resides. It is presumed the mound would extend to the eastern extent of the early chasma, as the Lower ILD does. Instead the mound ends abruptly and the Lower ILD continues for another 44 km.

2.6 Conclusions

The structure, stratigraphy and geomorphology of both Hebes Chasma and the ILDs it contains were studied using orbiter imagery and topographical data from HiRISE, CTX and HRSC cameras. CRISM hyperspectral observations further constrained past conditions within Hebes by verifying the ILD's mineralogy. Measuring layer attitudes and thicknesses revealed complex structures and three distinct units of ILD. Using these data in combination with general observations and known geological processes on Earth, the geologic history of Hebes Chasma can be described.

The Lower ILD exists in the lowest elevations of the chasma and contains the thickest average layering. Large-scale folding, hydrated sulfates, gypsum and clays were identified as well. An unconformity separates the Upper and Lower ILDs. Immediately above the

unconformity is a 900 m section of Upper ILD that contains no observable layering. Layering above this section is relatively thin and several thinning upwards sequences were observed. Hydrated sulfates and mafic minerals were detected including a horizontal boundary between mono and polyhydrated sulfates at an elevation between 800-900 m. This boundary also appears to be an erosional surface that is exposed at four landslide scars around the main mound. The Late ILD is contained to the valley between the main mound and the chasma's north wall. It possesses the chasma's thinnest average layers, and post depositional features include layered hummocks and polygons. Mono- and polyhydrated sulfates were detected in the Late ILD, however no boundary was found that corresponded to the mono/polyhydrated sulfate transition in the Upper ILD.

A hypothesis that explains all observations is proposed for the deposition of the ILDs. This hypothesis describes a complicated, multiple episodic, depositional regime that was influenced by variations in Martian climate and periodic ash fall from Tharsis related volcanic eruptions. The Lower ILD was deposited by ash fall within a proto-chasma that contained standing water or ice. After an interval of little or no deposition, ash fall deposited the Upper ILD, which was followed by further collapse of the chasma's walls. The Late ILD was deposited between the main mound and the chasma's north wall by ash fall or possibly by glaciers. Alteration of the ILDs produced the hydrated sulfates and gypsum, implying wet conditions within the chasma after ILD formation. Glacial morphology in the Late ILD implies colder periods and large amounts of ice within the chasma.

Future work involves further CRISM analysis, HiRISE coverage, and cleaner CTX topographical data. Present CTX DTMs can be noisy and missing entire sections of data, particularly on the westside of the chasma. The unconformity on the mound's western side is not

represented well with HRSC topography and could be better constrained with CTX or HiRISE DTMs. A systematic comparison of all layer thicknesses of VM and crater ILDs may reveal regional trends and further constrain ILD origin hypotheses.

Chapter 3: Perimeter Faults and Slump Blocks of Hebes Chasma, Mars: The dynamics of wall collapse and the relationship with ILD deposition

3.1 Introduction

The formation of Valles Marineris (VM) is thought to be the result of lithospheric stresses brought on by the formation of the Tharsis Bulge followed by collapse [Mege and Masson, 1996; Andrews-Hanna 2012] in the Late Noachian or Early Hesperian [Tanaka, 1997; Schultz, 1998; Okubo et al., 2008]. A system of early basins were eventually joined [Lucchitta, 1994] by the Early Hesperian [Schultz, 1998] creating the 4,000 km long, 200 km wide and 7-8 km deep structure that exists today. Chasma formation has previously been explained by loss of volume from melting of subsurface ice [Sharp, 1973], karst processes [Jackson et al., 2011], dyke intrusion [Mckenzie and Nimmo, 1999], and isostasy [Andrews-Hanna, 2012].

Hebes Chasma is the northernmost extent of VM residing on the edge of the Tharsis and Lunae Planum boundary. It is an isolated chasma with no outwash channel, distinguishing it from other chasmata in VM. This provides an ideal location to study the collapse formation processes of chasmata because the chasma perimeter is intact and the ILDs within are largely undisturbed. Within Hebes Chasma is a large 163 by 42 km ILD mound. The mound is nearly 8 km high, reaching elevations to within 200-300 m of the height of the surrounding plateau. The mound has uniform layering and contains an abundance of hydrous minerals including mono- and polyhydrated sulfates, gypsum and phyllosilicates.

This study interprets the mechanics of collapse of Hebes Chasma by examining perimeter cross-faults that vertically displace sections of the plateau and their relationship to slump blocks, landslides and other structures produced from mass wasting of the chasma wall. Contacts between ILDs and the chasma wall were examined to better understand the relationship between ILD and basin collapse, as well as constrain the timing of the formation of differing wall morphology.

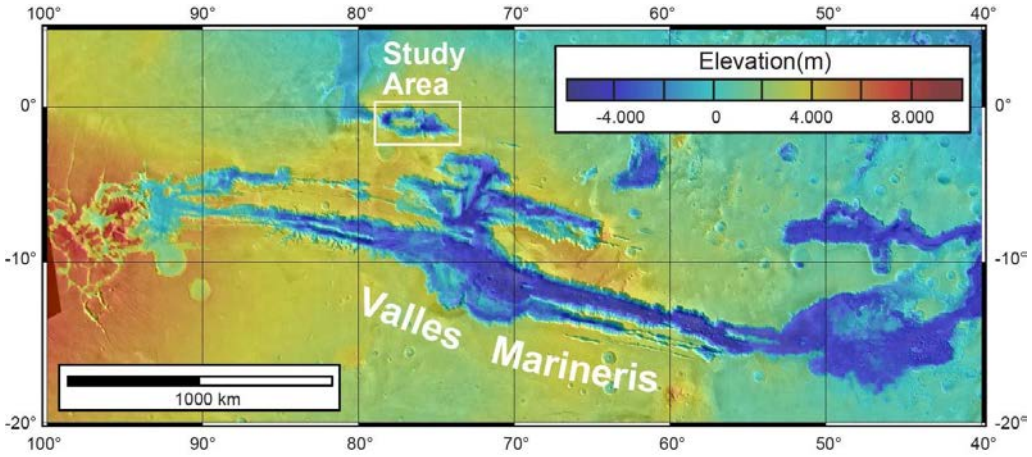

Figure 3.1: MOLA colorized DTM showing the location of Hebes Chasma

3.4.1 Background and Previous Work

The region surrounding Hebes Chasma is comprised of a multi-aged plateau influenced by tectonic contraction and the change in elevation at the edge of the Tharsis Buldge (Fig. 3.2). The north and east plateau is composed of tectonically contracted flood lavas of Early Hesperian age [Tanaka, 2014]. Distinguished by numerous faults and graben, the northwest plateau is a relatively small exposure of Noachian aged undifferentiated sedimentary and volcanic materials [Tanaka, 2014]. It is generally several kilometers thick and comprises the majority of walls in VM. The southern plateau is dominated by both Amazonian aged impact ejecta from the impact that formed Perrotin Crater and Hesperian aged aeolian, fluvial, and volcanic deposits [Tanaka,

2014]. Elevation of the plateau decreases more than 2 km over a distance of 400 km from the area south of Hebes towards Lunae Planum in the north.

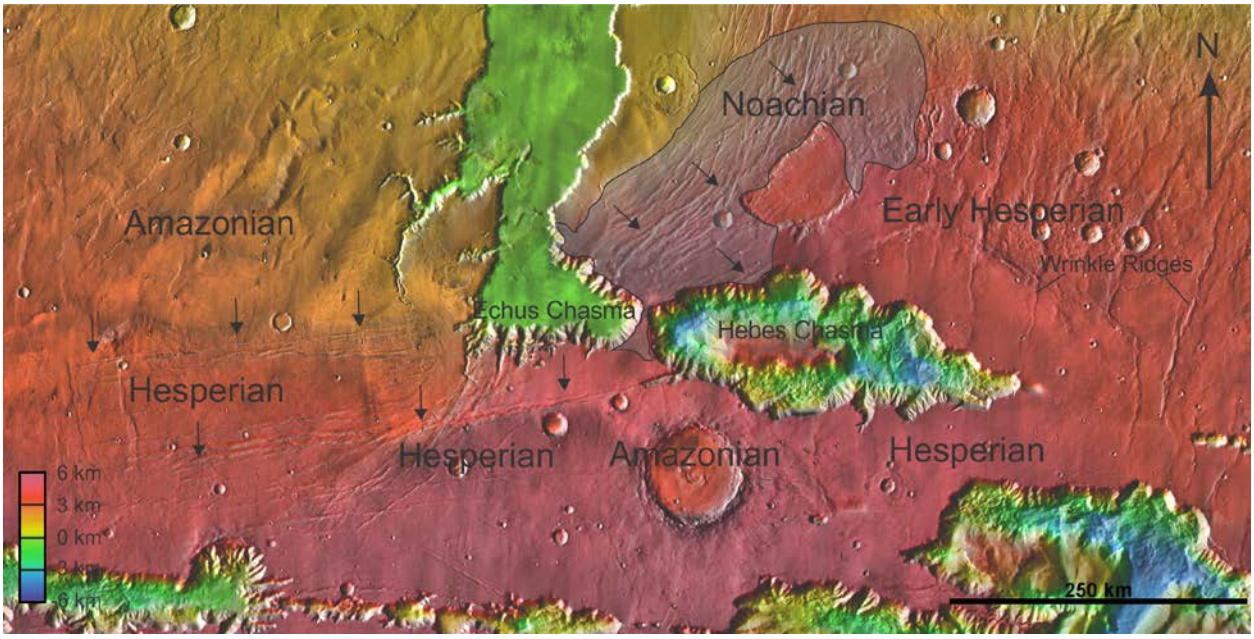

Figure 3.2: MOLA DEM and THEMIS imagery of the Hebes/Echus region. The plateau spans multiple geologic periods. The Noachian plateau has been outlined and shaded. Two wrinkle ridges have been labeled the northeast plateau, numerous others are running parallel in the area. Several grabens and faults in the northwest and far southwest are labeled with arrows. Plateau ages derived from Tanaka, [2014].

The Noachian exposure in the northwest plateau (shaded in fig. 3.2) provides a window into the abundant faulting throughout VM. More faulting can be observed southeast of Echus Chasma as the plateau grades into older Noachian/Hesperian material. Some of these Nochian faults express themselves in the Hesperian plateau surrounding Hebes, but are not easily identifiable. The origin of these faults is not fully understood, but they have been associated with the cooling of Tharsis [Tanaka, 1991]. The Hesperian aged plateau contains numerous wrinkle ridges that were not observed in the Noachian exposure.

The formation of Hebes Chasma has previously been explained by linear collapse of a pit chain by evaporation of ground ice along a graben [Peterson, 1981], and as karstic collapse through a system of subterranean piping [Jackson et al., 2011]. The latter model suggests

material drained through the ground by water and was carried west to the adjacent Echus Chasma, contributing to the large outwash event that flowed north and created Kasei Valles (Fig. 3.2). This piping system was eventually overwhelmed and plugged by the collapsed material. Grindrod and Balme [2010] proposed a similar model of flowing groundwater. Wilkins and Schultz [2003] studied faults in the perimeter of VM and concluded Hebes Chasma was best interpreted as a graben rather than a collapse depression. The absence of any outwash channel, coupled with the close proximity to Echus Chasma, makes groundwater models appealing to explain Hebes Chasma. Landslides in VM have been interpreted previously as sliding upon sub-surface ice [De Blasio, 2011] or water [Lucchitta, 1979].

Attempts to understand the relationship between collapse and ILD deposition have produced different models. Peterson [1981] suggested that infilling of the chasma may have occurred when the trough was only partially formed. Jackson et al., [2011] described a chasma formed from karstic collapse followed by diapiric arching that upwelled basement rock to create the central mound. However the amount of carbonates on Mars is limited [Ehlmann, 2008] and not adequate to create VM.

Perimeter faults around Hebes Chasma have been discussed and mapped previously [Peterson, 1981; Jackson et al., 2011; Witbeck et al., 1991; Wilkins and Schultz, 2003]. This study contributes to previous perimeter fault work by taking advantage of CTX imagery and topographical data with a resolution of 5 m/pixel. Several new faults have been discovered and vertical displacement was measured. Although Jackson et al., [2011] mapped several slump blocks in Hebes Chasma and described them as fault-bounded benches, this study investigates perimeter faults observed in the surrounding terrain adjacent to the chasma to determine if the slump blocks are fault controlled.

3.3 Methodology

A CTX mosaic registered to a HRSC composite DTM (orbits 0360, 2116, 2138, 2149, 5142, 5160, 5178) forms the base data for the study (Fig. 3.2a). CTX DTMs with a resolution of 5 m/pixel were used for measurements of the displacement of the perimeter faults. All CTX DTMs were calculated with the NASA Ames Stereo Pipeline [Moratto et al., 2010; Broxton and Edwards, 2008]. The strike of perimeter faults were plotted on a rose diagram created using the program SpheriStat3 [Stesky and Pearce, 2014]. JMARS software was used to create a regional cross section of Echus Chasma, Hebes Chasma, and a pit chain located to the southeast of Hebes [Christensen et al., 2014].

3.4 Results

A cross-section was created from Echus Chasma, across Hebes Chasma, to a 95 km pit chain located 147 km east of Hebes (Fig. 3.3). The map suggests that these three features are collinear with an orientation of 102˚ and form a large single regional feature that runs parallel to Valles Marineris. The cross-section is subdivided into sections A-F that represent significant features. Section A-B includes Echus Chasma, an open ended flat-floored chasma that measures 115 km across and contains no ILDs. The elevation of the floor is approximately -1,000 m. The plateau on the western side of Echus is younger Hesperian-Amazonian with an elevation of approximately 1,500 m, nearly 2,500 m lower than the older Noachian aged plateau between Echus and Hebes which has an elevation of about 4,000 m [Tanaka, 2014]. Section B-C includes Hebes Chasma and central ILD mound up to the eastern-most exposure of the Lower ILD. These ILD units and their associated unconformity are discussed in the geologic map presented in

Chapter 2 (Fig. 2.4). Hebes Chasma measures 314 km across and is nearly 8 km deep, approximately 3,500 m deeper than Echus Chasma. Section C-D represents the eastern collapse of Hebes and indicates two benches in the wall at elevations of 0 and 3,000 m. The VM cap unit discussed in section 3.4.2 was observed along the benches' edges. Section D-E includes the Hesperian aged plateau west of Hebes Chasma [Tanaka, 2014]. Section E-F includes the pit chain that ranges in depth to approximately 3,000 m.

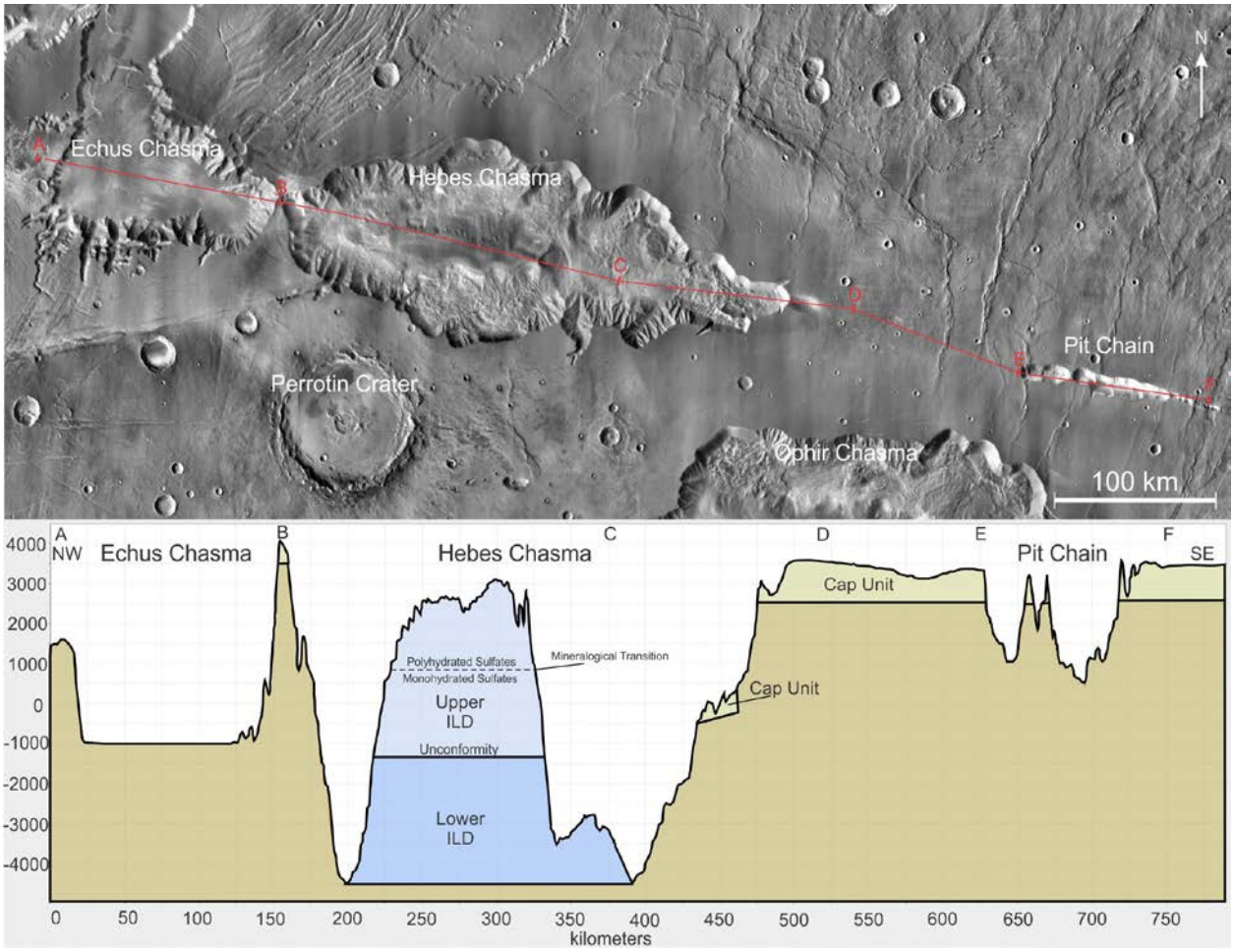

Figure 3.3: Regional cross-section between Echus Chasma, Hebes Chasma, and the pit chain using THEMIS day IR imagery and MOLA topography (Vertical exaggeration 26X).

3.4.2 Wall Morphology and Cap Unit

Two types of wall morphologies were observed: smooth talus (Figs. 3.4, 3.6, 3.7) and spur and gully (Figs. 3.6, 3.7). Spur and gully morphology is the most common wall type in VM

[Lucchitta, 1977] characterized by steep cliffs that are dissected into alternating spurs (topographic highs) and gullies (topographic lows) which are subparallel and inclined 15˚ to 30˚. Spur and gully morphology is thought to be one of the oldest features created during VM formation [Mege, 2011; Lucchitta, 1999; Lucchitta, 1978; Sharp, 1973]. Sections of smooth talus create concave swaths of wall where mass wasting events appear to have destroyed the spur and gully morphology. Extensive material at the base of these smooth talus sections also appears to bury parts of the wall up to several kilometers.

Throughout VM is a 500-2000 m thick “plateau-capping unit” [Lucchitta, 1979; Lucchitta, 1999; McEwen et al., 1999; William et al., 2003]. It is also present around the perimeter of Hebes Chasma (Fig. 3.4) [Peterson, 1981; Jackson et al., 2011], as well as the collinear pit-chain observed in the southeast. The cap unit is up to 2 km thick and is useful in identifying slump blocks. The unit contains what appear to be thin layers. In some areas it is unclear if this unit’s emergence is compositional or erosional.

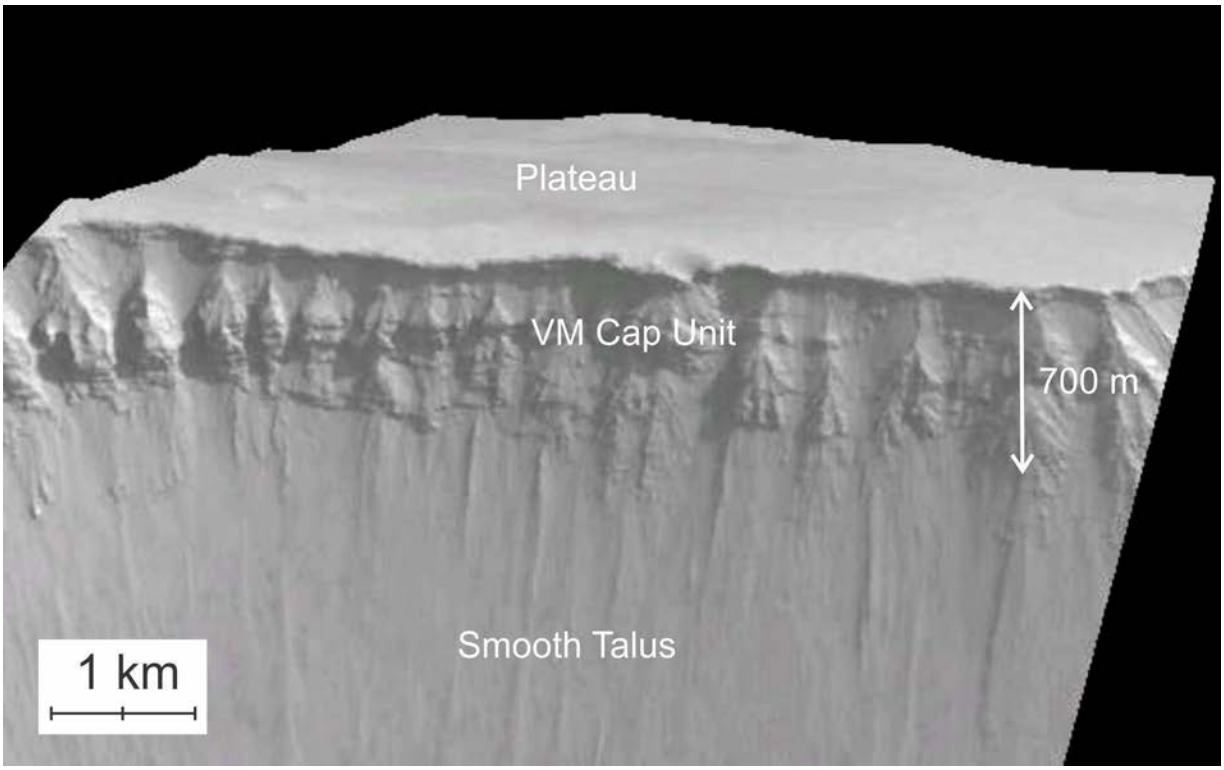

Figure 3.4: 3D view of VM cap unit in Hebes Chasma.

3.4.3 Perimeter Faulting and Proto-Blocks

A total of 27 faults were identified on the plateau within 20 km of Hebes Chasma (Fig. 3.5b). Only faults that cross-cut the chasma's edge or vertically offset the surrounding plateau were considered for this study. Perimeter faults can be recognized as linear depressions or troughs where a proto-block has not been downthrown. In some instances parallel faults create graben (Fig. 3.8).

Faults range from 5 to 35 km in length with 40-500 m of vertical displacement. Lateral displacement was not observed. Fault strikes were measured and three preferred orientations were identified (Fig. 3.5c). Set 1 strikes 101˚, which is similar to the 102-105˚ orientation of

VM. Faults in Set 1 generally have the largest vertical offset (500 m) as well. Set 2 strikes 65˚ and Set 3 strikes 145˚. All faults appear to have steep dips. When two orientations cross at the chasma edge, the resulting structures are 35-300 km^2 proto-blocks that have been dropped 40-500 m from the plateau (Fig. 3.6-3.8).

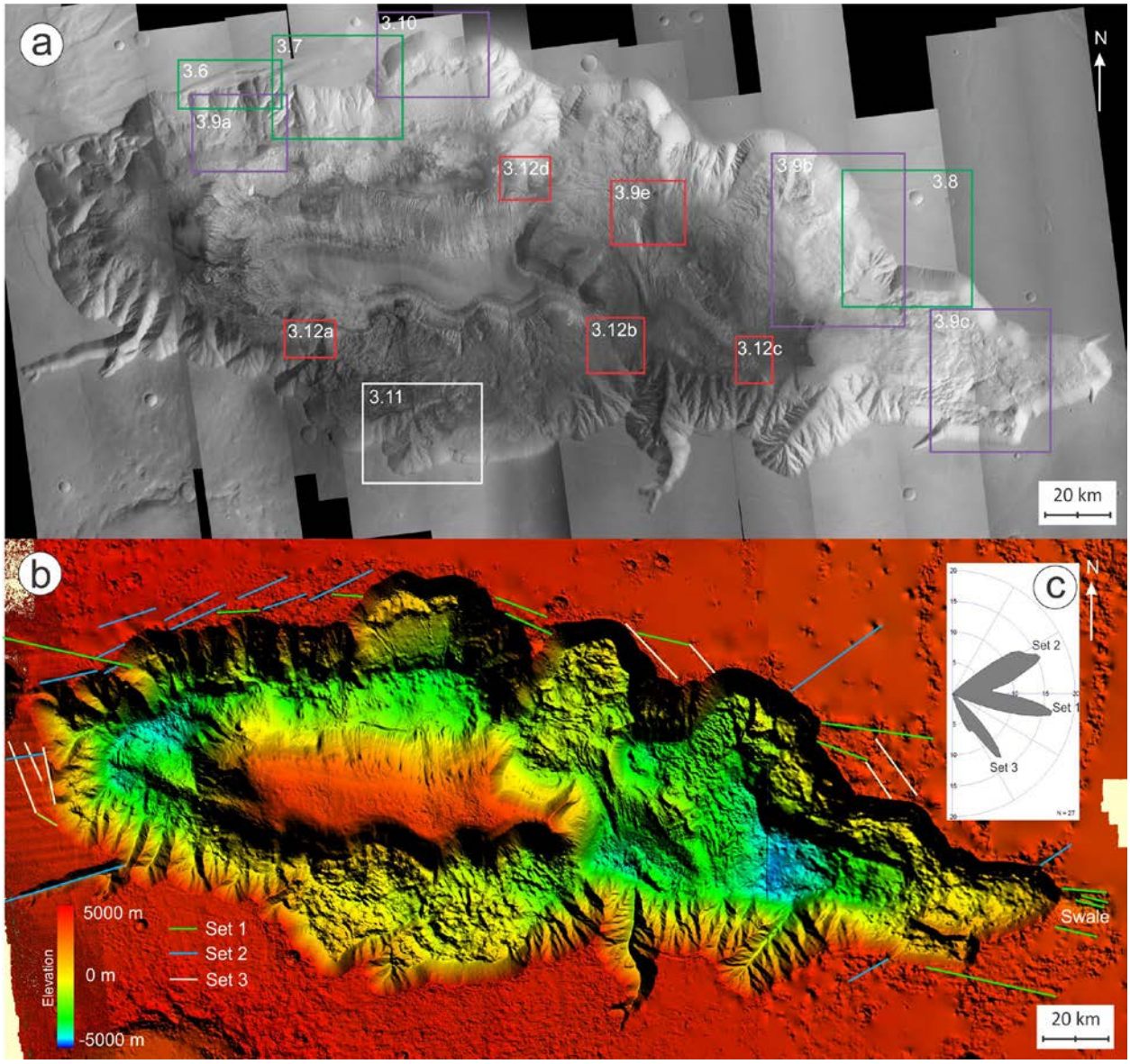

Figure 3.5: Imagery and elevation of Hebes Chasma. (a) CTX mosaic with locations of other figures in the paper outlined. Green indicates the location of proto-blocks. Purple indicates the location of slump blocks. Red indicates the location of contacts between the chasma wall and ILDs. White indicates the location of a sackung structure. (b)

HRSC DTM of Hebes Chasma with perimeter faults traced. (c) Rose diagram showing three preferred orientations (101˚, 65˚ and 145˚) of the perimeter faults.

Faults in Sets 1 and 2 primarily cross the northwestern plateau (Fig. 3.5-3.7). Faults in Sets 1 and 3 cross the northeastern plateau (Fig. 3.5, 3.8). A 750 m deep depression, referred to as “The Swale” by Jackson et al., [2011], that marks the easternmost extent of the chasma is bounded by Set 1 faults (Fig. 3.5b). Few faults were observed in the southern plateau likely due to extensive ejecta cover from Perrotin Crater impact (Fig. 3.3) [Tanaka, 2014].

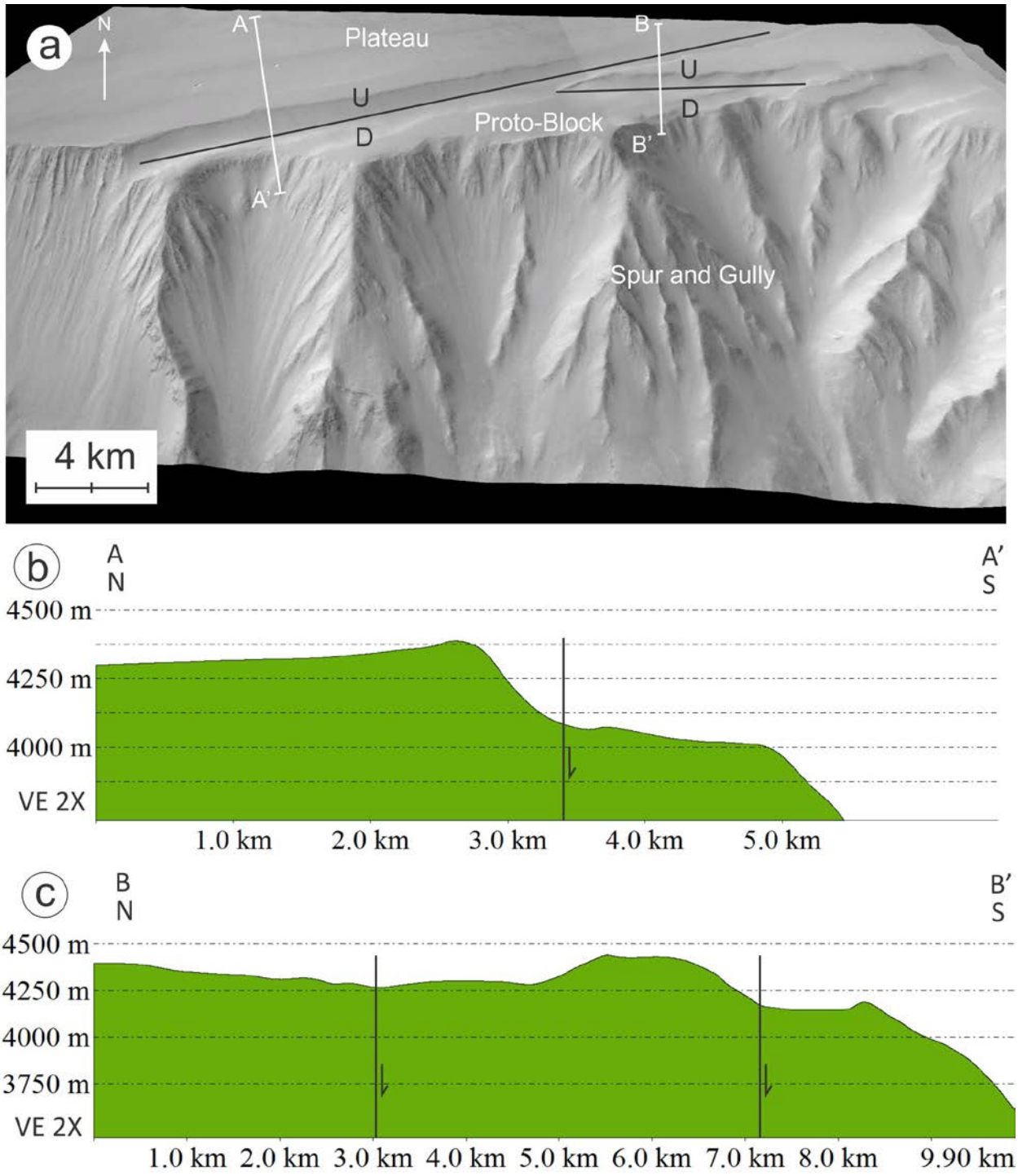

Figure 3.6: A proto-block observed in the northwest area of Hebes Chasma. (a) 3D view of the proto-block. Faults marked with black lines. Cross-sections marked by white lines lines. (b-c) Cross-sections of the proto-block.

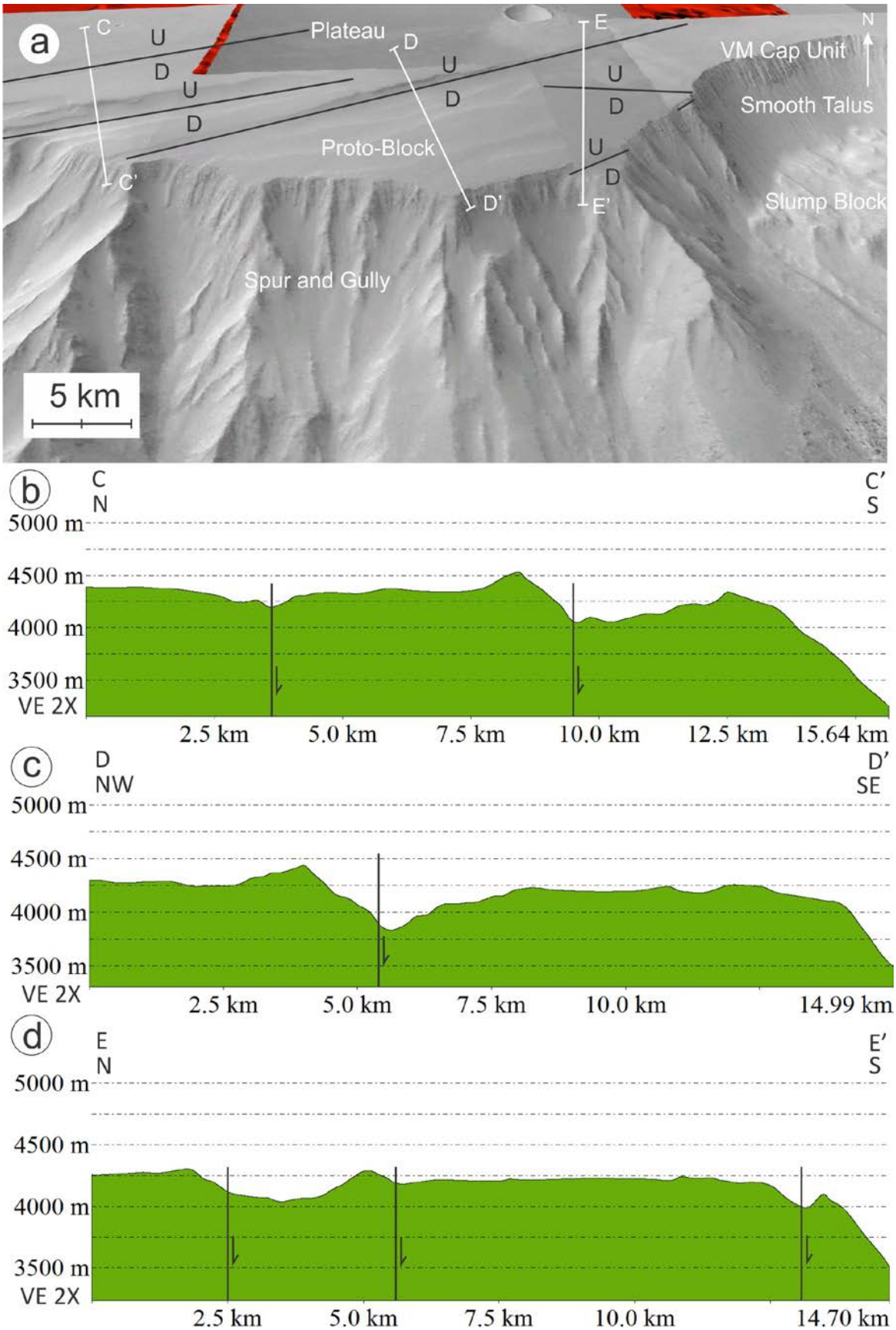

Figure 3.7: Adjacent proto-block observed in the northwest. (a) 3D view of the proto-blocks. Faults marked with black lines. Cross-section marked by white lines. (b-d) Cross-sections of the proto-block.

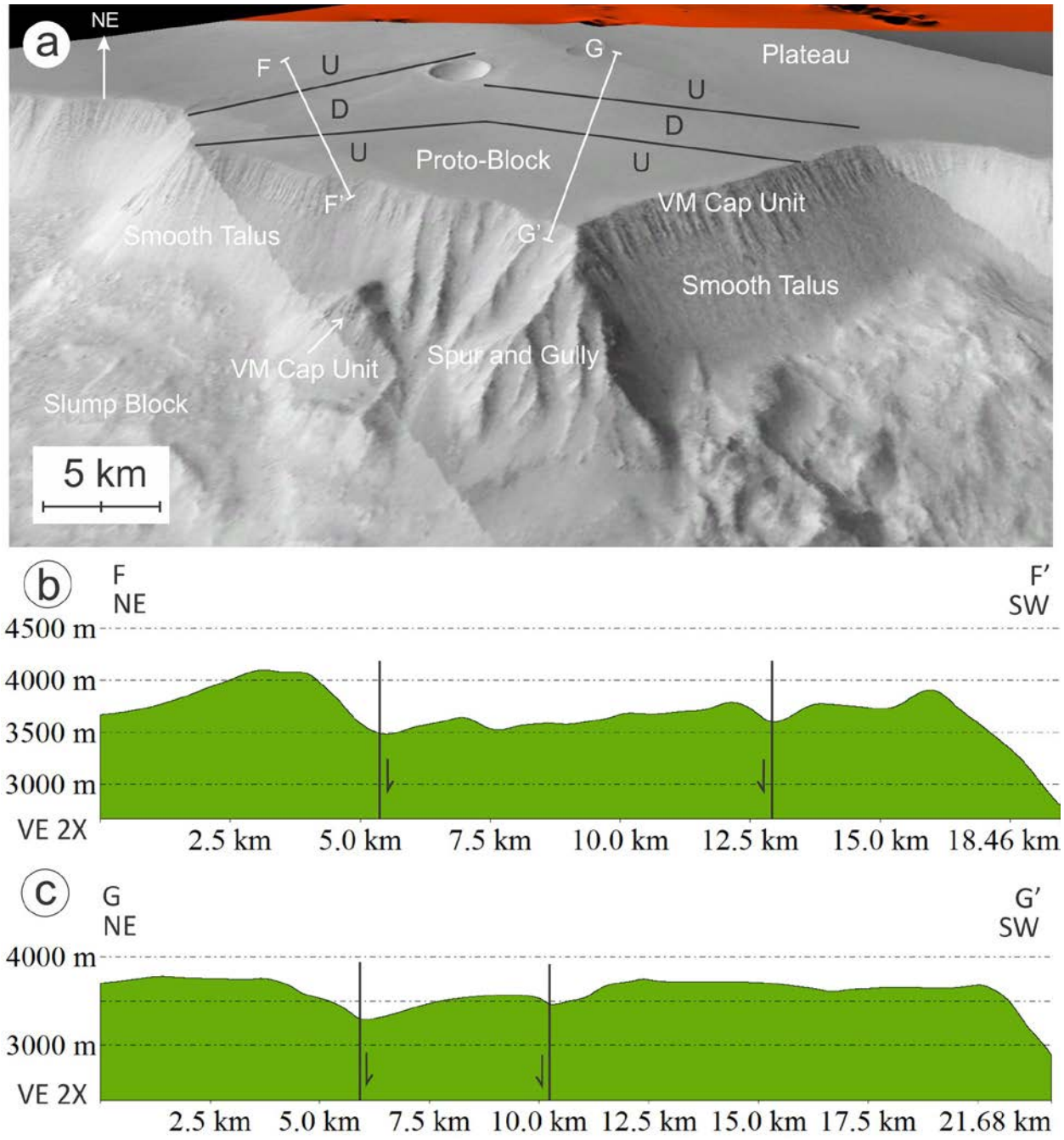

Figure 3.8: Large proto-block observed in the northeast area of Hebes Chasma. (a) 3D view of the proto-block. Faults marked with white lines. Cross-sections marked by red lines. (b-c) Cross-sections of the proto-block.

3.4.4 Slump Blocks

Slump blocks and landslides share many of the same mechanisms, faulting, freeze/thaw processes, marsquakes and saturation/lubrication of the underlying rock [Nemčok, 1972; Lucchitta, 1979]. However they differ in several respects, notably the speed of movement and competency of material. Landslides are rapid moving masses of mixed rock, while slump blocks are detached sections of wall that slide downward at varying speeds. They can often be associated with coherent blocks riding upon landslide debris [Lucchitta, 1979].

The VM Cap Unit was observed in multiple locations throughout the chasma's interior where pieces of recognizable cap unit is dispersed throughout landslide debris. Slump blocks tend to preserve the planar layering of the cap unit. In several areas, the cap unit is intact and can be traced around the entire slump blocks. While there are also many instances of the cap unit outcropping in fragments, only large and intact sections of the cap unit that had an easily recognizable plateau surface are considered slump blocks in this study.

A total of seven slump blocks were observed that vary in size and vertical displacement (Fig. 3.5 and geologic map presented in Chapter 2 Fig. 2.4). They are surrounded and partially buried by landslide debris. A 2 km-thick exposure of the northwest slump block is 69 km^2 in size and has dropped vertically over 4 km from the plateau (Fig. 3.9a). In the northeast three slump blocks are adjacent to one another and range in size from 36 km^2 to 226 km^2 (Fig. 3.9b). The smaller two slump blocks are 36 km^2 and 49 km^2 in size both are 1 km thick exposures and have collapsed over 3 km. South of them is a 3 km-thick exposure 226 km^2 in size, which has dropped vertically 4 km. In the southeast side of the chasma a 54 km^2, 2 km-thick slump block has traveled 10 km laterally from the wall (Fig. 3.9c) and is surrounded by landslide debris on all sides. There is also a 121 km^2, 1 km-thick slump block located north and center (Fig. 3.10). This

block is unusual relative to the other blocks in that it has broken up into numerous smaller sections each varying from horizontal to backward and inward inclinations relative to the chasma wall.

The morphology of the chasma wall alternates from spur and gully to concave sections of smooth talus (Fig. 3.5a). Sections of smooth talus are always associated with slump blocks or landslides and are thus thought to be younger than the spur and gully formations. In general, the eastern wall is dominated by smooth talus and the western wall is dominated by spur and gully.

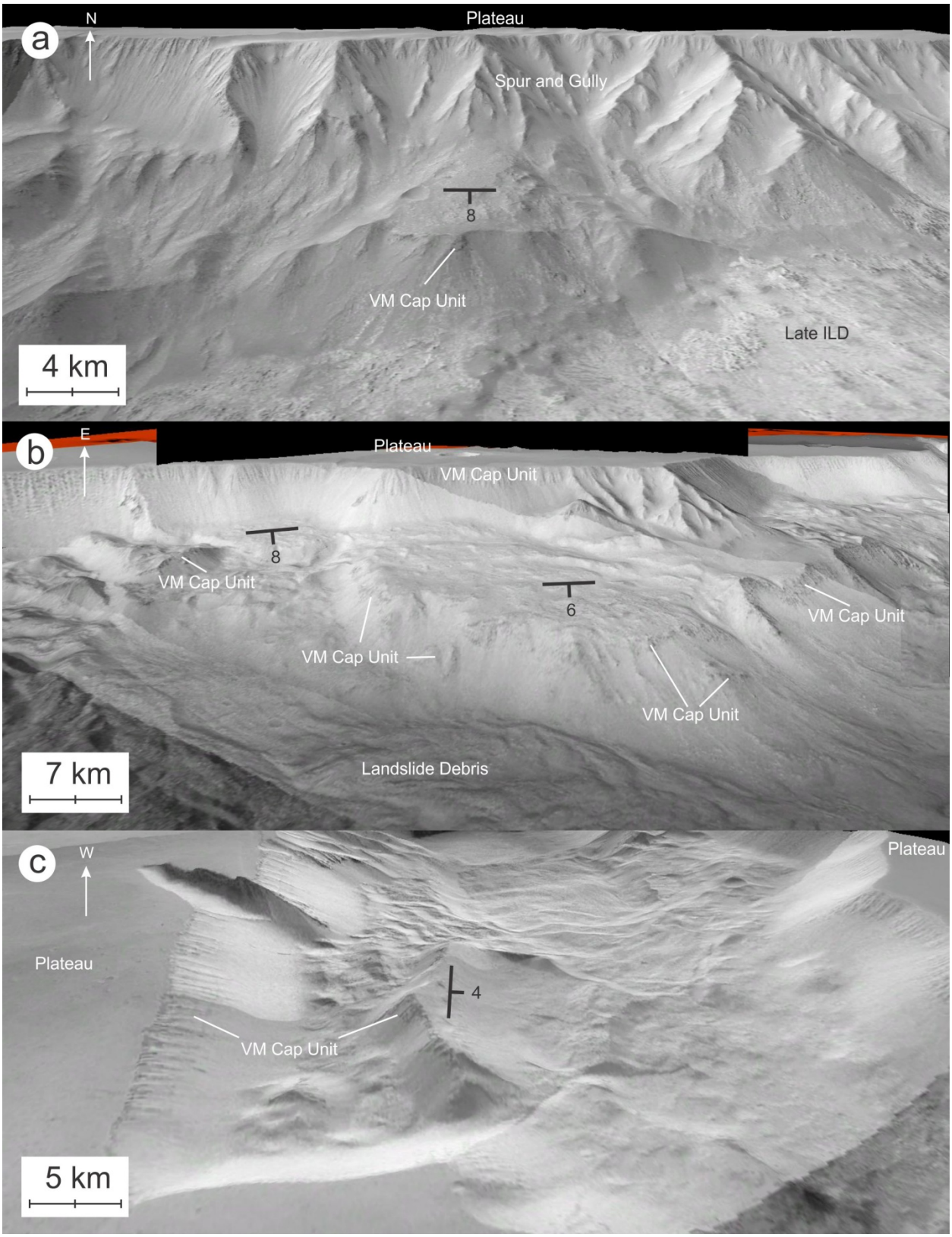

Figure 3.9: 3D view of slump blocks. (a) Northwest slump block adjacent to spur and gully wall that is tilted inwards 8˚. (b) Three slump blocks located in the northeast tilting inwards 6-8˚. Far left slump block is fragmented, but essentially horizontal. (c) Eastern slump block completely surrounded by landslide debris that has traveled 10 km from the wall.

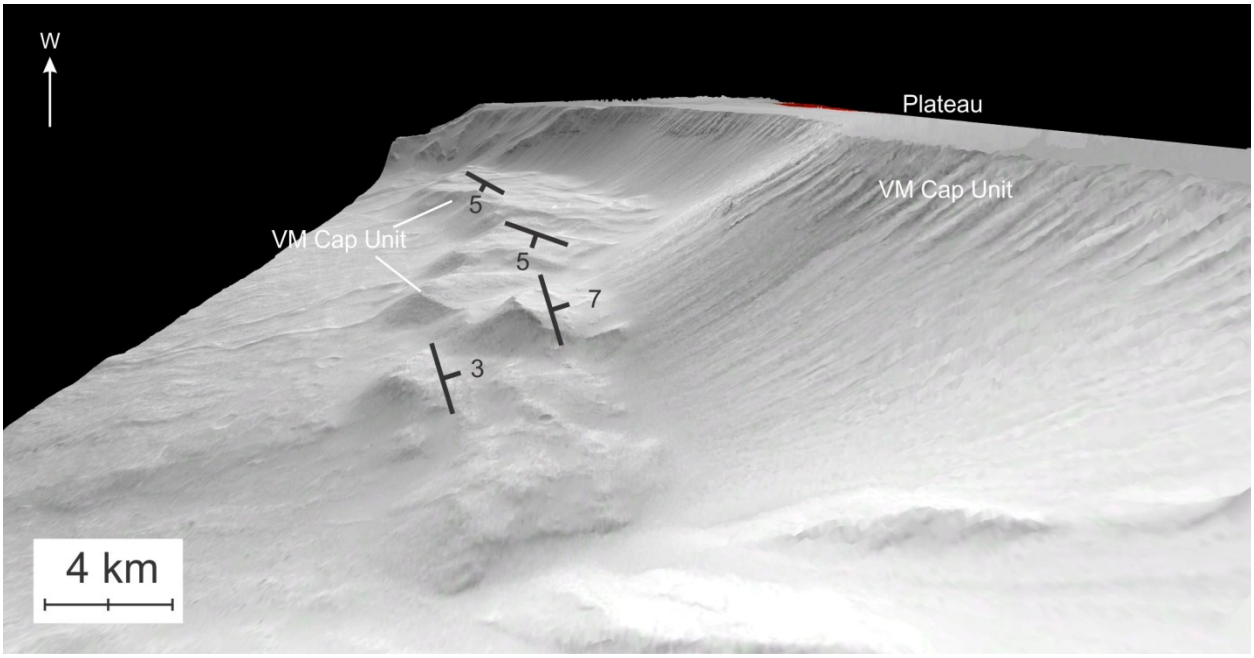

Figure 3.10: 3D view of the north-center fragmented slump block.

3.4.5 Southern Collapse

Few faults were observed in the southern plateau although scarps created by late collapse of the wall were observed due south of Hebes Mensa trending 136˚ (Fig. 3.11) and similar in orientation to Set 3 faults at ~145˚. Similar collapse structures in VM have previously been interpreted as sackungs [Lucas et al., 2011; Mege, 2011]. A sackung is a geomorphic landform produced by gravitational spreading in slopes which creates uphill-facing scarps often attributed to deglacial unloading in oversteepend slopes [Agliardi, 2005]. Movement can be described as dip-slip displacement that occurs along fault planes dipping steeply into the slope or by forward toppling [Gutiérrez-Santolalla, 2005].

The terrain that composes the floor of Hebes varies greatly throughout the chasma. The elevation of the southern floor is more than a kilometer higher than the northern floor and is significantly covered with mass wasted material from the southern wall. This material is

observed overtop ILD. The scarps and ridges within the topography of the southern floor mimic the concave shapes of the sections of smooth talus wall around the chasma.

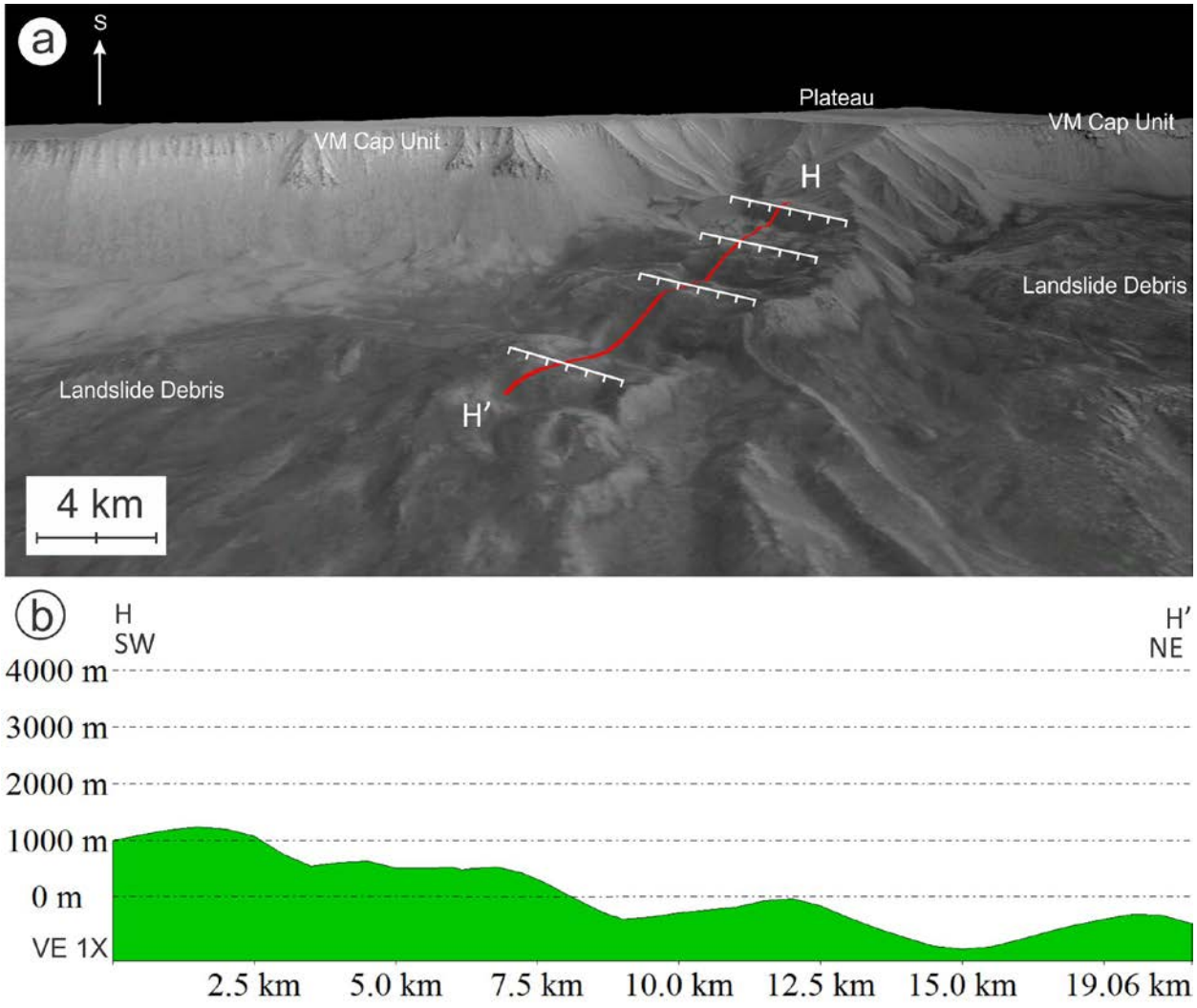

Figure 3.11: Sackung structure observed in the southern side of Hebes Chasma. (a) 3D view of the sackung structure protruding from the chasma wall. Scarps are marked and trend 136˚

3.4.6 Chasma Wall and ILD Relationship

There are five locations where ILD is observed in contact with spur and gully wall (Fig. 3.12). These areas are important because they show the inferred extent of the chasma during ILD deposition. The contacts occur at elevations ranging from -3,300 to 500 m. Layer attitudes in these areas generally dip toward the chasma wall and away from the chasma center.

Contacts between the ILD and the southern wall are abrupt and distinct (Fig. 3.12a-c). Figure 3.12b illustrates ILD layering beneath the main mound and landslide debris that extends to the

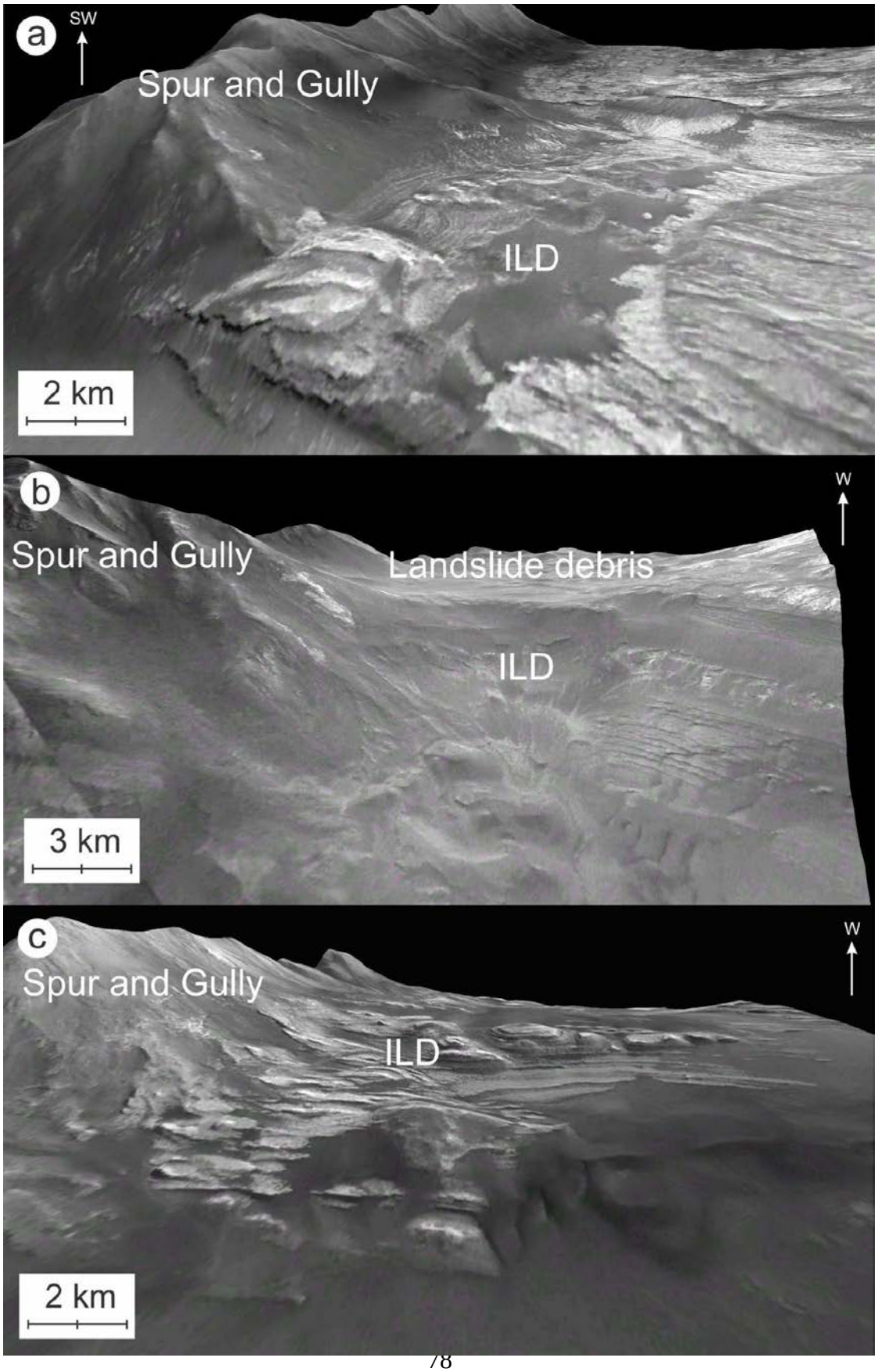
a
SW
Spur and Gully
ILD
2 km
b
W
Spur and Gully
Landslide debris
ILD
3 km
c
W
Spur and Gully
ILD
2 km

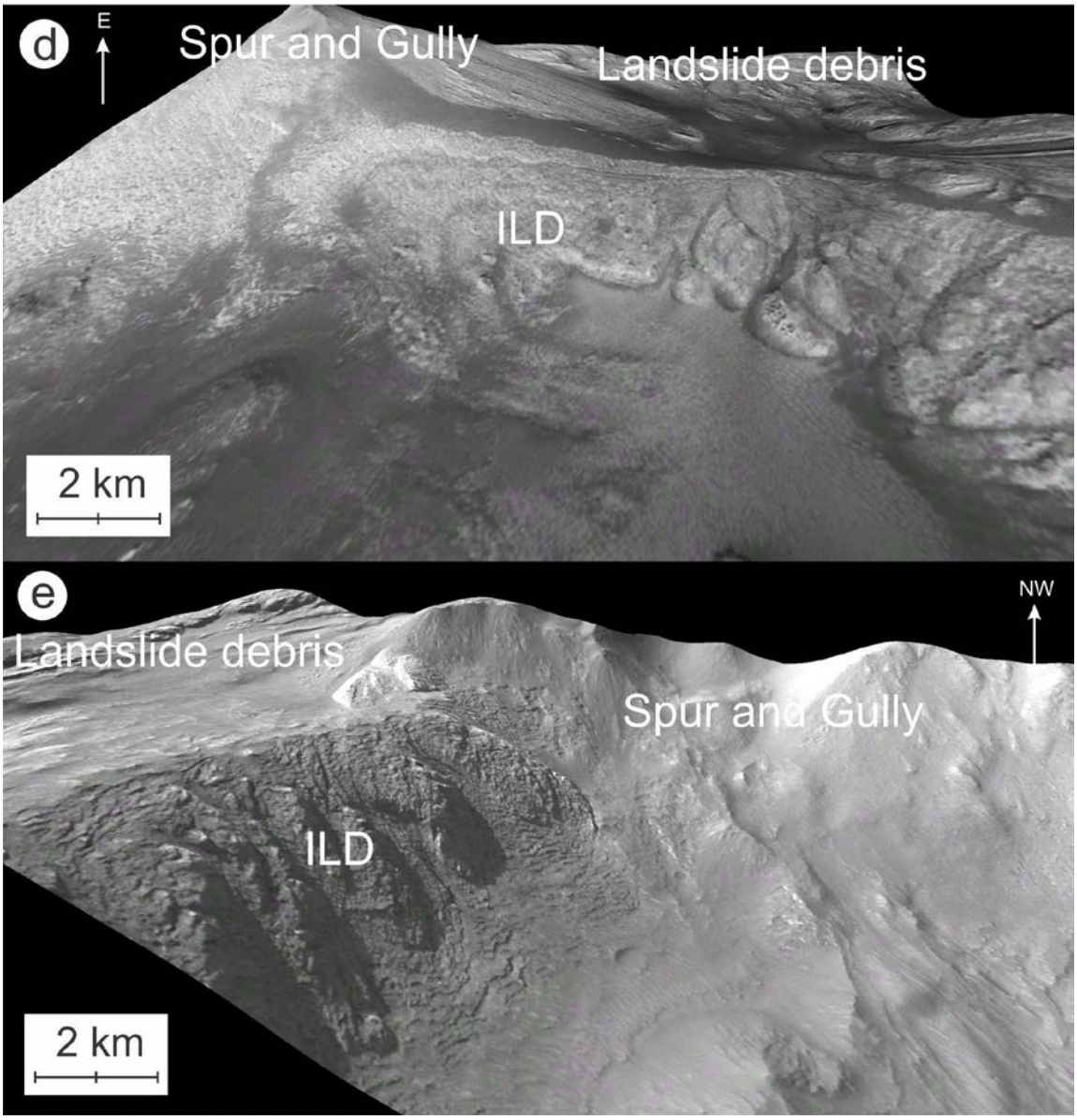

Figure 3.12: 3D view of the five locations of the ILD in contact with the spur and gully wall.

chasma wall. The ILD has some minor collapse features at this contact. Figure 3.12c shows the deepest visible ILD in Hebes where it is in contact with the chasma wall at about -3,300 m. Two contacts in the north were observed as well (Fig. 3.12d-e).

3.5 Discussion

By combining observations of faults, slump blocks, and contacts between the chasma wall and ILDs, a fault controlled collapse driven by the loss of subsurface volume is proposed as

a contending mechanism for the formation of Hebes Chasma. By comparing a regional topographic profile of Echus and Hebes to the timing of both Kasei Valles' formation and the ILDs deposition, various scenarios of water table elevation and groundwater flow are discussed. Lastly, a four stage formation model describes asynchronous timing of the chasma's collapse and the ILDs' deposition, where different depositional events occur within progressive phases of chasma collapse.

3.5.1 Collapse Mechanism

Our observations expand upon several aspects of previous work that describe the collapse of Hebes Chasma and VM. Previously proposed mechanisms tend to group into two principal ideas, that collapse was driven either by ILD mound related subsidence, or by a loss of volume from beneath the chasma.

Isostatic subsidence induced by the structural load of ILDs has been proposed as a contributing cause of basin collapse [Andrews-Hanna, 2012]. In this setting, the absence of ILD within Echus Chasma may explain why the floor of Hebes is 3.5 km deeper than the floor of Echus. However, Echus is the same age as other VM chasmata, which contain extensive ILDs [Lucchitta, 1994; Schultz, 1998] and have mature spur and gully wall morphology. Furthermore, Ius Chasma and other areas of VM are also without ILD, but exceed 7 km in depth. It is possible that Echus Chasma did contain ILDs, but were swept away in the outwash event that created Kasei Valles. In Hebes, areas of the Upper and Lower ILD are observed in contact with spur and gully wall at depths exceeding -3 km. Layers at these ILD-chasma wall contacts are relatively undisturbed and uniform, suggesting that the chasma had already collapsed to these depths at the time of ILD deposition. Although isostatic subsidence caused by the ILDs should have occurred, there is no evidence that the ILDs within Hebes Chasma have subsided significantly.

Our observations are more in agreement with a collapse mechanism that involves a loss of volume from beneath the chasma. Slump blocks next to and transported away from the wall within Hebes have been mentioned previously [Croft, 1989; Jackson et al., 2011]. Rotational slump blocks tilted backward towards the wall have also been observed throughout VM [Lucchitta, 1979], however our measurements indicate inward tilting slump blocks are predominant within Hebes. These are likely produced from large scale toppling failure that detaches proto-blocks under stress along perimeter cross-faults, creating a forward rotation. Detachment is caused by gravity, as there is a high level of potential energy [Lucchitta, 1979], and aided by the loss of volume due to the removal of subsurface ice or the release of water contained in aquifers (Figs. 3.13, 3.14). The loss of volume caused by melting subsurface ice is a more appealing collapse mechanism because there is a 9% loss of volume during the phase change of ice to water. Water would then be forced from containment within the wall into the chasma and along the perimeter faults (Figs. 3.13 Stage 1, 3.14 Stage 1). As water migrated along perimeter faults a freeze-thaw process may have occurred, agitating the faults and encouraging proto-block detachment. Marsquakes in response to the thermoelastic cooling of Tharsis [Phillips, 1991] may have played a role as well [Lucchitta, 1979]. Saturated or less competent lower sections of the wall give way to landslides during toppling of the proto-block (Fig. 3.14). The block can be transported away from the wall with the landslide (Fig. 3.14 Stage 2). Intact slump blocks could represent a slower toppling event, whereas areas of extensive landslide debris could represent a faster more chaotic event perhaps controlled by differences in saturation within the chasma wall or marsquakes.

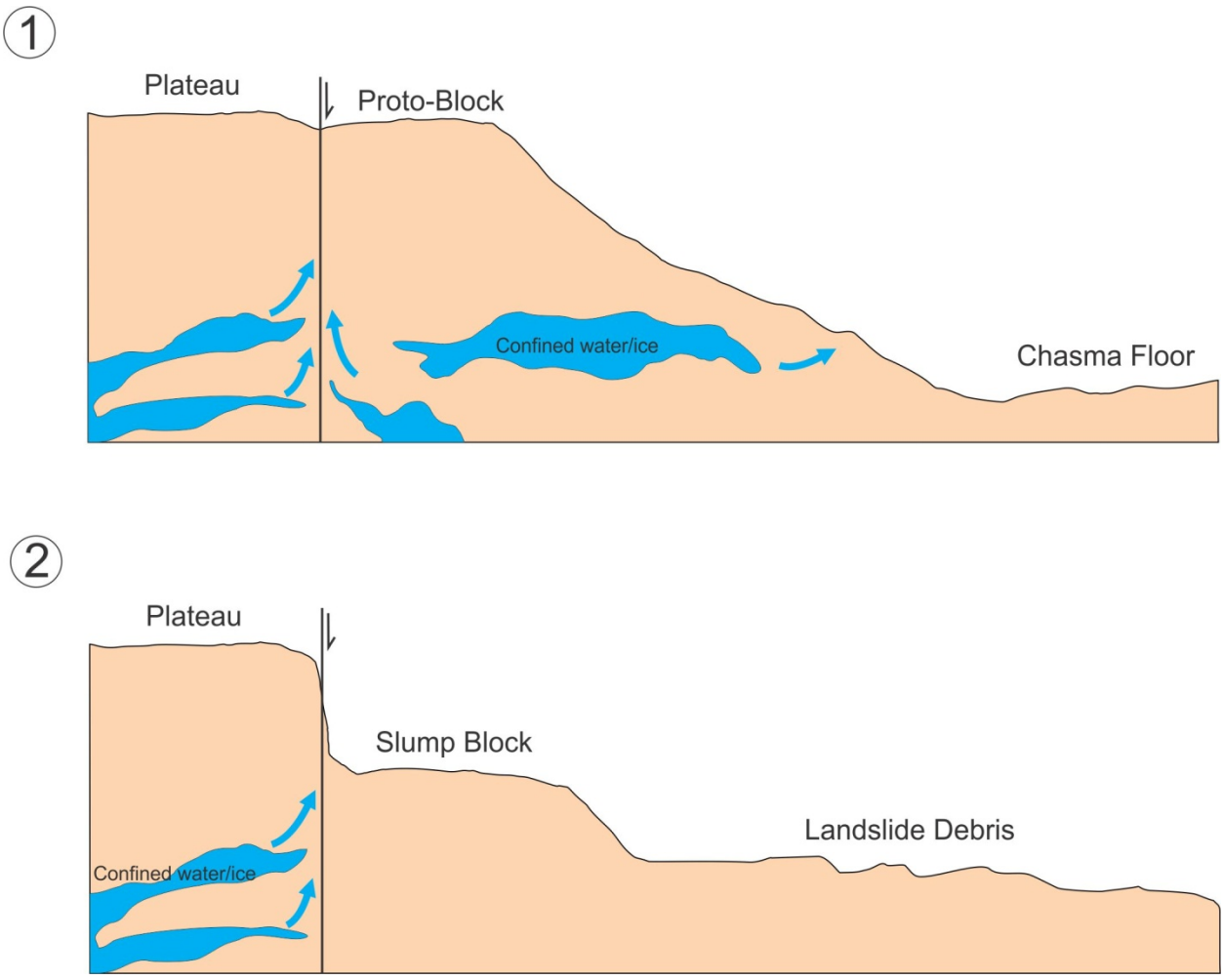

Figure 3.13: Sketch of two stage wall collapse. (Stage 1) The evolution of subsurface ice or the release of confined water creates void space within the wall. Water can be released in outbursts from the wall or migrate along perimeter faults. A freeze-thaw process may occur along the faults. (Stage 2) The proto-block collapses at a slow to moderate rate as sections of the lower wall become weakened from volume loss and the fault is agitated from migrating water and marsquakes.

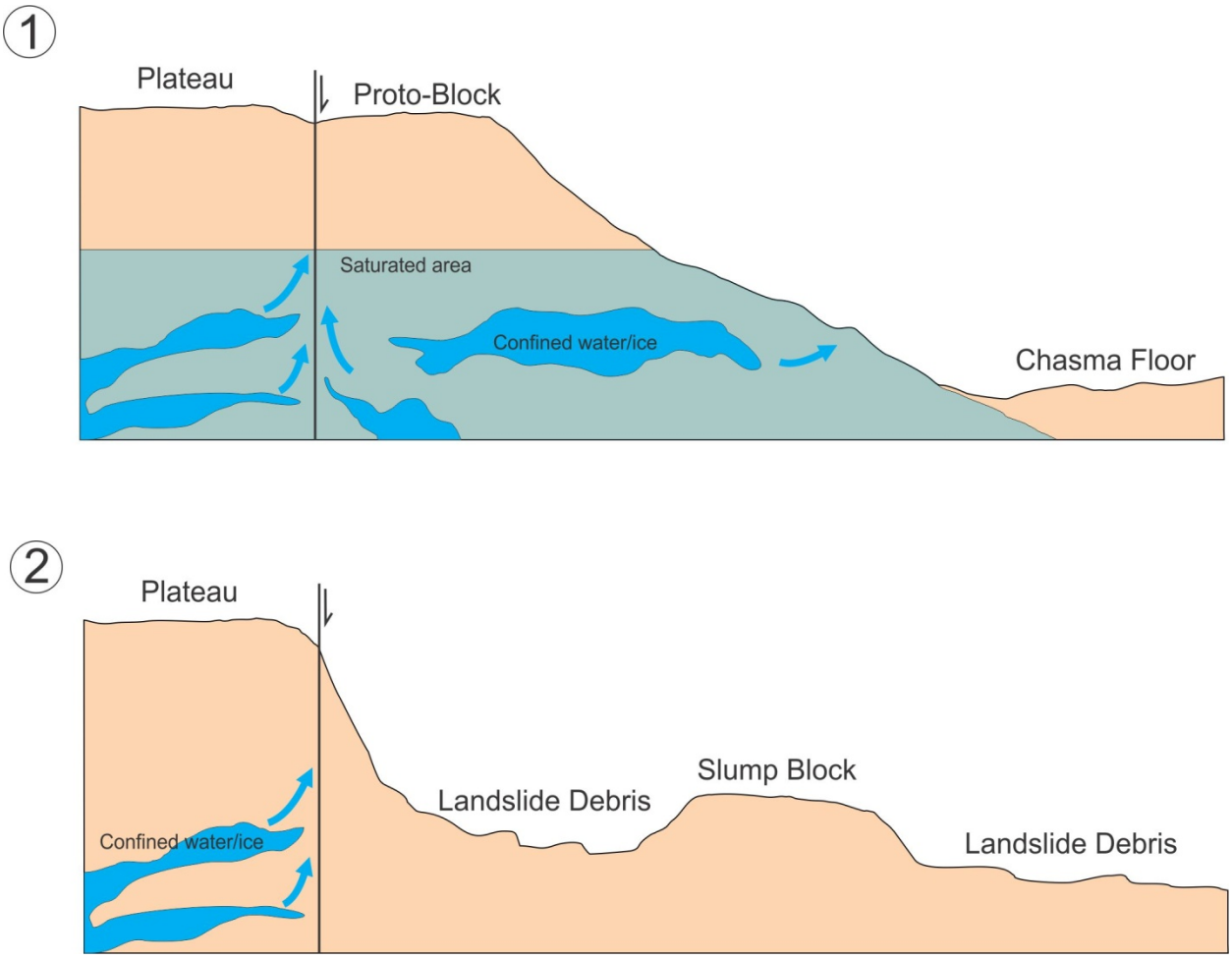

Figure 3.14: Sketch of two stage wall collapse during a saturated lower wall section scenario. (Stage 1) The evolution of subsurface ice or the release of confined water creates void space within the wall. The walls lower section may be less competent or more permeable. Water may seep out through lower wall sections or release in outbursts. Water also migrates along perimeter faults and a freeze-thaw process may occur. (Stage 2) Failure of the saturated lower wall section results in a more catastrophic landslide where the proto-block is transported away from the wall on top of the landslide.

When collapse occurs along perimeter cross-faults, incurvate sections of smooth talus wall are created. To demonstrate this process, Fig. 3.15 illustrates how the outline of the northern wall would change if the proto-blocks collapsed. The resulting future outline is similar to the present undulated outline suggesting perimeter faults have always controlled wall collapse. Furthermore, only the slump block in figure 3.8a is adjacent to spur and gully wall whereas all

the other slump blocks are adjacent to sections of smooth talus wall. Since spur and gully wall morphology

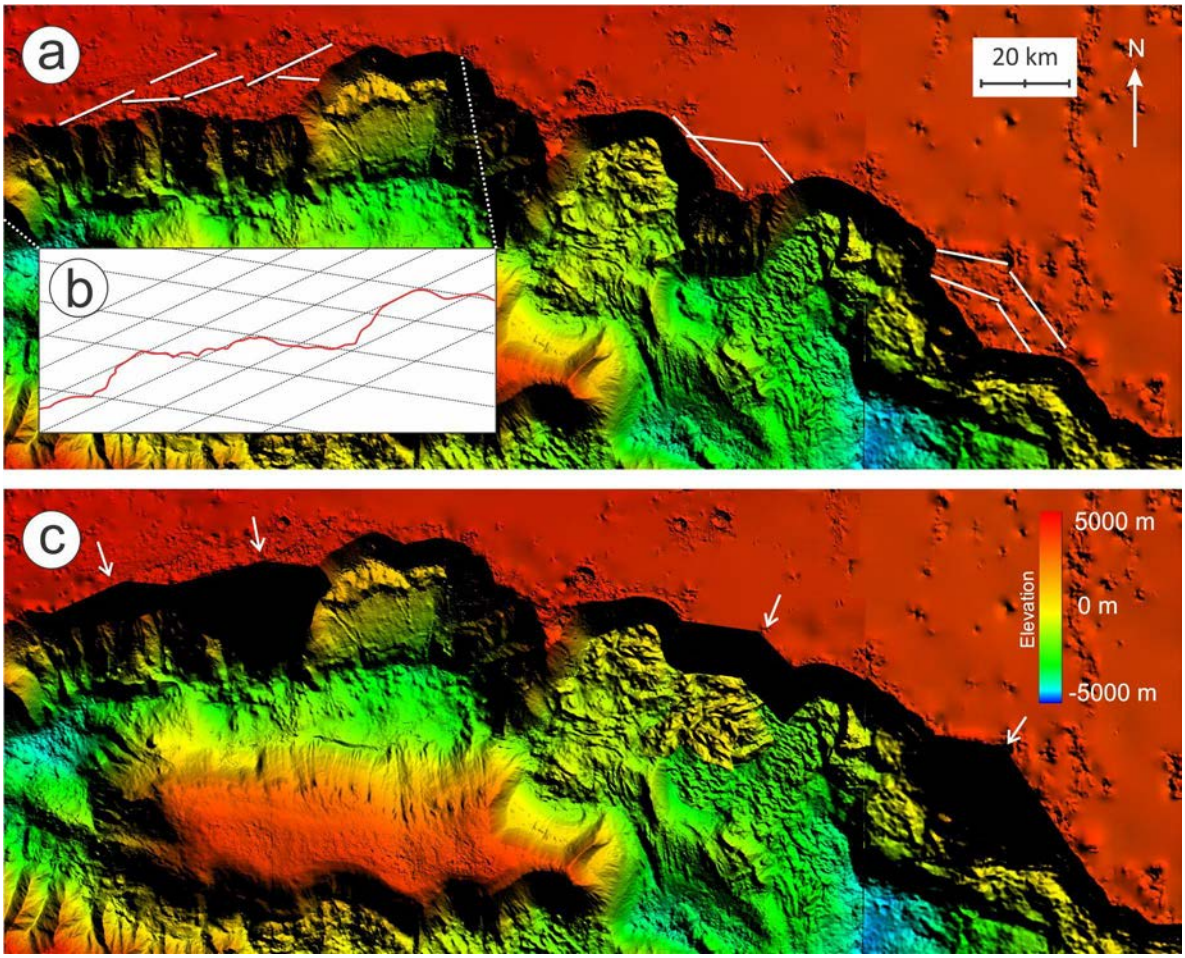

Figure 3.15: Outlines of the northern wall before and after the collapse of proto-blocks. (a) Shows the present chasma and several of its perimeter faults. (b) Generalized conception of how fault Sets 1 and 2 control the outline of the northwest wall. (c) Hypothesized future outline of the north wall if proto-blocks collapsed. Collapsed sections indicated by white arrows.

represents the early history of VM and is considered to require a significant amount of time to form [Peulvast, 2001; Lucchitta, 1979], the collapse of this particular slump block was likely earlier than the other slump blocks.

This mechanism of volume loss induced collapse along cross-faults was likely consistent throughout chasma formation. The wall retreated one proto-block at a time until the chasma

reached its present extent. As the chasma grew and more subsurface ice melted, water collected within the chasma possibly using the pre-existing faults as pathways.

3.5.2 Groundwater flow between Echus and Hebes Chasma

Drainage between Echus and Hebes Chasma [Croft, 1989; Robinson and Tanaka, 1990; Jackson et al., 2011] is a reasonable interpretation given the short distance between the two chasmata and the heavily faulted plateau between them (Fig. 3.16). Several faults observed connecting the two chasmata may have directed water flow. However, Echus Chasma is a flat floored depression with no evidence of flow entering from below [Chapman, 2010]. Our observations do not refute or support a groundwater drainage hypothesis, but do constrain several parameters if groundwater drainage between the two chasmata occurred.

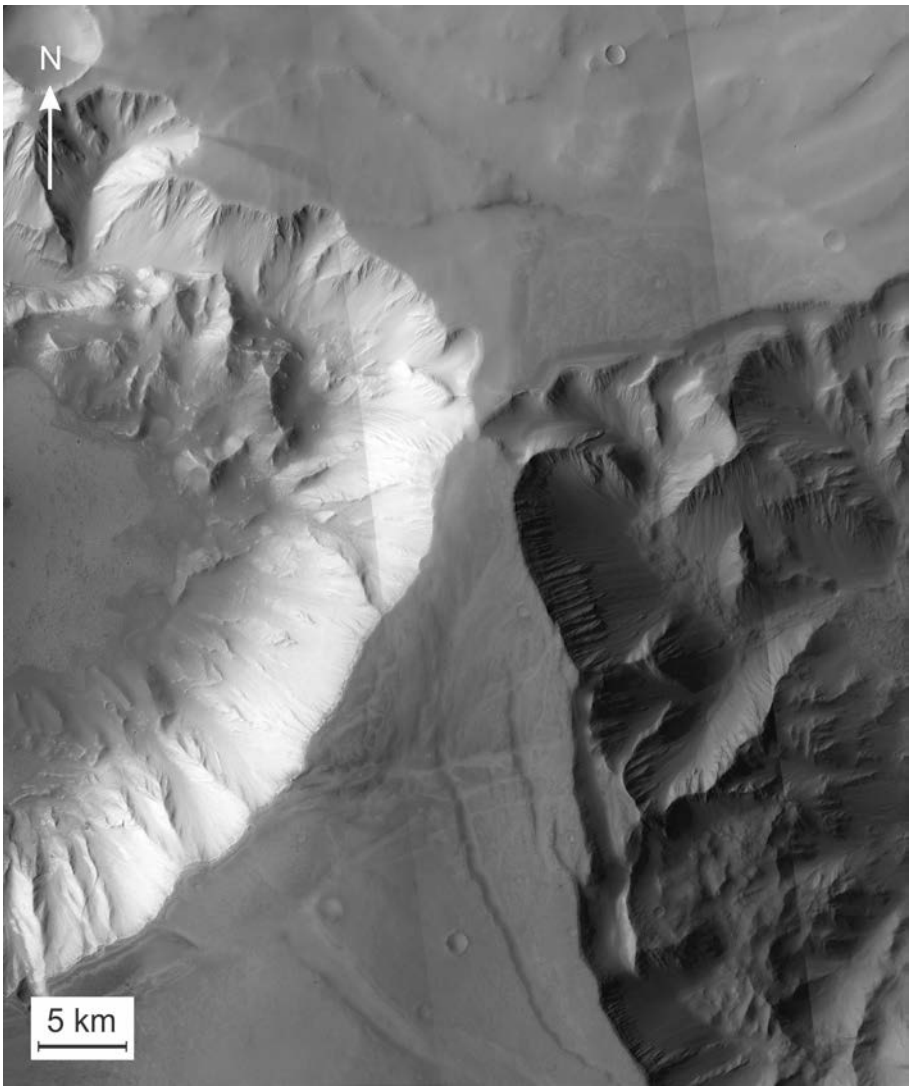

Figure 3.16: Adjacent sides of Hebes (right) and Echus Chasma (left).

Depending on the timing and elevation of the water level in Hebes, several drainage scenarios may have existed. There is a 3,500 m elevation difference between the floors of Echus (approx. -1,000 m) and Hebes (approx. -4,500) (Fig. 3.3). The north side of Echus leads into the Kasei Valles outflow system, which is thought to have initially formed during a Late Hesperian outflow event [Chapman, 2010]. The elevation difference between the floors of the chasmata suggests water would have flowed more easily from Echus to Hebes. During periods when the water level in Hebes dropped to elevations ≤ -1,000 m, a significant pressure gradient would be

needed for the water to flow into Echus. Prior to the formation of Kasei Valles, during the Early to Mid Hesperian, the chasmata may have shared a water table. During and after the Late Hesperian, Kasei Valles would have limited the water level in Hebes to -1,000 m if drainage to Echus existed and a strong pressure gradient did not. The identification of gypsum and hydrous sulfates within Hebes' ILD at an elevations < -2,000 m (discussed in Chapter 2) indicates that there were periods of evaporation in areas that could not be drained. Absolute timing of the gypsum formation is not known, the relative timing of alteration of the ILD is younger than the Early Hesperian.

There is a relatively small elevation difference between the ILD mound's unconformity (-1,400 m) discussed in Chapter 2 and the floor of Echus Chasma (-1,000 m). It is reasonable to suggest Echus contained ILD and was an isolated chasma like Hebes until the formation of Kasei Valles in the Late Hesperian [Chapman, 2010]. Once Kasei Valles formed, ILD within Echus was either immediately eroded away during the initial outflow event or began to erode away in subsequent outflow events that persisted into the Amazonian [Chapman, 2010]. If the ILD was deposited in a lacustrine setting, then the similar elevations of the Hebes mound unconformity and the floor of Echus may suggest that water was not contained within Echus at the time of the Lower ILD's deposition, if groundwater flow existed between Echus and Hebes.

3.5.3 Collapse History

To explain the described relationship between chasma formation and ILD deposition, we propose a four stage history that constrains and expands upon previous models [Peterson, 1982; Lucchitta, 1994; Fueten, 2014] is suggested (Fig. 3.17). Our model describes a complicated geologic history of chasma formation where ILDs are deposited within a basin that is structurally controlled by episodic faulting along three preferred orientations of faults of differing origins.

3.5.3.1 Faulting

The 101˚ strike of Set 1 faults is likely related to the regional orientation of 102˚ along which Echus, Hebes, and the pit chain occur as well as the general orientation of VM. If VM formation was the result of graben formation [Tanaka and Golombek, 1989; Mege and Masson, 1996; Schultz, 1998], it is reasonable to suggest these faults are related as well. This interpretation agrees with measured strikes of early compressional wrinkle ridges (Zuber, 1994) observed in the plateau that are perpendicular to strikes in Set 1. Faults in Set 2 tend to dominate the northwest Noachian aged plateau possibly due to cooling and contraction dynamics along the edge of the Tharsis Bulge. Faults in Set 3 may be related to Set 2 or more likely formed in response to tension created from extension along faults in Set 1. Wrinkle ridges do not appear to influence the chasma wall. The three fault sets match preferred fault orientations of 101-107˚, 70˚ and 135-150˚ that were measured previously in West Candor Chasma [Birnie, 2012]. These sets match in order of predominance as well, however the West Candor study observed faults within the chasma and ILD, not in the perimeter. The three fault sets also appear to share similar orientations to the valleys of Noctis Labyrinthus further south in the Tharsis upland [Masson, 1977].

3.5.3.2 Stage of Collapse

This scenario proposes the combination of multiple episodes of ILD deposition within an early chasma that undergoes multiple episodes of collapse and is envisaged to have taken place in several stages (Figs. 3.17-3.20). Groundwater flow is also proposed to have existed between Echus and Hebes due to either permeable wall material or subterranean piping. During Stage 1, Hebes was approximately 30% smaller in surface area than it is presently and the floor was at an elevation of approximately -3,500 m. Echus was enclosed and lakes were contained within both

chasmata. Due to the groundwater connection between them, the Echus and Hebes have a shared water level which is shown at an arbitrary elevation, below the rim of Echus. Any water above the rim of Echus would have spilled over onto the plateau and thus marks the maximum water level that could exist in Hebes. During Stage 2, the Lower ILD was deposited into Hebes and settled at the bottom of the lake. The Lower ILD was presumably deposited into Echus as well, but eroded away in the subsequent outwash events that eventually formed Kasei Valles. The ILDs deposited as sequences of ash fall as described in Chapter 2 and bury slump blocks from the initial formation of the chasma. The present shape of the ILD mound roughly reflects the undulated outline of the chasma walls, particularly in the south, suggesting that ILDs filled most or all of the chasma. At the beginning of Stage 3, the northern wall of Echus gave way to an outwash event that drained the lake it contained and created an outwash channel. Any ILD within Echus was eroded away during this event, or possibly over time by several outwash events. Water in Hebes was drained into Echus and through the outwash channel until the water level reached the elevation of the floor of Echus, approximately -1,000 m. At the end of Stage 3, the exposed Lower ILD was eroded to approximately this level, creating the erosional surface that would become the unconformity. During Stage 4, the Upper ILD was deposited on the Lower ILD and the unconformity was created. If the Upper ILD is lacustrine, then the groundwater flow between Echus and Hebes must have ceased. Some wall collapse may have occurred during the deposition of the Upper ILD, but timing is not certain. Further collapse of Hebes is more apparent during stages 5 and 6. During Stage 5, the mineralogical transition between mono- and polyhydrated sulfates was produced within the Upper ILD and wall collapse begins to dominate the setting. By Stage 6 Hebes had collapsed significantly and space is created between the ILDs and chasma wall, specifically in the north and west sides of the chasma. This period of collapse

formed the slump block in figure 3.8a. Slump scars within the Upper ILD also form and water is withdrawn from the chasma, possibly by evaporation. At the end of Stage 6 aeolian and glacial activity began eroding the ILD mound. During Stage 7 the Late ILD is deposited within the northern valley between the chasma wall and the ILD mound. Although timing is unclear, glacial activity played a major role in the morphology of the ILDs and chasma throughout stages 7 and 8. The polygons and hummocks observed on the Late ILD were produced, followed by the large valley that cuts through the Lower ILD discussed in Chapter 2. Stage 8 is dominated by debris flows from the ILDs and further wall collapse. A series of collapses in the north, east, and south walls created the slump blocks in figures 3.8b and 3.9, followed by the sackung structure in figure 3.10. Lastly, further collapse in the east created the slump block in figure 3.8c.

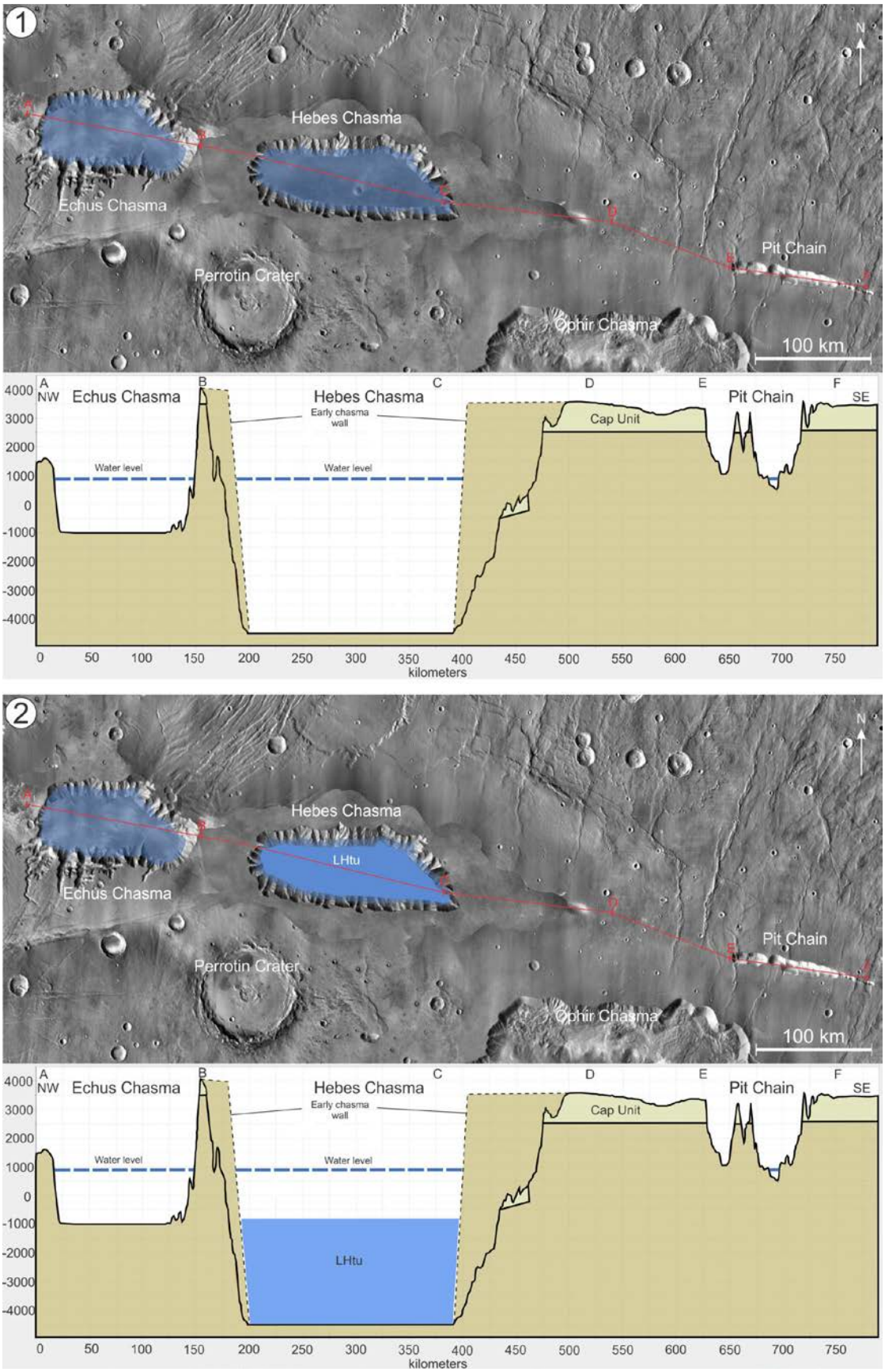

Fig. 3.17: Formation stages 1 and 2. VE=26X. (1) Early Echus and Hebes basins form and are filled with water. Groundwater flow between the two chasmata creates a shared water level. The Echus outwash channel has not formed. Hebes is approximately 30% smaller than it is presently. (2) The Lower ILD (LHtu) is deposited in Hebes.

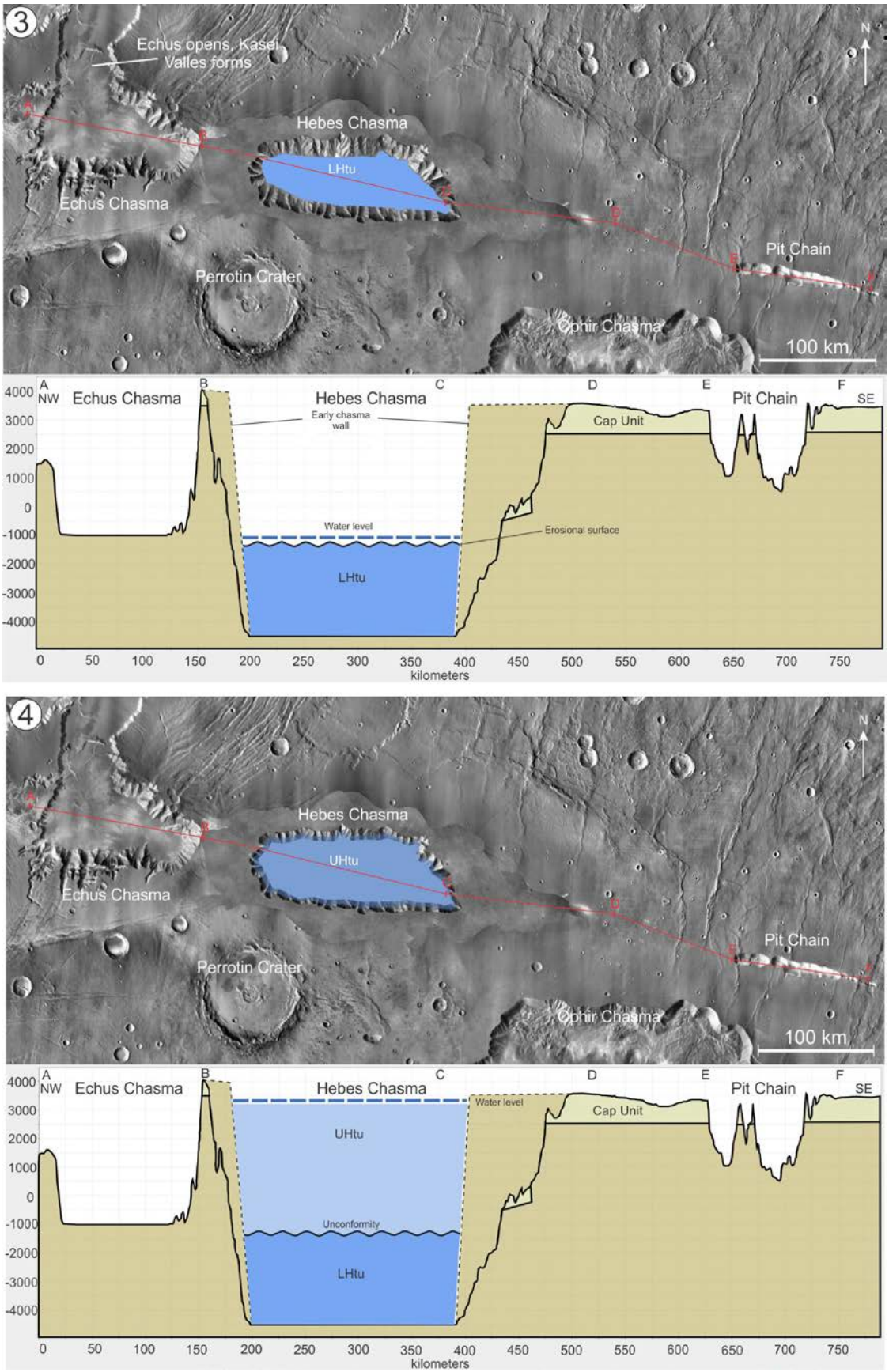

Fig. 3.18: Formation stages 3 and 4. VE=26X. (3) The outwash channel that leads to the formation of Kassei Valles is produced which subsequently drains water from Echus. Groundwater flow between Echus and Hebes allows water in Hebes to drain, creating a new water level that is approximately the same elevation as the floor of Echus. LHtu becomes exposed and is eroded to this new water level. (4) The Upper ILD (UHtu) is deposited on the erosional surface, creating the unconformity. If UHtu is lacustrine, then groundwater flow between Echus and Hebes must cease.

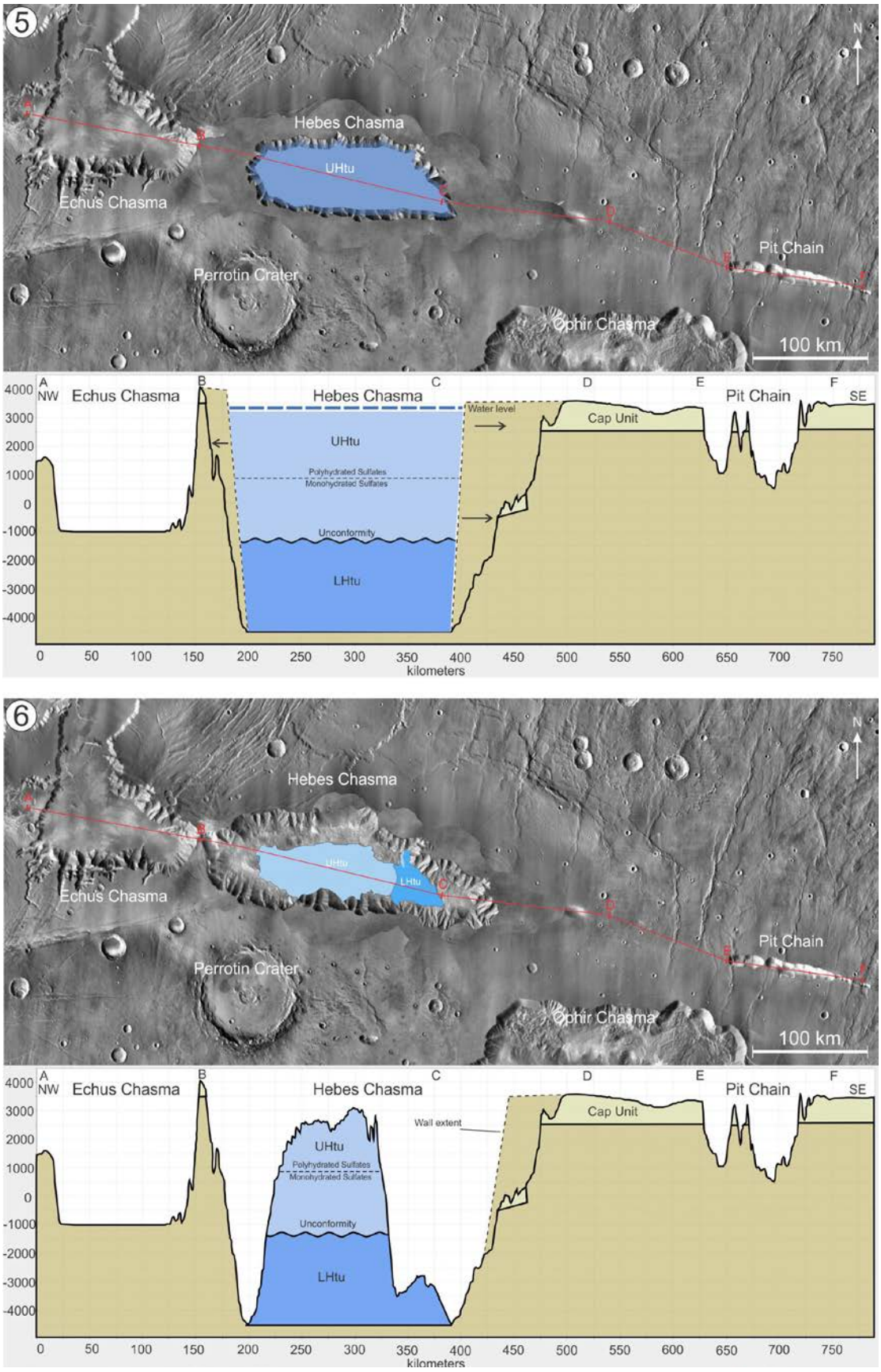

Fig. 3.19: Formation stages 5 and 6. VE=26X. (5) The mineralogical transition in UHtu forms. Hebes begins to collapse further, either late in the deposition of UHtu or immediately after. (6) Hebes is enlarged significantly and any water contained within is withdrawn, possibly by evaporation. ILD slump scars form and the ILDs are eroded to present extent.

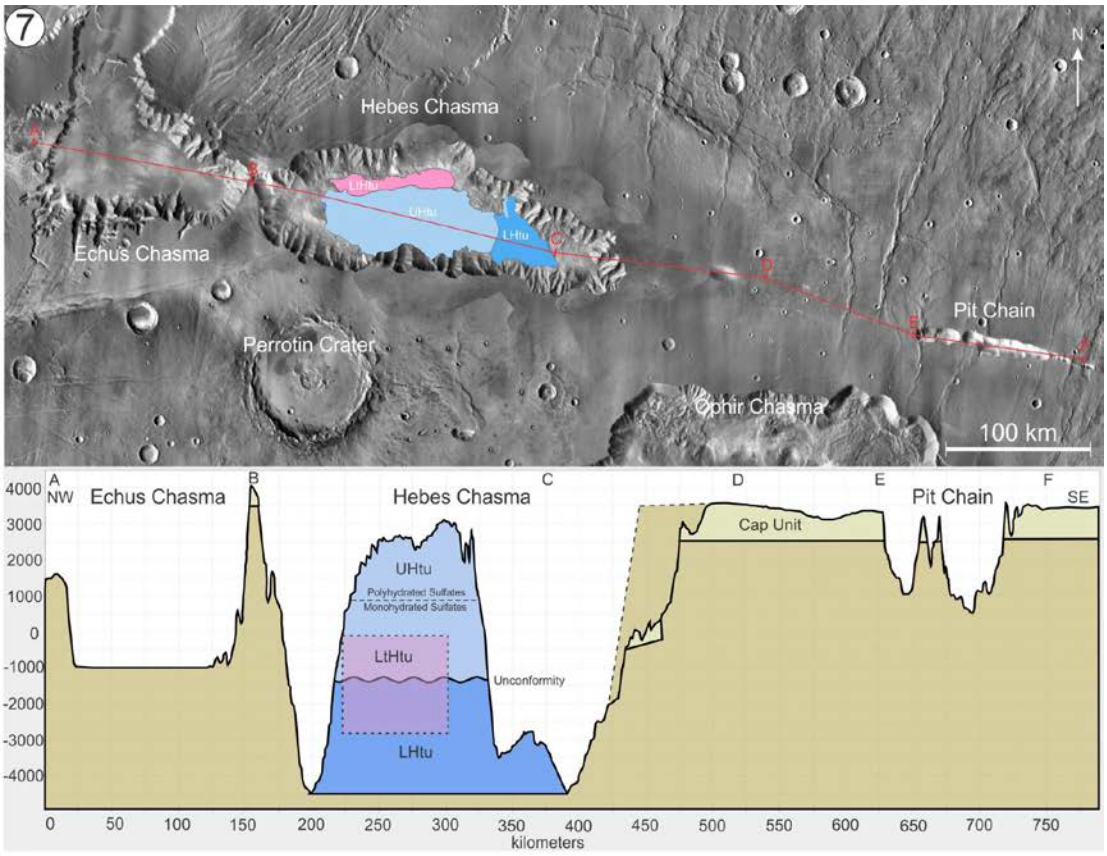

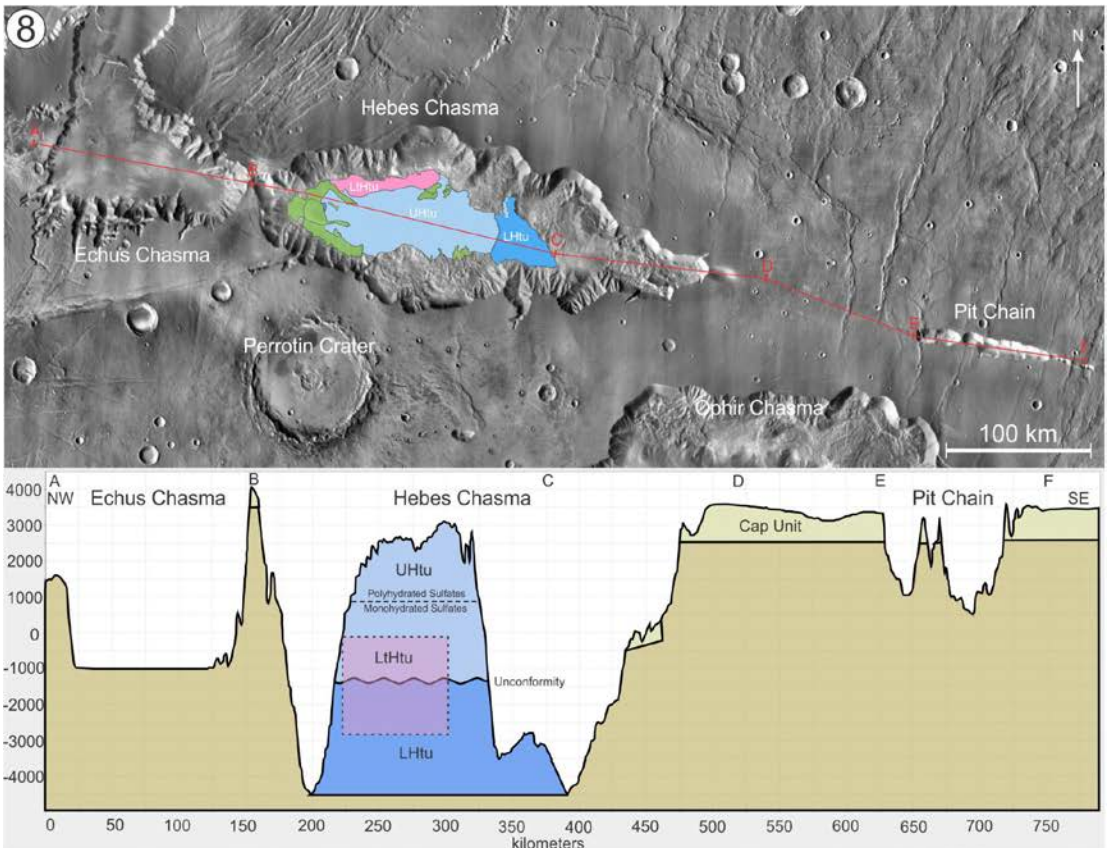

Fig. 3.20: Formation stages 7 and 8. VE=26X. (7) The Late ILD (LtHtu) is deposited in the northern valley between the chasma wall and the ILD mound. LtHtu is roughly represented by the dashed square in the cross-section. (8) ILD debris flows form (green) and Hebes collapses to the present extent. The southern and eastern portions of the chasma are the last to collapse.

3.6 Conclusions

This study examined the geology of Hebes Chasma in order to understand the collapse mechanism that formed the ancestral basins of VM and their continued, post-ILD collapse. The collapse dynamics that dominated the late formation of the chasma are more easily interpreted. Observations are best described by a loss of volume from confined aquifers or subsurface ice behind the chasma walls that created a toppling failure along fault-controlled sections, or proto-blocks. Lower sections of wall may have been more saturated and gave way to catastrophic landslides that carried intact blocks, but also slowed downward movement of blocks. Faults show three preferred orientations 101˚, 65˚ and 145˚ that are regionally consistent and have been measured previously in VM. These provide insight into Tharsis related stresses and suggest multiple, long-term, episodes of faulting.

The contacts between ILD and spur and gully wall have important implications to wall collapse. No major deformation in the ILD was observed at these contacts. Layers at the contacts are uniform and dip shallowly towards the wall. These observations are inconsistent with the isostatic subsidence model for basin collapse proposed by Andrews-Hanna, [2012], where one would expect to see deformed contacts.

Evidence for groundwater flow between Hebes and Echus is inconclusive, but a rough framework based on inferred outcomes that arise from differing water levels before and after the formation of Kasei Valles can be produced. Regional topography suggests that generally water would have flowed eastwards into Hebes. The similar elevations of the floor of Echus and the ILD unconformity in Hebes are possibly related by erosion of the Lower ILD to a water level that was created by the draining of lakes through the outwash channel that eventually formed Kasei Valles.

A systematic examination of the perimeters of other chasma in VM should be examined to see if the three preferred orientations of 101˚, 65˚ and 145˚ occur elsewhere. In particular the north side of Ophir Chasma which displays similar concave sections of smooth talus wall in between spur and gully wall. Perimeter faults in the plateau were mapped previously [Lucchitta, 1999]; however, a new look with higher resolution topographical data could reveal more faults. A concise evaluation of perimeter faults around VM similar to previous work by Wilkins and Schultz, [2003] and Birnie, [2012] could provide insight into the technicalities of VM collapse. Future work may also reveal if spur and gully wall morphology is fault controlled.

Chapter 4: Final Discussion and Overall Conclusions

Analyses of the layer thicknesses, layer attitudes, geomorphology and mineralogy of the ILD in Hebes Chasma provided several insights into the timing, deposition, alteration and erosion of the mound. Analyses of perimeter faults, slump blocks and wall morphology provided insight into the timing and mechanism of chasm collapse. Examining the margin and topography between Echus and Hebes constrained hypothetical groundwater flow and lake levels within the chasma.

The ILD of Hebes Chasma was deposited by ash fall in three episodes, forming the Lower ILD, Upper ILD and Late ILD. Some observations suggest a glacial origin for the Late ILD. The lack of an out-wash channel limited the possibility of erosion and kept the majority of the ILD intact. Each of these units displays differing mineralogy, erosional features, layer thicknesses and layer attitudes.

Topographical relief within the chasma floor formed large-scale, gently dipping folds within the Lower ILD. The fold hinges have a similar orientation to Set 2 faults observed in the northwest Noachian plateau suggesting the faults may be present in the chasma floor as well. This is the first observation of large folds within Valles Marineris. The Lower ILD also contains the chasma's thickest layers (averaging 24.17 m) as well as gypsum. An unconformity separates the Upper and Lower ILD indicating erosion. The unconformity was observed at an elevation of approximately -1,400 m and produced by the draining of water within Hebes to the elevation of the floor of Echus. This left the Lower ILD in Hebes exposed above the water level and was subsequently eroded to this level. Above the unconformity is a 900 m section of the Upper ILD that contains no visible layering suggesting that its deposition may have been rapid and constant in a low energy lacustrine condition, or possibly as the result of the melting of a frozen lake that

had accumulated a thick deposit of sediment. Layers are observed above this 900 m section averaging 6.73 m. Layer attitudes of the Upper ILD dip outward like other ILD mounds observed in Valles Marineris.

The Late ILD has layer attitudes similar to the Upper ILD, however certain aspects including layer thickness, composition and erodibility distinguish them. The Late ILD has thin layering averaging less than one meter and lacks the mono/polyhydrated boundary that the Upper ILD has. Most striking is the unit's layered hummocks, features not seen anywhere else in the chasma. Layer attitude can be explained by draping over the central mound's slope. After deposition of the Upper and Lower ILD, the chasma northern wall collapsed to its current extent which was followed by deposition of the Late ILD. Deposition by ash fall is supported by its composition, however glaciers are known to form layered hummocks on Earth so a glacial deposition may be possible as well. This area is a valley between the central mound and the chasma wall, ideal for containing a lake or "moat".

A mineralogical transition exists at an elevation between 800-900 m. Below 800 m are monohydrated sulfates and above 900 m are polyhydrated sulfates. This indicates the lower section of the Upper ILD is more competent and/or resistant and the upper section is porous and may have become more saturated. Four large landslide scars were formed at this boundary and are further evidence of the lower sections higher competence. Hydrated sulfates were detected at these slump scars and suggest that they comprise the bulk of the mound.

Given their sizable mafic and sulfur content, draping structure and sheer height, the Upper and Lower ILD are best described as ash fall deposits within standing water or possibly formed during intervals of melting ice. Layer thickness measurements revealed several sequences of thinning upwards within the layers of the Upper ILD, possibly indicating eruptions

of differing intensity and duration. The sulfates were produced after deposition by alteration and since they are detected at slump scars, likely form the bulk of Hebes ILD mound. On Earth, sulfates are often formed in periglacial environments. However in these instances the alteration is limited to a few millimeters at most. Water is a significantly more powerful weathering agent compared to ice when forming hydrated minerals. For these reasons, a scenario of ash fall involving standing water is more convincing than one with ice.

At the time of the Upper and Lower ILD deposition, the chasma perimeter was about 30% smaller than it is presently. Spur and gully wall morphology represents the oldest formations in Valles Marineris. Areas of the Upper and Lower ILD are seen in contact with spur and gully wall at depths exceeding -3 km. Layers at these contacts are relatively undisturbed and uniform. No evidence was found in Hebes Chasma to support subsidence coinciding with deposition. This suggests that the chasma had already collapsed to these depths at the time of deposition and the mass of the ILDs did not cause significant further collapse. Measurements of 27 vertical faults observed within the plateau around the perimeter of the chasma indicate three preferred orientations 101˚, 65˚, 145˚ (Sets 1, 2 and 3 respectively) and various amounts of vertical relief up to 500 m. When these faults intersect, sections of wall referred to as proto-blocks are created which are susceptible to collapse along the fault planes. Seven slump blocks that have collapsed several kilometers were observed throughout the chasma. A loss volume from either melting ice or the release of confined aquifers behind the chasma walls provides the simplest explanation for wall collapse. The loss of volume from ice is a slightly more attractive mechanism as there is a 9% loss of volume during the phase change of ice to water.

Some observations pose problems. The absence of Lower ILD in a large 281 km^2 area between two contacts of Lower ILD and chasma wall cannot be easily explained. Most puzzling

is the absence of Upper ILD above the eastern outcrop of Lower ILD.

This work is meant to contribute our understanding of the formation of Valles Marineris as well as resolve the timing and depositional mechanism of the ILDs. ILDs contain information that aids the construction of past atmospheric conditions on Mars. The overwhelming evidence from ILDs suggesting that significant liquid water existed at the surface is vital to our understanding of Mars. Our findings demonstrate that: 1) Hebes Chasma formed from a loss of volume rather than ILD induced subsidence. 2) Wall collapse is fault controlled. 3) There were three separate periods of deposition of ILDs. 4) ILD deposition occurred before the chasma was completely formed. 5) Substantial water and some glacial activity were present during and after ILD deposition.

Future research should include a complete survey of all ILDs in VM using HiRISE imagery and CRISM spectroscopy to analyze bed thickness distribution and composition in an effort to correlate ILDs in different regions. Correlations between ILDs in VM and craters may also be important. An examination of perimeter faults throughout VM should be undertaken as well to see if the three preferred orientations of 101˚, 65˚, and 145˚ propagate elsewhere. In particular the north side of Ophir Chasma which displays similar concave sections of smooth talus wall in between spur and gully wall should be examined. Perimeter faults in the plateau were mapped previously [Lucchitta, 1999], however a new look with higher resolution topographical data could reveal more faults. Future work may also reveal spur and gully wall morphology is fault controlled.

References

Agliardi, F., Crosta, G., Zanchi, A. (2001), Structural constraints on deep-seated slope deformation kinematics. Engineering Geology, 59, 83–102.

Anderson, R. B. and Bell, J. F. (2010), Geologic mapping and characterization of Gale Crater and implications for its potential as a Mars Science Laboratory landing site. The Mars Journal, 5, 76–128.

Andrews-Hanna, J. C., Phillips, R. J., and Zuber, M. T. (2007), Meridiani Planum and the global hydrology of Mars. Nature, 446(7132), 163-166.

Andrews-Hanna, J.C. (2012), The formation of Valles Marineris: 3. Trough formation through super-isostasy, stress, sedimentation, and subsidence. J. Geophys. Res., 117, E06002, doi:10.1029/2012JE004059

Armstrong, J. C., & Leovy, C. B. (2005). Long term wind erosion on Mars. *Icarus*, *176*(1), 57-74.

Baker, V. R. and Partridge, J. B. (1986), Small martian valleys: Pristine and degraded morphology. J. Geophys. Res. 84, 3561–3572

Balme, M. R., Bargery, A.S., Gallagher, C.J., and Gupta, S., (2011), Martian Geomorphology, Geological Society Special Publication 356.

Baum, R.L. and Odum, J.K. (1996), Geologic map of slump-block deposits in part of the Grand Mesa area, Delta and Mesa Counties, Colorado. U.S.G.S. Open-File Report 96-017.

Bibring, J.-P., Langevin, Y., Gendrin, A., Gondet, B., Poulet, F., Berthé, M., Soufflot, A., Arvidson, R., Mangold, N., Mustard, J., Drossart, P., the OMEGA team (2005), Mars surface diversity as revealed by the OMEGA/Mars Express observations. Science, 307, 1576 – 1581, doi:10.1126/science.1108806.

Bibring, J.-P., Langevin, Y., Mustard, J. F., Poulet, F., Arvidson, R., Gendrin, A., Gondet, B., Mangold, N., Pinet, P., Forget, F., the OMEGA team (2006), Global mineralogical and aqueous Mars history derived from OMEGA/Mars Express data. Science, 312, 400 – 404, doi:10.1126/science.1122659.

Birnie, C., Fueten, F., Stesky, R., & Hauber, E. (2012). Underlying structural control of small-scale faults and fractures in West Candor Chasma, Mars. Journal of Geophysical Research: Planets (1991–2012), 117(E11).

Bishop, J. L., Parente, M., Weitz, C. M., Noe Dobrea, E. Z., Roach, L. H., Murchie, S. L., McGuire, P.C., McKeown, N.K., Rossi, C.M., Brown, A.J., Calvin, W.M., Milliken, R., and Mustard, J. F. (2009). Mineralogy of Juventae Chasma: Sulfates in the light-toned mounds, mafic minerals in the bedrock, and hydrated silica and hydroxylated ferric sulfate on the plateau. Journal of Geophysical Research: Planets (1991–2012), 114(E2).

Brown, W.G. (1988), Deformational style of Laramide uplifts in the Wyoming foreland. GSA, Memoir 171.

Broxton, M.J. and Edwards, L.J. (2008), The Ames Stereo Pipeline: Automated 3D Surface Reconstruction from Orbital Imagery. LPSC XXXIX, Abstract #2419.

Carr, M.H. and Head, J.W. (2010), Geologic history of Mars, Earth and Planet. Sci. Let., 294, 185-203, doi:10.1016/j.epsl.2009.06.042.

Catling, D. C., Wood, S. E., Leovy, C., Montgomery, D. R., Greenberg, H. M., Glein, C. R., and Moore, J. M. (2006), Light-toned layered deposits in Juventae Chasma, Mars. Icarus, 181(1), 26-51.

Chapman, M. G., (2002), Layered, massive, and thin sediments on Mars: Possible Late Noachian to Late Amazonian tephra? In: Volcano-Ice Interactions on Earth and Mars. Geol. Soc. Spec. Publ., London, 202, 273–203.

Chapman, M.G. and Tanaka, K.L. (2001), Interior trough deposits on Mars: Subice volcanoes?, J. Geophys. Res., 106(E5), 10087-10100, doi:10.1029/2000JE001303

Chapman, M. G., Neukum, G., Dumke, A., Michael, G., van Gasselt, S., Kneissl, T., Zuschneid, W., Hauber, E., Ansan, V., Mangold, N., and Mason, P., (2010), Noachian-Hesperian geologic history of the Echus Chasma and Kasei Valles system on Mars: New data and interpretations. Earth and Planet. Sci. Let., 296, 256-271, doi:10.1016/j.epsl.2009.11.032.

Chojnacki, M. and Hynek, B.M. (2008), Geological context of water-altered minerals in Valles Marineris, Mars, JGR: Planets (1991–2012*)* 113.E12.

Christensen, P.R., Engle, E., Anwar, S., Dickenshied, S., Noss, D., Gorelick, N., Weiss-Malik, M., JMARS – A Planetary GIS, http://adsabs.harvard.edu/abs/2009AGUFMIN22A..06C

Croft, S. K. (1989), Spelunking on Mars: the carbonate-tectonic hypothesis for the origin of Valles Marineris. Tectonic Features on Mars, 1, 21-24.

Croft, S. K. (1990), Geologic map of the Hebes Chasma quadrangle, VM 500K 00077 (abstract), NASA Tech. Memo 4210, 539–541.

De Blasio, F.V. (2011), Landslides in Valles Marineris (Mars): A possible role of basal lubrication by sub-surface ice. Planetary and Space Science, 59, 1384-1392.

De Pablo, M.A. (2003), An Alternative Hypothesis for the Origin and Evolution of Hebes Chasma, Mars. 34th LPSC, Abstract #1072.

Ehlmann, B. L., Mustard, J. F., Murchie, S. L., Poulet, F., Bishop, J. L., Brown, A. J., Calvin, W.M., Clark, R.N., Des Marais, D., Milliken, R.E., Roach, L.H., Roush, T.L., Swayze, G.A., and Wray, J. J. (2008). Orbital identification of carbonate-bearing rocks on Mars. *Science*, *322*(5909), 1828-1832.

Mustard, J. F., Ehlmann, B. L., Murchie, S. L., Poulet, F., Mangold, N., Head, J. W., and Roach, L. H. (2009), Composition, morphology, and stratigraphy of Noachian crust around the Isidis basin. Journal of Geophysical Research: Planets (1991–2012), 114(E2).

Flahaut, J., Quantin, C., Allemand, P., and Thomas, P. (2010), Morphology and Geology of the ILD in Capri/Eos Chasma (Mars) from Visible and Infrared Data. Icarus, 207, 175-185, doi:10.1016/j.icarus.2009.11.019.

Fueten, F., Flahaut, J., Le Deit, L., Stesky, R., Hauber, E., and Gwinner, K. (2011), Interior layered deposits within a perched basin, southern Coprates Chasma, Mars: Evidence for their formation, alteration, and erosion. Journal of Geophysical Research: Planets (1991–2012), 116(E2).

Fueten, F., Flahaut, J., Stesky, R., Hauber, E., and Rossi, A. P. (2014), Stratigraphy and mineralogy of Candor Mensa, West Candor Chasma, Mars: Insights into the geologic history of Valles Marineris. Journal of Geophysical Research: Planets, 119(2), 331-354.

Gangale, T., "Planetary Timescales" *Palaeos: Time: Geologic Time Scales on Earth, Mars, and the Moon*. n.p., 2007. Web. 23 Sept. 2015.

Gendrin, A., Mangold, N., Bibring, J.-P., Langevin, Y., Gondet, B., Poulet, F., Bonello, G., Quantin, C., Mustard, J., Arvidson, R., LeMouélic, S. (2005), Sulfates in Martian layered terrains: The OMEGA/Mars Express view. Science, 307, 1587–1591, doi:10.1126/science.1109087.

Golombek, M. P., Plescia, J. B., and Franklin, B. J. (1991), Faulting and folding in the formation of planetary wrinkle ridges. In Lunar and Planetary Science Conference Proceedings, 21, 679-693.

Gortzinger, J.P. and Milliken, R.E., (2012), The Sedimentary Rock Record of Mars: Distribution, Origins, and Global Stratigraphy. Sedimentary Geology of Mars, SEPM, 102, 1.

Gourronc, M., Bourgeois, O., Mège, D., Pochat, S., Bultel, B., Massé, M., and Mercier, D., (2014), One million cubic kilometers of fossil ice in Valles Marineris: Relicts of a 3.5 Gy old glacial landsystem along the Martian equator. Geomorphology, 204, 235-255.

Grindrod, P.M. and Balme, M.R. (2010), Groundwater processes in Hebes Chasma, Mars. Geophysical Research Letters, 37, doi:L13202.

Grindrod, P.M. and Warner, N.H. (2014), Erosion rate and previous extent of interior layered deposits on Mars revealed by obstructed landslides. Geology, 42, 795-798, doi:10.1130/G35790.1

Gutiérrez-Santolalla, F., Acosta, E., Ríos, S., Guerrero, J., and Lucha, P. (2005), Geomorphology and geochronology of sackung features (uphill-facing scarps) in the Central Spanish Pyrenees. Geomorphology, 69(1), 298-314.

Haberle, R.M. (1998), Early Mars climate models. Journal of Geophysical Research: Planets (1991–2012), 103, E12, 28467-28479.

Harrison, K. P. and Grimm, R. E. (2005), Groundwater-controlled valley networks and the decline of runoff on early Mars. J. Geophys. Res. 110.

Hartmann, W. K., & Neukum, G. (2001), Cratering chronology and the evolution of Mars. *Chronology and evolution of Mar*s, 165-194. Springer Netherlands.

Hauber, E., Gwinner, K., Gendrin, A., Fueten, F., Stesky, R., Pelkey, S., Wulf, H., Reiss, D., Zegers, T., MacKinnon, P., Michael, G., Jaumann, R., Bibring, J.-P., Neukum, G., and HRSC Co-Investigator Team. (2006), An Integrated Study of Interior Layered Deposits in Hebes Chasma, Valles Marineris, Mars, Using MGS, MO, and MEX Data. 37th LPSC, Abstract #2022.

Hauber, E., Gwinner, K., Gendrin, A., Fueten, F., Stesky, R., Pelkey, S., Reiss, D., Zegers, T., MacKinnon, P., Jaumann, R., Bibring, J.-P., and Neukum, G. (2008), Hebes Chasma, Mars: Slopes and stratigraphy of interior layered deposits, 39th LPSC, Abstract #2375.

Head, J. W., Greeley, R., Golombek, M. P., Hartmann, W. K., Hauber, E., Jaumann, R., and Carr, M. H. (2001), Geological processes and evolution. In *Chronology and Evolution of Mars* (pp. 263-292). Springer Netherlands.

Head, J. W., Marchant, D. R., Agnew, M. C., Fassett, C. I., & Kreslavsky, M. A. (2006), Extensive valley glacier deposits in the northern mid-latitudes of Mars: Evidence for Late Amazonian obliquity-driven climate change. Earth and Planet. Sci. Let., 241, 663-671, doi:10.1016/j.epsl.2005.11.016

Hore, A., Fueten, F., Hauber, E., Flahaut, J. (2013), Structural analysis, layer thickness measurements and mineralogical investigation of the largest interior layered deposit within Ganges Chasma, 44th LPSC, Abstract 1070.

Howard, A.D. (1988), Introduction: groundwater sapping on Mars and Earth. Sapping Features of the Colorado Plateau, NASA Spec. Publ., 491, 1-5.

Hynek, B. M. and Phillips, R. J. (2003), New data reveal mature, integrated drainage systems on Mars indicative of past precipitation. Geology 31, 757–760.

Jackson, M. P. A., Adams, J. B., Dooley, T. P., Gillespie, A. R., and Montgomery, D. R. (2011), Modeling the collapse of Hebes Chasma, Valles Marineris, Mars. Geological Society of America Bulletin, 123(7-8), 1596-1627.

Jakosky, B. M., Henderson, B. G., and Mellon, M. T. (1995), Chaotic obliquity and the nature of the Martian climate. JGR: Planets (1991–2012), 100, E1, 1579-1584.

Kite, E. S., Lewis, K. W., Lamb, M. P., Newman, C. E., and Richardson, M. I. (2013), Growth and form of the mound in Gale Crater, Mars: Slope wind enhanced erosion and transport. Geology, 41(5), 543-546.

Komatsu, G., Geissler, P. E., Strom, R. G., and Singer, R. B. (1993). Stratigraphy and erosional landforms of layered deposits in Valles Marineris, Mars. Journal of Geophysical Research: Planets (1991–2012), 98(E6), 11105-11121.

Komatsu, G., Ori, G. G., Ciarcelluti, P., and Litasov, Y. D. (2004), Interior layered deposits of Valles Marineris, Mars: analogous subice volcanism related to Baikal Rifting, Southern Siberia. Planetary and Space Science, 52(1), 167-187.

Le Deit, L., Bourgeois, O., Mège, D., Hauber, E., Le Mouélic, S., Massé, M., and Bibring, J. P. (2010), Morphology, stratigraphy, and mineralogical composition of a layered formation covering the plateaus around Valles Marineris, Mars: Implications for its geological history. Icarus, 208(2), 684-703.

Leshin, L. A., Mahaffy, P. R., Webster, C. R., Cabane, M., Coll, P., Conrad, P. G., and Peret, L. (2013). Volatile, isotope, and organic analysis of martian fines with the Mars Curiosity rover. Science, 341(6153), 1238937.

Lewis, K. W., Aharonson, O., Grotzinger, J. P., Kirk, R. L., McEwen, A. S., and Suer, T. A. (2008), Quasi-periodic bedding in the sedimentary rock record of Mars. Science, 322(5907), 1532-1535.

Lucas, A., Mangeney, A., Mege, D., and Bouchut, F. (2011), Influence of the scar geometry on landslide dynamics and deposits: Application to Martian landslides. Journal of Geophysical Research: Planets (1991–2012), 116(E10).

Lucchitta, B.K. (1973), Morphology of chasma walls, Mars, Journal of Geophysical Research, 6, 651-662.

Lucchitta, B.K. (1978), Morphology of chasma walls, Mars. USGS Journal of Research, 6(5), 651-662.

Lucchitta, B. K. (1979), Landslides in Valles Marineris, Mars. Journal of Geophysical Research, 84(B14), 8097–8113, doi:10.1029/JB084iB14p08097.

Lucchitta, B.K., (1990), Young volcanic deposits in the Valles Marineris, Mars. Icarus, 86, 476–509. doi:10.1016/0019-1035(90)90230-7.

Lucchitta, B. K., Isbell, N. K., and Howington-Kraus, A. (1994), Topography of Valles Marineris: Implications for erosional and structural history. Journal of Geophysical Research: Planets (1991–2012), 99(E2), 3783-3798.

Lucchitta, B.K. (1999), USGS Map I-2568.

Lucchitta, B.K. (2010). Lakes on Mars, doi:10.1016/B978-0-444-52854-4.00005-2.

Madeleine, J. B., Forget, F., Head, J. W., Levrard, B., Montmessin, F., and Millour, E. (2009), Amazonian northern mid-latitude glaciation on Mars: A proposed climate scenario. Icarus, 203(2), 390-405.

Mangold, N., Allemand, P., Thomas, P. G. (1998), Wrinkle ridges of Mars: Structural analysis and evidence for shallow deformation controlled by ice-rich décollements. Planetary Space and Science, 46, 345-356.

Mangold, N., Gendrin, A., Gondet, B., LeMouelic, S., Quantin, C., Ansan, V., and Neukum, G. (2008), Spectral and geological study of the sulfate-rich region of West Candor Chasma, Mars. Icarus, 194(2), 519-543.

Malin, M.C. and Edgett, K.S. (2000), Sedimentary Rocks of Early Mars. Science, 290, 5498, 1927-1937.

Masson, P. (1977), Structure pattern analysis of the Noctis Labyrinthus-Valles Marineris regions of Mars. Icarus, 30(1), 49-62.

McEwen, A. S., Malin, M. C., Carr, M. H., and Hartmann, W. K. (1999). Voluminous volcanism on early Mars revealed in Valles Marineris. Nature, 397(6720), 584-586.

McKenzie, D. and Nimmo, F. (1999), The generation of martian floods by the melting of ground ice above dykes. Nature, 397, 231-233, doi:10.1038/16649

Mege, D., and Masson, P. (1996), Amounts of crustal stretching in Valles Marineris, Mars. Planetary Space and Science, 44, 749-782.

Mege, D., and Masson, P. (1996), A plume tectonics model for the Tharsis province, Mars. Planetary and Space Science, 44(12), 1499-1546.

Mege, D. and Bourgeois, O. (2011), Equatorial glaciations on Mars revealed by gravitational collapse of Valles Marineris wallslopes. Earth and Planetary Science Letters, 310(3), 182-191.

Michalski, J. and Niles, P.B. (2012), Atmospheric origin of Martian interior layered deposits:Links to climate change and the global sulfur cycle. Geology, 40, 5, 419-422.

Milliken, R., J. Grotzinger, R. Beyer, S. Murchie, A. McEwen, and the CRISM Science Team

(2007), Evidence for salt tectonics in Valles Marineris, Mars. 7th International Mars Conference, Abstract 3383.

Moratto, Z.M., Broxton, M. J., Beyer, R. A., Lundy, M., and Husmann, K. (2010), Ames Stereo Pipeline, NASA's Open Source Automated Stereogrammetry Software. LPSC XLI, Abstract # 2364.

Murchie, S., Arvidson, R., Bedini, P., Beisser, K., Bibring, J. P., Bishop, J., and Wolff, M (2007), Compact Reconnaissance Imaging Spectrometer for Mars (CRISM) on Mars Reconnaissance Orbiter (MRO). Journal of Geophysical Research, 112, E05S03, doi:10.1029/2006JE002682.

Murchie, S. L., Mustard, J. F., Ehlmann, B. L., Milliken, R. E., Bishop, J. L., McKeown, N. K., Dobrea, E., Seelos, F., Buczkowski, D., Wiseman, S., Arvidson, R., Wray, J., Swayze, G., Clark, R., Des Marais, D., McEwen, A., and Bibring, J. P. (2009), A synthesis of Martian aqueous mineralogy after 1 Mars year of observations from the Mars Reconnaissance Orbiter. Journal of Geophysical Research: Planets (1991–2012), 114(E2).

Murchie, S.L., Roach, L.H., Seelos, F.P., Milliken, R.E., Mustard, J.F., Arvidson, R.E., Wiseman, S.M., Lichtenberg, K.A., Andrews-Hanna, J.C., Bibring, J.-P., Bishop, J.L., Parente, M., Morris, R.V., (2009), Evidence for the origin of layered deposits in Candor Chasma, Mars, from mineral composition and hydrologic modeling, Journal of Geophysical Research, 114, E00D05, doi:10.1029/2009JE003343.

Mustard, J. F., Murchie, S. L., Pelkey, S. M., Ehlmann, B. L., Milliken, R. E., Grant, J. A., and Wolff, M. (2008), Hydrated silicate minerals on Mars observed by the Mars Reconnaissance Orbiter CRISM instrument. Nature, 454(7202), 305-309.

Nedell, S. S., Squyres, S. W., Andersen, D. W., (1987), Origin and evolution of the layered deposits in the Valles Marineris, Mars. Icarus, 70, 409–441.

Nemčok, A., Pašek, J., and Rybář, J. (1972), Classification of landslides and other mass movements. Rock Mechanics, 4(2), 71-78.

Okubo, C.H., Lewis, K.H., McEwen, A.S., and Kirk, R.L. (2008), Relative Age of Interior Layered Deposits in Southwest Candor Chasma Based on High-Resolution Structural Mapping. Journal of Geophysical Research, 113, E12002, doi: 10.1029/2008JE003181.

Pangaea Scientific (2006-2011), *Orion: Orientation Hunter [computer software]*. Supported by Canada Centre for Remote Sensing, Natural Resources Canada. Brockville, Ontario, Canada.

Peterson, C. (1981), A secondary origin for the central plateau of Hebes Chasma, Proc. Lunar Planet. Sci., 12B, 1459-1471.

Peulvast, J. P., Mege, D., Chiciak, J., Costard, F., and Masson, P. L. (2001), Morphology, evolution and tectonics of Valles Marineris wallslopes (Mars). Geomorphology, 37(3), 329-352.

Phillips, R. J., and Grimm, R. E. (1991), Martian seismicity. Lunar and Planetary Science Conference, 22, 1061.

Pieri, D.C. (1980), Martian Valleys: Morphology, Distribution, Age, and Origin, Science, 210, 4472, 895-897.

Pollack, J. B., Kasting, J. F., Richardson, S. M. and Poliakoff, K. (1987), The case for a wet, warm climate on early Mars. Icarus 71, 203–224.
Poulet, F., Bibring, J.-P., Mustard, J. F., Gendrin, A., Mangold, N., Langevin, Y., Arvidson, R. E., Gondet, B., Gomez, C., the OMEGA Team, (2005), Phyllosilicates on Mars and implications for the early Mars history. Nature, 438, 623–627, doi:10.1038/nature04274.

Quantin, C., Gendrin, A., Mangold, N., Bibring, J.P., Poulet, F., Allemand, P., and the OMEGA Team (2005), Sulfate deposits identified by Omega in Melas Chasma. 36th LPSC, Abstract #1789.

Quantin, C., Mangold, N., Hauber, E., Flahaut, J., Le Deit, L., Fueten, F., Zegers, T., and ISSI internationnal Team on ILD (2010), Timing Constraints of Interior Layered Deposit Emplacement in Valles Marineris, First International Conference on Mars Sedimentology and Stratigraphy; no. 6048.

Roach, L. H., Mustard, J. F., Swayze, G., Milliken, R. E., Bishop, J. L., Murchie, S. L., and Lichtenberg, K. (2010), Hydrated mineral stratigraphy of Ius Chasma, Valles Marineris. Icarus, 206(1), 253-268.

Robinson, M. S., and Tanaka, K. L. (1990), Magnitude of a catastrophic flood event at Kasei Valles, Mars. Geology, 18(9), 902-905.

Rossi, A. P., G. Neukum, M. Pondrelli, S. van Gasselt, T. Zegers, E. Hauber, A. Chicarro, and B. Foing (2008), Large-scale spring deposits on Mars? Journal of Geophysical Research, 113, E08016, doi:10.1029/2007JE003062.

Schultz, R. A. (1998), Multiple-process origin of Valles Marineris basins and troughs, Mars. Planetary and Space Science, 46(6), 827-834. doi:10.1016/S0032 -0633(98)00030-0.

Schultz, R.A. (2000), Localization of bedding plane slip and backthrust faults above blind thrust faults: Keys to wrinkle ridge structure. Journal of Geophysical Research, 105, 12,035– 12,052.

Sharp, R. B. (1973), Mars: Troughed terrain. Journal of Geophysical Research, 78, 4063–4072, doi:10.1029/JB078i020p04063.

Sharp, R.P. and Malin, M.C. (1975), Channels on Mars, GSA Bulletin, 86, 5, 593-609, doi:10.1130/0016-7606

Soffen, G. A. (1977), The Viking Project. Journal of Geophysical Research, 82, 28, 3959-3970.

Sowe et al., (2011), A comparative study of interior layered deposits on Mars, Martian Geomorphology, 356, 281.

Spencer, J. R., and F. P. Fanale (1990), New models for the origin of Valles Marineris closed depressions. Journal of Geophysical Research, 95(B9), 14,301–14,313.

Stesky, R.M and G.W. Pearce. (2014), *Pangaea Scientific: Spheristat 3.2 [computer software]*. Obtained from: http://www.pangaeasci.com.

Tanaka, K. L., and Golombek, M.P. (1989), Martian tension fracture and the formation of grabens and collapse features at Valles Marineris, Lunar and Planetary Science, 19, 383–396.

Tanaka, K. L., Golombek, M. P., and Banerdt, W. B. (1991), Reconciliation of stress and structural histories of the Tharsis region of Mars. Journal of Geophysical Research: Planets (1991–2012), 96(E1), 15617-15633.

Tanaka, K.L. (1997), Origin of Valles Marineris and Noctis Labyrinthus, Mars, by Structurally Controlled Collapse and Erosion of Crustal Materials. Lunar Planet. Sci. XXVIII, Abstract 1169.

Tanaka, K.L. (2014), USGS Map 3292, 43.

Viviano-Beck and Murchie, S.L. (2014), Hydrothermally Altered Stratigraphy in the Walls of Valles Marineris. Lunar Planet. Sci. XLV, Abstract #1963.

Wietz, M. (1999), A volcanic origin for the interior layered deposits in Hebes Chasma, Mars, 30th LPSC, Abstract #1277.

Watters, T. R. (1993), Compressional tectonism on Mars. Journal of Geophysical Research: Planets (1991–2012), 98(E9), 17049-17060.

Wilkins, S.J. and Schultz, R.A. (2003), Cross faults in extensional settings: Stress triggering, displacement localization, and implications for the origin of blunt troughs at Valles Marineris, Mars, Journal of Geophysical Research, 108, 5056, doi:10.1029/2002JE001968.

Williams, J.-P., Paige, D.A., and Manning, C.E. (2003), Layering in the wall rock of Valles Marineris: instrusive and extrusive magmatism. Geophys. Res. Lett., 30, 1623, doi: 10.1029/2003GL017662

Williams, J. P., and Nimmo, F. (2004), Thermal evolution of the Martian core: Implications for an early dynamo. Geology, 32(2), 97-100.

Williams, R. M. E. and Phillips, R. J. (2001), Morphometric measurements of martian valley networks from Mars Orbiter Laser Altimeter (MOLA) data. J. Geophys. Res. 106, 23737–23751

Witbeck, N.E., Tanaka, K.L., and Scott, D.H. (1991), Geologic map of the Valles Marineris region, Mars. USGS IMAP 2010.

Wordsworth, R., Forget, F., Millour, E., Head, J. W., Madeleine, J. B., and Charnay, B. (2013), Global modelling of the early martian climate under a denser CO 2 atmosphere: Water cycle and ice evolution. Icarus, 222(1), 1-19.

Zuber, M. T. (1995), Wrinkle ridges, reverse faulting, and the depth penetration of lithospheric strain in Lunae Planum, Mars. Icarus, 114(1), 80-92.